(12) INTERNATIONAL APPLICATION PUBLISHED UNDER THE PATENT COOPERATION TREATY (PCT)

(19) World Intellectual Property Organization
International Bureau

(43) International Publication Date
19 June 2025 (19.06.2025)

WIPO | PCT

(10) International Publication Number
WO 2025/128969 A1

(51) International Patent Classification:
A61K 33/38 (2006.01) *A61P 19/10* (2006.01)
A61K 47/62 (2017.01) *A61K 33/34* (2006.01)
A61L 27/54 (2006.01) *B82Y 5/00* (2011.01)

(21) International Application Number:
PCT/US2024/059993

(22) International Filing Date:
13 December 2024 (13.12.2024)

(25) Filing Language: English

(26) Publication Language: English

(30) Priority Data:
63/610,188 14 December 2023 (14.12.2023) US

(71) Applicant: **THE TEXAS A&M UNIVERSITY SYSTEM** [US/US]; 3369 Tamu, College Station, TX 77843-3369 (US).

(72) Inventors: **GAHARWAR, Akhilesh**; 3369 Tamu, College Station, TX 77843-3369 (US). **KERSEY, Anna**; 3369 Tamu, College Station, TX 77843-3369 (US). **SINGH, Irtisha**; 3369 Tamu, College Station, TX 77843-3369 (US).

(74) Agent: **WILSON, Kristi D.**; Dentons US LLP, P.O. Box 1302, Chicago, IL 60606 (US).

(81) Designated States *(unless otherwise indicated, for every kind of national protection available)*: AE, AG, AL, AM, AO, AT, AU, AZ, BA, BB, BG, BH, BN, BR, BW, BY, BZ, CA, CH, CL, CN, CO, CR, CU, CV, CZ, DE, DJ, DK, DM, DO, DZ, EC, EE, EG, ES, FI, GB, GD, GE, GH, GM, GT, HN, HR, HU, ID, IL, IN, IQ, IR, IS, IT, JM, JO, JP, KE, KG, KH, KN, KP, KR, KW, KZ, LA, LC, LK, LR, LS, LU, LY, MA, MD, MG, MK, MN, MU, MW, MX, MY, MZ, NA, NG, NI, NO, NZ, OM, PA, PE, PG, PH, PL, PT, QA, RO, RS, RU, RW, SA, SC, SD, SE, SG, SK, SL, ST, SV, SY, TH, TJ, TM, TN, TR, TT, TZ, UA, UG, US, UZ, VC, VN, WS, ZA, ZM, ZW.

(84) Designated States *(unless otherwise indicated, for every kind of regional protection available)*: ARIPO (BW, CV, GH, GM, KE, LR, LS, MW, MZ, NA, RW, SC, SD, SL, ST, SZ, TZ, UG, ZM, ZW), Eurasian (AM, AZ, BY, KG, KZ, RU, TJ, TM), European (AL, AT, BE, BG, CH, CY, CZ, DE, DK, EE, ES, FI, FR, GB, GR, HR, HU, IE, IS, IT, LT, LU, LV, MC, ME, MK, MT, NL, NO, PL, PT, RO, RS, SE, SI, SK, SM, TR), OAPI (BF, BJ, CF, CG, CI, CM, GA, GN, GQ, GW, KM, ML, MR, NE, SN, TD, TG).

Published:
— *with international search report (Art. 21(3))*
— *with sequence listing part of description (Rule 5.2(a))*

WO 2025/128969 A1

(54) Title: INORGANIC IONS AND BIOMATERIALS TO DRIVE STEM CELL DIFFERENTIATION

(57) Abstract: The present disclosure provides compositions and methods for increasing osteoblast or chondrocyte differentiation. The present disclosure further provides inorganic ion compositions, including silver ion composition and copper ion compositions. Aspects of the disclosure further relate to methods for treating diseases or disorders associated with altered osteoblast or chondrocyte differentiation, growth, or function.

TITLE OF THE INVENTION

INORGANIC IONS AND BIOMATERIALS TO DRIVE STEM CELL DIFFERENTIATION

CROSS-REFERENCE TO RELATED APPLICATIONS

[0001] This application claims the priority of U.S. Provisional Appl. Ser. No. 63/610,188, filed December 14, 2023, the entire disclosure of which is incorporated herein by reference.

STATEMENT OF GOVERNMENT RIGHTS

[0002] This invention was made with government support under DP2-EB026265 and R21NS121945 awarded by the National Institutes of Health and under W81XWH2210932 awarded by the Department of Defense. The government has certain rights in the invention.

INCORPORATION OF SEQUENCE LISTING

[0003] A sequence listing containing the file named "TAMC081WO_ST26.xml" which is 23.3 kilobytes (measured in MS-Windows®) and created on December 4, 2024, and comprises 26 sequences, is incorporated herein by reference in its entirety.

FIELD OF THE INVENTION

[0004] This present disclosure relates to the field of diseases or conditions associated with altered osteoblast or chondrocyte growth, differentiation, or function.

BACKGROUND OF THE INVENTION

[0005] Inorganic biomaterials are attractive in regenerative medicine as their physical and chemical properties can direct cell behavior and fate. Recent strategies have capitalized on the unique properties of inorganic biomaterials, using their ability to release ionic dissolution products to stimulate *in situ* tissue regeneration. These strategies harness the body's innate regenerative capabilities, potentially revolutionizing therapeutic approaches and offering significant advancements in the field of regenerative medicine. Complementing this, the high tunability, extended shelf-life, and capacity of inorganic biomaterials to orchestrate cellular and molecular processes enhance their suitability for clinical translation. For example,

bioactive glasses, such as 45S5 Bioglass®, stimulate bone growth by gradually dissolving and releasing essential ions like calcium, silicon, and phosphate. These ions promote osteogenesis and angiogenesis, aiding tissue regeneration and healing. The unique composition of Bioglass® enables it to bond with living tissues, making it suitable for clinical applications like dental and orthopedic implants or bone graft substitutes. Similarly, nanosilicates are shown to release ions such as silicon, magnesium, and lithium to stimulate endochondral differentiation in absence of any osteoinductive drugs or growth factors. Similarly, others have shown that delivering magnesium using microspheres can effectively guide *in situ* bone growth. These studies underscore the potential to harness the release of inorganic ions from biomaterials in the development of next-generation bioactive materials, specifically for *in situ* tissue regeneration.

[0006] Despite the promising advances in the use of inorganic biomaterials for tissue regeneration, a significant knowledge gap remains in understanding the effects of inorganic ions on cellular functions. To address this intricate problem, the present disclosure employed whole transcriptome sequencing (RNA-seq) to examine the comprehensive impact of inorganic ions on the transcriptomic profile. RNA-seq offers an unbiased interrogation of all expressed genes within a cell, thus significantly augmenting the potential to identify influenced molecular targets and signaling pathways. It has been documented that bioactive ions exert influence on an extensive array of complex biological processes, often at minimally detectable levels. Consequently, the highly granular insights provided by RNA-seq hold substantial promise for illuminating the intricate and dynamic processes modulated by bioactive inorganic ions at the transcriptomic level.

[0007] While the therapeutic roles of prevalent inorganic ions such as calcium, silicon, and magnesium, are relatively well-understood, the therapeutic roles and mechanisms of certain trace elements, particularly transition metals (d-block elements), is not well understood. For instance, copper (Cu) has been associated with diverse biological processes, including neuronal differentiation, antiviral activity, and immune modulation. Similarly, silver (Ag), renowned for its unique antimicrobial properties, has been increasingly recognized as a pro-regenerative material. Yet, the mechanisms governing these effects remain elusive. A thorough understanding of the role of copper and silver ions as bioactive dissolution agents is still underexplored. To address this gap, the present disclosure provides a significant advance in the field by utilizing the powerful tool of RNA-seq to delve into the effects of copper and silver ions on the transcriptomic landscape of human mesenchymal stem cells (hMSCs). The present

disclosure also describes metals with well-characterized roles as benchmarks for inert (such as tantalum (Ta) and titanium (Ti)) and toxic (such as platinum (Pt)) effects. By uncovering the detailed molecular mechanisms driven by these inorganic ions, the present disclosure provides compositions and methods for the design of inorganic biomaterials with tunable properties for advanced applications in regenerative medicine.

SUMMARY OF THE INVENTION

[0008] In one aspect the present disclosure provides a method of inducing osteoblast differentiation of a stem cell in a subject in need thereof, the method comprising administering to the subject an effective amount of a silver ion composition to induce osteoblast differentiation. In one embodiment, the silver ion composition is defined as a silver salt composition. The silver salt composition, in another embodiment, comprises a silver salt selected from the group consisting of silver acetate, silver nitrate, silver chloride, silver bromide, silver iodide, silver fluoride, silver sulfide, silver phosphate, silver chromate, and silver sulfate. In yet another embodiment, the silver salt composition is defined as an aqueous solution comprising the silver salt. In still yet another embodiment, the silver ion composition is defined as a silver biomaterial composition. Non-limiting examples of silver biomaterial compositions include a silver nanoparticle composition, a silver microparticle composition, a silver hydrogel composition, a silver microgel composition, a silver nanofiber composition, a silver microfiber composition, a silver polymer composition, a silver biomaterial coating, a silver depot, and a silver microneedle composition. In one embodiment, the effective amount of silver ions in the silver ion composition is a concentration sufficient to produce a local effective concentration of about 0.1 μM to about 100 μM or about 0.1 μM to about 29.95 μM. In another embodiment, the silver ion composition further comprises a targeting molecule. The stem cell, in yet another embodiment, is a mesenchymal stem cell. In still yet another embodiment, the subject is afflicted with or at risk of developing a disease or condition associated with altered osteoblast growth, differentiation, or function. Non-limiting examples of diseases or conditions associated with altered osteoblast growth, differentiation, or function include a fracture, a bone injury, rheumatoid arthritis, spondylarthritis, osteoarthritis, osteoporosis, a bone infection (osteomyelitis), a congenital bone disorder, a tumor-related bone defect, age-related bone loss, and a metabolic bone disease. In still yet another embodiment, administering comprises injection, microneedle administration, oral administration, buccal administration, vaginal administration, inhalation, intraosseous administration, trans nasal

application, topical administration, transdermal application, or rectal administration. In one embodiment, the present disclosure provides a method comprising administering a pharmaceutical composition comprising the effective amount of the silver ion composition to the subject.

[0009] In another aspect, the present disclosure provides a method of inducing chondrocyte differentiation of a stem cell in a subject in need thereof, the method comprising administering to the subject an effective amount of a copper ion composition to induce chondrocyte differentiation. In one embodiment, the copper ion composition is defined as a copper salt composition. The copper salt composition, in another embodiment, comprises a copper salt selected from the group consisting of copper acetate, copper nitrate, copper sulfate, copper chloride, copper carbonate, copper oxide, copper hydroxide, copper bromide, copper iodide, copper chloride, and copper oxide. In still yet another embodiment, the copper salt composition is defined as an aqueous solution comprising the copper salt. The copper ion composition, in one embodiment, is defined as a copper biomaterial composition. Non-limiting examples of a copper biomaterial composition include a copper nanoparticle composition, a copper microparticle composition, a copper hydrogel composition, a copper microgel composition, a copper nanofiber composition, a copper microfiber composition, a copper polymer composition, a copper biomaterial coating, a copper depot, and a copper microneedle composition. In another embodiment, the effective amount of copper ions in the copper ion composition is a concentration sufficient to produce a local effective concentration of about 0.1 μM to about 100 μM or about 0.1 μM to about 26.66 μM. In yet another embodiment, the copper ion composition further comprises a targeting molecule. The stem cell, in still yet another embodiment, is a mesenchymal stem cell. In one embodiment, the subject is afflicted with or at risk of developing a disease or condition associated with altered chondrocyte growth, differentiation, or function. Non-limiting examples of diseases or conditions associated with altered chondrocyte growth, differentiation, or function include a cartilage injury, costochondritis, an intervertebral disc herniation, polychondritis, osteoarthritis, rheumatoid arthritis, a traumatic joint injury, an ACL tear, a cartilage lesion or defect, a hip labral tear, osteonecrosis, juvenile idiopathic arthritis, avascular necrosis, chondromalacia patellae, post-traumatic osteoarthritis, a cartilage tumor, and an achondroplasia-like condition. In another embodiment, administering comprises injection, microneedle administration, oral administration, buccal administration, vaginal administration, inhalation, intraosseous administration, trans nasal application, topical administration,

transdermal application, or rectal administration. In yet another embodiment, the present disclosure provides a method comprising administering a pharmaceutical composition comprising the effective amount of the copper ion composition to the subject.

[0010] In yet another aspect, the preset disclosure provides a pharmaceutical composition comprising: a) a silver ion composition capable of producing a local effective silver ion concentration of about 0.1 μM to about100 μM or about 0.1 μM to about 29.95 μM; or b) a copper ion composition capable of producing a local effective copper ion concentration of about 0.1 μM to about 100 μM or about 0.1 μM to about 26.66 μM. In one embodiment, the silver ion composition is defined as a silver salt composition. In another embodiment, the copper ion composition is defined as a copper salt composition. The silver salt composition, in yet another embodiment, comprises a silver salt selected from the group consisting of silver acetate, silver nitrate, silver chloride, silver bromide, silver iodide, silver fluoride, silver sulfide, silver phosphate, silver chromate, and silver sulfate. The copper salt composition, in still yet another embodiment, comprises a copper salt selected from the group consisting of copper acetate, copper nitrate, copper sulfate, copper chloride, copper carbonate, copper oxide, copper hydroxide, copper bromide, copper iodide, copper chloride, and copper oxide. In one embodiment, the silver salt composition is defined as an aqueous solution comprising the silver salt. In another embodiment, the copper salt composition is defined as an aqueous solution comprising the copper salt. The silver ion composition, in yet another embodiment, is defined as a silver biomaterial composition. The copper ion composition, in still yet another embodiment, is defined as a copper biomaterial composition. Non-limiting examples of silver biomaterial compositions include a silver nanoparticle composition, a silver microparticle composition, a silver hydrogel composition, a silver microgel composition, a silver nanofiber composition, a silver microfiber composition, a silver polymer composition, a silver biomaterial coating, a silver depot, and a silver microneedle composition. Non-limiting examples of copper biomaterial compositions include a copper nanoparticle composition, a copper microparticle composition, a copper hydrogel composition, a copper microgel composition, a copper nanofiber composition, a copper microfiber composition, a copper polymer composition, a copper biomaterial coating, a copper depot, and a copper microneedle composition. In one embodiment, the silver ion composition further comprises a targeting molecule. In another embodiment, the copper ion composition further comprises a targeting molecule.

BRIEF DESCRIPTION OF THE DRAWINGS

[0011] The following drawings form part of the present specification and are included to further demonstrate certain aspects of the present invention. The invention may be better understood by reference to one or more of these drawings in combination with the detailed description of specific embodiments presented herein.

[0012] FIG. 1 hMSC compatibility with ion solutions. FIG. 1A - Viability assessment of hMSCs treated with varying concentrations of inorganic ions evaluated by MTT assay. Concentration resulting in ~10% reduction in viability (IC_{10}), compared to nontreated control, is denoted. FIG. 1B - LIVE/DEAD staining of hMSCs treated with low concentrations of inorganic ions for 72 hours. Live cells stained with calcein AM. Dead cells stained with ethidium homodimer-1. Images are representative of n = 3 total samples. Scale bar 100 μm. FIG. 1C - Cell cycle analysis via flow cytometry of hMSCs treated with low concentrations of inorganic ions for 72 hours.

[0013] FIG. 2 shows inorganic ion solution pH in deionized water (stock) and cell culture medium (working).

[0014] FIG. 3 demonstrates the transcriptome perturbation by inorganic ions. FIG. 3A - Experimental setup to investigate whole transcriptome response to inorganic ion treatment. FIG. 3B - Principal component analysis (PCA) of replicate samples of hMSCs cultured with and without inorganic ions based on RNA expression from RNA-seq w.r.t 50% most variable genes across all replicates where rows represent expressed genes (tpm, N = 3,864). FIG. 3C - Minus average (MA) representation of gene expression differences between hMSCs with and without inorganic ion treatment, where significant events are determined using GLM (*P*adjust < 0.05). FIG. 3D - Significant DEGs in hMSCs cultured with and without inorganic ions. Filled and unfilled bars depict significance cutoff *P*adjust < 0.05 and 0.01, respectively. FIG. 3E - Hierarchical clustering of replicate samples of hMSCs cultured with and without inorganic ions w.r.t mRNA expression from RNA-seq. DGE (*P*adjust < 0.05) across all replicates are depicted as rows (n = 3,864). Z-scoring represents row-scaled values.

[0015] FIG. 4 shows common transcriptome features between ion treatments. FIG. 4A - Shared differentially expressed genes (DEGs) between individual inorganic ion treatment groups. Exploded slice corresponds to the number of significant (*P*adjust < 0.05) DEGs uniquely enriched by the primary ion, and all other slices represent DEGs shared between other ions. FIG. 4B - Gene ontology (GO) biological processes (BP) shared between inorganic ions.

Circle size represents the number of DEGs corresponding to each term, and color intensity represents significance (FDR).

[0016] FIG. 5 shows the shared GO terms between ion treatments. FIG. 5A - GSEA database *GO Cellular Components*. Enrichment map of GSEA terms enriched (FDR < 0.05) by inorganic ion treatment. Node size represents number of total DEGs mapped to each term and color corresponds to enrichment by certain inorganic ions. Edge width represents similarity coefficient between terms. FIG. 5B - GSEA database *GO Molecular Functions*. Enrichment map of GSEA terms enriched (FDR < 0.05) by inorganic ion treatment. Node size represents number of total DEGs mapped to each term and color corresponds to enrichment by certain inorganic ions. Edge width represents similarity coefficient between terms.

[0017] FIG. 6 demonstrates the osteogenic influence of Ag ions on hMSCs. FIG. 6A - Grouped gene ontology (GO) evidence of osteogenic differentiation regulation by Ag ions. Bars represent -Log10 *P* value for each GO term. FIG. 6B - Volcano plot representation of significant DEGs (*P*adjust < 0.05) within Skeletal System Development (GO:0001501) comparing hMSCs with and without Ag ion treatment. FIG. 6C - Volcano plot representation of significant DEGs (*P*adjust < 0.05) within Ossification (GO:0001503) comparing hMSCs with and without Ag ion treatment. FIG. 6D - Qualitative assessment of Ag ion influence on alkaline phosphatase (ALP) production (left) and mineralized extracellular matrix production (right) staining at Day 7 and 21, respectively. hMSCs cultured in normal (ALP) and osteoconductive (ARS) media is used as negative control and hMSCs cultured in presence of osteogenic induction agent dexamethasone (DEX) represent positive control. Representative images from 3 independent replicates. Scale bar 100 μm. FIG. 6E - ALP activity is evaluated using kinetic assay at Day 7 (n = 2; mean ± s.d.; $^{**}P < 0.01$; ns, nonsignificant; unpaired two-tailed *t*-test). FIG. 6F - Calcium deposition is quantified using CPC extraction of stained nodules at Day 21 (n = 3; mean ± s.d.; $^{****}P < 0.0001$; $^{***}P < 0.001$; $^{**}P < 0.01$; unpaired two-tailed *t*-test). FIG. 6G - Qualitative histological assessment of Ag ion osteogenic influence on ALP and mineralized matrix production in 3D hMSC spheroids at Day 10 and 21, respectively. Representative images from 3 independent sections. Scale bar 100 μm. FIG. 6H - Effect of Ag ion on production of osteogenic-specific protein osteopontin (OPN) is determined via Western blot at Day 21. Housekeeping protein β-actin is used as internal control for quantitative assessment (n = 3; mean ± s.d.; $^{**}P < 0.01$; unpaired two-tailed *t*-test). Representative images shown.

[0018] FIG. 7 demonstrates that Ag triggers competitive MAPK signaling to initiate osteogenesis in stem cells. FIG. 7A - Volcano plot representation of significant DEGs (*P*adjust < 0.05) within Positive Regulation of MAPK Cascade (GO:0043410) comparing hMSCs with and without Ag ion treatment. FIG. 7B - Volcano plot representation of significant DEGs (*P*adjust < 0.05) within Response to BMP (GO:0071772) comparing hMSCs with and without Ag ion treatment. FIG. 7C - Volcano plot representation of significant DEGs (*P*adjust < 0.05) within Regulation of Non-Canonical Wnt Signaling Pathway (GO:200050) comparing hMSCs with and without Ag ion treatment. FIG. 7D - UpSet plot of significant GO terms reveals overlap between signaling mechanism and osteogenesis. Gene ratios are determined from number of genes (*P*adjust < 0.05) divided by the total size of the term (horizontal bars). The number of interactions between GO terms are depicted for each pair(s) of terms (vertical bars) with the pair being evaluated highlighted (dark gray) in the boxplot. FIG. 7E - RNA-seq track plots of normalized mRNA expression (aligned reads normalized to total library size - transcript per million (tpm)) at genomic locus of Gremlin 1 (*GREM1*), Fibroblast growth factor receptor 2 (*FGFR2*), Mitogen-activated protein kinase 3 (*MAP2K3*), and Bone morphogenetic protein 4 (*BMP4*). These data illustrate differential coverage induced by Ag ion treatment. FIG. 7F - Western blot of RUNX2 protein expression by Ag ion-treated hMSCs with and without pathway inhibitors Wnt (cadamonin), MEK (PD185342), and BMP (LDN 193189). Quantification normalized to GAPDH expression (n = 3; mean ± s.d.; $^{**}P < 0.01$; ns, nonsignificant; unpaired two-tailed *t*-test). FIG. 7G - Overlap of processes regulating MAPK signaling (DEGs from GO:0043410) and osteogenesis (DEGs from GO:0001501, GO:0001503, GO:0060348) is assessed by network visualization in Cytoscape. Node size corresponds to Log2 *P*adjust of each gene. Uniform edge width illustrates interactions within a previously identified signaling pathway (generated via GeneMANIA plugin) where the arrow indicates directionality of source and target gene.

[0019] FIG. 8 demonstrates that Ag ion treatment induces oxidative stress response in hMSCs. FIG. 8A - Volcano plot representation of significant DEGs (*P*adjust < 0.05) within Positive Regulation of Reactive Oxygen Species Metabolic Process (GO:2000379) comparing hMSCs with and without Ag ion treatment. FIG. 8B - GSEA enrichment plot revealing hypoxia by Ag ion treatment against curated *Hallmark* database (FDR < 0.05). NES values correspond to the magnitude of correlation that genes in the ranked list have with the term normalized to term size; -Log2 transformed FDR value. Enrichment profile is depicted in the upper portion of the plot. Bars represent gene "hits" in the ranked list ordered by positive correlation (left) and

negative (right) to the term. Ranking metric scores are depicted in the bottom portion of the plot corresponding to the position of individual genes within the input pre-ranked list. FIG. 8C - Reactive oxygen species (ROS) staining by superoxide probe DHE after 24 hours of Ag ion treatment. Images are representative of n = 3 total samples. Scale bar 100 μm.

[0020] FIG. 9 shows the intracellular signaling mechanism of silver-induced osteogenic differentiation supported by the present disclosure.

[0021] FIG. 10 demonstrates the chondrogenic influence of Cu ion on hMSCs. FIG. 10A - Volcano plot representation of significant DEGs (*P*adjust < 0.05) within Cartilage Development (GO:0051216) comparing hMSCs with and without Cu ion treatment. FIG. 10B - Volcano plot representation of significant DEGs (*P*adjust < 0.05) within Glycosaminoglycan Biosynthetic Process (GO:0006024) comparing hMSCs with and without Cu ion treatment. FIG. 10C - Hierarchical clustering of replicate samples of hMSCs cultured with and without Cu ions w.r.t mRNA expression from RNA-seq. DGE (*P*adjust < 0.05) comprising genes related to chondrogenic differentiation across all hMSC and Cu replicates are depicted as rows (n = 99). Z-scoring represents row-scaled values. FIG. 10D - RNA-seq track plots of normalized mRNA expression (aligned reads normalized to total library size - transcript per million (tpm)) at genomic locus of Aggrecan (*ACAN*), Cartilage oligomeric protein (*COMP*), and Transforming growth factor beta 1 (*TGFB1*). These data illustrate differential coverage induced by Cu ion treatment. FIG. 10E - Western blot of ACAN protein expression by Cu ion-treated hMSCs at Day 7. Quantification normalized to β-actin expression (n = 3; mean ± s.d.; $^{*}P < 0.05$; unpaired two-tailed *t*-test). FIG. 10F - Western blot of COMP protein expression by Cu ion-treated hMSCs at Day 21. Quantification normalized to β-actin expression (n = 2; mean ± s.d.; $^{*}P < 0.05$; unpaired two-tailed *t*-test). FIG. 10G - Assessment of 2D proteoglycan generation via Safranin O (Saf. O.) staining at Day 21. Quantification via stain dissolution and absorbance measurement at 560 nm (n = 3; mean ± s.d.; $^{****}P < 0.0001$; $^{***}P < 0.001$; $^{**}P < 0.01$; unpaired two-tailed *t*-test). All groups normalized to hMSCs cultured in chondroconductive media. Representative images from 3 independent replicates. Scale bar 100 μm. FIG. 10H - Qualitative histological assessment of Cu ion chondrogenic influence on ECM protein (proteoglycan, glycosaminoglycan) production in 3D hMSC spheroids at Day 21. Representative images from 3 independent sections. Scale bar 100 μm. FIG. 10I - GO Bubble plot of compiled signaling terms enriched by Cu ion treatment, arranged by significance (-Log10 FDR) and Z-score. Bubble size corresponds to gene ratio. These data illustrate TGFβ pathways are key mediators of Cu-induced chondrogenesis. FIG. 10J - GO

Circle plot depicting fold change values of significant DEGs contributing to enriched signaling GO terms. Outer ring: Individual DEGs represented as circular nodes corresponding to downregulation and upregulation; radial location corresponds to significance (-Log_{10} *P* value) of the gene. Inner ring: GO term Z-score depicted with decreasing to increasing gradient; height corresponds to significance (-Log_{10} *P* value) value of the term.

[0022] FIG. 11 shows that Cu ion treatment suppresses osteoarthritic cartilage degradation markers. FIG. 11A - RNAseq tracks of normalized mRNA expression (aligned reads normalized to total library size - transcript per million (tpm)) at genomic locus of Matrix metalloproteinase 13 (*MMP13*). FIG. 11B - Normalized fluorescent intensity of superoxide production by hMSCs treated with Cu ion (n = 3, mean ± s.d.; ***$P < 0.001$; ****$P < 0.0001$; unpaired two-tailed *t* test).

[0023] FIG. 12 shows the differentiation effects of Cu ion treatment in 2D seeded hMSCs. FIG. 12A - Qualitative assessment of Cu ion chondrogenic influence on ECM protein (proteoglycan, glycosaminoglycan) production in 2D hMSC monolayer culture at Day 21. Representative images from 3 independent sections. Scale bar 100 μm. FIG. 12B - Qualitative assessment of Cu ion influence on ALP production in 2D hMSC culture at Day 7. Representative images from 3 independent sections. Scale bar 5 mm. FIG. 12C - ALP activity is evaluated using kinetic assay at Day 7 (n = 3; mean ± s.d.). These data indicate Cu ion suppression of ALP activity in hMSCs.

[0024] FIG. 13 shows the similarity between GO signaling terms enriched by Cu ion treatment. Term correlation is evaluated via similarity score (black) from 0 to 1 representing shared DEGs, where higher score corresponds to higher connection between two terms. Data normalized to gene ratio.

[0025] FIG. 14 shows the network visualization of signaling processes regulating Cu-induced chondrogenic differentiation in Cytoscape. DEGs annotated to GO processes or clusters of GO processes are depicted in circular layout. Node size corresponds to significance and color corresponds to Log2 transformed fold change of each gene; upregulation and downregulation. Uniform edge width illustrates co-expression of genes in the network or interactions within a previously identified signaling pathway or predicted pathway where the arrow indicates directionality of source and affected gene. Edges are generated in Cytoscape via GeneMANIA plugin.

[0026] FIG. 15 demonstrates that Cu ion treatment has a broad impact on hMSC immunomodulatory characteristics. FIG. 15A - Schematic representation of hMSC immunomodulation resulting in different biomaterial outcomes. Left: pro-inflammatory immune niche can cause tissue degeneration or implant rejection. Right: anti-inflammatory niche driven by M2 macrophages promotes tissue regeneration. FIG. 15B - Significantly ($P <$ 0.05) enriched GO terms related to immune processes. Circle size and border width denote - Log10 FDR and Gene Ratio (number of genes divided by term size) values, respectively. Overlap of contributing DEGs represented by line between GO term (left) and gene (right). Log2 FC represented as significantly downregulated or significantly upregulated. These data illustrate the broad impact of Cu ion treatment on hMSCs immune processing, primarily by downregulating inflammatory cytokines. FIG. 15C - Gene expression of immune targets assessed via qRT-PCR at Day 7 with and without Cu ion treatment. Bars represent Log2 FC normalized to *GAPDH* expression and untreated hMSC condition (n = 3; mean ± s.d.; $^{**}P <$ 0.01; $^{****}P < 0.0001$; unpaired two-tailed *t*-test).

[0027] FIG. 16 demonstrates immune modulation of hMSCs following Cu ion treatment. FIG. 16A - Gene set enrichment analysis (GSEA) assessing immune signaling including JAK/STAT pathway, inflammation, and apoptosis against curated *Hallmark* database (FDR < 0.05). FIG. 16B - RNA-seq track plots of normalized mRNA expression (aligned reads normalized to total library size - transcript per million (tpm)) at genomic locus of Interleukin 7 (*IL7*) and Signal transducer and activator of transcription 2 (*STAT2*). These data illustrate differential coverage induced by Cu ion treatment. FIG. 16C - Gene expression of immune targets assessed via qRT-PCR at Day 3 with and without Cu ion treatment. Bars represent Log2 FC normalized to *GAPDH* expression and untreated hMSC condition (n = 3; mean ± s.d.; $^{*}P < 0.05$; $^{**}P < 0.01$; $^{***}P < 0.001$; unpaired two-tailed *t*-test). FIG. 16D - Secreted IL1B protein expression by THP-1-derived macrophages determined through direct enzyme linked immunosorbent assay (ELISA). Pharmacologically polarized macrophages M0 (100 nM PMA), M1 (20 ng/mL IFNγ, 10 pg/mL LPS), M2 (20 ng/mL IL4, 20 ng/mL IL13) are used as internal negative controls. Co-culture of M0 cells and hMSCs with and without Cu ion treatment were sampled at 24, 48, and 72 hours (n = 3; mean ± s.d.; $^{****}P < 0.0001$; one-way ANOVA). FIG. 16E - Relative protein expression (normalized to GAPDH expression for each condition) determined through indirect ELISA assessing intracellular macrophage IL7 production (n=3; mean ± s.d.).

[0028] FIG. 17 shows disruption of hMSC energy metabolism and mitochondrial function by Pt ion. FIG. 17A - Grouped gene ontology (GO) evidence of metabolic regulation by Pt ion.

Bars represent -Log10 *P* value for each GO term. These data provide strong indication of Pt ion impact on hMSC regulation of energy metabolic processes. FIG. 17B - Gene set enrichment analysis (GSEA) assessing trends in metabolic processes including oxidative phosphorylation and respiratory electron transport function against curated *Hallmark* and *Reactome* databases (FDR < 0.05). FIG. 17C - RNA-seq track plots of normalized mRNA expression (aligned reads normalized to total library size - transcript per million (tpm)) at genomic locus of Cytochrome C1 (*CYC1*), Cytochrome C oxidase subunit 6A1 (*COX6A1*), and Voltage-dependent anion-selective channel protein 2 (*VDAC2*). These data illustrate differential coverage induced by Pt ion treatment. FIG. 17D - Relative mitochondrial copy number was assessed via qRT-PCR at Day 3. Total DNA was extracted from hMSCs treated with and without Pt ion and amplification of Nidogen 2 (*ND2*) was quantified w.r.t. *GAPDH* control (n = 6; mean ± s.d.; ****$P < 0.0001$; unpaired two-tailed *t*-test). FIG. 17E - Immunofluorescent staining of mitochondria (stained via MitoView Green) and nucleic (stained via DAPI). Scale bar 100 μm; magnified scale bar 50 μm. FIG. 17F - Quantified immunofluorescence intensity of mitochondria (stained via MitoView Green) normalized to nuclear content (stained via DAPI). hMSCs treated with and without Pt ion. Mitochondrial membrane uncoupler, carbonyl cyanide m-chlorophenyl hydrazone (CCCP), used as internal reference for depleted membrane potential (n = 2; mean ± s.d., **$P < 0.01$; one-way ANOVA). FIG. 17G - Mitochondrial membrane potential was quantified as red:green fluorescent intensity ratio after staining with JC-1 dye and normalized w.r.t. nuclear content (stained via DAPI). Red and green signals correspond to high and low potential, respectively. hMSCs treated with and without Pt ion. CCCP was used as internal reference for depleted membrane potential (n = 2; mean ± s.d., **$P < 0.01$; unpaired two-tailed *t*-test). FIG. 17H - Immunofluorescent staining of JC-1 dye as it is processed by hMSCs treated with and without Pt ion or CCCP. Scale bar 100 μm. FIG. 17I - Schematic representation of proposed Pt ion mechanism initiating mitochondrial-induced apoptosis pathway.

[0029] FIG. 18 shows differentially regulated genes related to each complex within mitochondrial respiratory electron transport chain in response to Pt ion treatment. Bars correspond to Log2 FC expression.

[0030] FIG. 19 shows a volcano plot representation of significant DEGs (Padjust < 0.05) within Positive Regulation of Cytosolic Calcium Ion Concentration (GO:0007204) and Response to Calcium Ion (GO:0051592) comparing hMSCs with and without Pt ion treatment.

BRIEF DESCRIPTION OF THE SEQUENCES

[0031] SEQ ID NO:1 – representative forward primer sequence for amplification of alkaline phosphatase (*ALP*).

[0032] SEQ ID NO:2 - representative reverse primer sequence for amplification of alkaline phosphatase (*ALP*).

[0033] SEQ ID NO:3 representative forward primer sequence for amplification of osteocalcin (*OCN*).

[0034] SEQ ID NO:4 representative reverse primer sequence for amplification of osteocalcin (*OCN*).

[0035] SEQ ID NO:5 representative forward primer sequence for amplification of osteopontin (*OPN*).

[0036] SEQ ID NO:6 representative reverse primer sequence for amplification of osteopontin (*OPN*).

[0037] SEQ ID NO:7 representative forward primer sequence for amplification of integrin-binding sialoprotein (*IBSP*).

[0038] SEQ ID NO:8 representative reverse primer sequence for amplification of integrin-binding sialoprotein (*IBSP*).

[0039] SEQ ID NO:9 representative forward primer sequence for amplification of runt-related transcription factor 2 (*Runx2*).

[0040] SEQ ID NO:10 representative reverse primer sequence for amplification of runt-related transcription factor 2 (*Runx2*).

[0041] SEQ ID NO:11 representative forward primer sequence for amplification of collagen 1 A1 (*Col1a1*).

[0042] SEQ ID NO:12 representative reverse primer sequence for amplification of collagen 1 A1 (*Col1a1*).

[0043] SEQ ID NO:13 representative forward primer sequence for amplification of tumor necrosis factor alpha (*TNFα*).

[0044] SEQ ID NO:14 representative reverse primer sequence for amplification of tumor necrosis factor alpha (*TNFα*).

[0045] SEQ ID NO:15 representative forward primer sequence for amplification of interlukin-6 (*IL6*).

[0046] SEQ ID NO:16 representative reverse primer sequence for amplification of interlukin-6 (*IL6*).

[0047] SEQ ID NO:17 representative forward primer sequence for amplification of mitogen-activated protein kinase (*MEK1*).

[0048] SEQ ID NO:18 representative reverse primer sequence for amplification of mitogen-activated protein kinase (*MEK1*).

[0049] SEQ ID NO:19 representative forward primer sequence for amplification of extracellular signal-regulated kinase 1 (*ERK1*).

[0050] SEQ ID NO:20 representative reverse primer sequence for amplification of extracellular signal-regulated kinase 1 (*ERK1*).

[0051] SEQ ID NO:21 representative forward primer sequence for amplification of SRY-BOX transcription factor 9 (*Sox9*).

[0052] SEQ ID NO:22 representative reverse primer sequence for amplification of SRY-BOX transcription factor 9 (*Sox9*).

[0053] SEQ ID NO:23 representative forward primer sequence for amplification of aggrecan (*ACAN*).

[0054] SEQ ID NO:24 representative reverse primer sequence for amplification of aggrecan (*ACAN*).

[0055] SEQ ID NO:25 representative forward primer sequence for amplification of glyceraldehyde 3-phosphate dehydrogenase (*GAPDH*).

[0056] SEQ ID NO:26 representative reverse primer sequence for amplification of glyceraldehyde 3-phosphate dehydrogenase (*GAPDH*).

DETAILED DESCRIPTION OF THE INVENTION

[0057] The present disclosure provides compositions and method for inducing osteoblast or chondrocyte differentiation of a stem cell. The present disclosure provides a significant advance in the art by providing inorganic biomaterials for tissue regeneration with the potential to enhance clinical outcomes that currently predominately rely on growth factors and small molecule therapeutics.

[0058] The present disclosure provides inorganic ion compositions for inducing osteoblast or chondrocyte differentiation of a stem cell. As used herein the term "inorganic ion composition" refers to a composition comprising inorganic ions. Non-limiting examples of inorganic ions that may be used in an inorganic ion composition of the present disclosure include silver, copper, platinum, tantalum, and titanium ions. As used herein the term "silver ion composition" refers to a composition comprising silver ions. In some embodiments, a silver

ion composition may be a silver salt composition or a silver biomaterial composition. As used here the term "silver salt composition" refers to a chemical composition comprising a chemical compound formed between silver cations and non-metal anions. Non-limiting examples of such chemical compounds include silver acetate, silver nitrate, silver chloride, silver bromide, silver iodide, silver fluoride, silver sulfide, silver phosphate, silver chromate, silver sulfate. As used herein the term "silver biomaterial composition" refers to a composition comprising silver ions which has been engineered to interact with biological systems. Any biomaterial composition known in the art may be used according to the compositions and methods of the present disclosure. Non-limiting examples of silver biomaterial compositions include silver nanoparticle compositions, silver microparticle compositions, silver hydrogel compositions, silver microgel compositions, silver nanofiber compositions, silver microfiber compositions, silver polymer compositions, silver biomaterial coatings, silver depots, and silver microneedle compositions. As used herein the term "copper ion composition" refers to a composition comprising copper ions. In some embodiments, a copper ion composition may be a copper salt composition or a copper biomaterial composition. As used here the term "copper salt composition" refers to a chemical composition comprising a chemical compound formed between copper cations and non-metal anions. Non-limiting examples of such chemical compounds include copper acetate, copper nitrate, copper sulfate, copper chloride, copper carbonate, copper oxide, copper hydroxide, copper bromide, copper iodide, copper chloride, and copper oxide. As used herein the term "copper biomaterial composition" refers to a composition comprising copper ions which has been engineered to interact with biological systems. Any biomaterial composition known in the art may be used according to the compositions and methods of the present disclosure. Non-limiting examples of copper biomaterial compositions include copper nanoparticle compositions, copper microparticle compositions, copper hydrogel compositions, copper microgel compositions, copper nanofiber compositions, copper microfiber compositions, copper polymer compositions, copper biomaterial coatings, copper depots, and copper microneedle compositions.

[0059] In certain embodiments, the effective amount of silver ions in a silver ion composition or the effective amount of copper ions in a copper ion composition is a concentration sufficient to produce a local effective concentration of about 0.1 μM to about 100 μM, about 1 μM to about 100 μM, about 5 μM to about 90 μM, about 10 μM to about 80 μM, about 10 μM to about 70 μM, about 10 μM to about 60 μM, about 10 μM to about 50 μM, about 10 μM to about 40 μM, about 20 μM to about 35 μM, about 25 μM to about 35 μM, about 20 μM to

about 25 μM, about 0.1 μM to about 29.95 μM, or about 0.1 μM to about 26.66 μM, including all ranges and values derivable therebetween. As used herein the term "local effective concentration" refers to the concentration of metal ions present at the location of a stem cell to be differentiated. In particular embodiments, the effective amount of silver ions in a silver ion composition or the effective amount of copper ions in a copper ion composition is approximately equal to or greater than the half maximal effective concentration (EC_{50}) of silver ions required to induce osteoblast differentiation of a stem cell or of copper ions required to induce chondrocyte differentiation of a stem cell.

[0060] The inorganic ion compositions of the present disclosure can, through their released ions, shape cellular behavior and interactions, crucially influencing cell identity and promoting tissue-specific functions. Silver, as evidenced by the data provided in the present disclosure, stimulates osteogenic differentiation and mineralization in mesenchymal stem cells, uniquely inducing osteogenesis by stimulating MAPK and Wnt signaling pathways while circumventing BMP signaling. Copper, conversely, stimulates chondrogenesis. As evidenced by the data provided by the present disclosure, copper induces chondrogenic differentiation via the TGFβ receptor pathway upon activation of cell surface mediators, and concurrently suppresses pro-inflammatory modulators such as IL1β, fostering M2 macrophage polarization conducive to regeneration.

[0061] In certain aspects, the present disclosure provides pharmaceutical and therapeutic compositions comprising the inorganic ion compositions of the present disclosure. In some embodiments, the inorganic ion compositions of the present disclosure may be combined with a pharmaceutically acceptable carrier. As used herein, a "pharmaceutically acceptable carrier," "pharmaceutically acceptable adjuvant," or "adjuvant" refers to reagents, cells, compounds, materials, compositions, and/or dosage forms that are not only compatible with the inorganic ion compositions or other agents to be administered therapeutically, but also are, within the scope of sound medical judgment, suitable for use in contact with the tissues of human beings and animals without excessive toxicity, irritation, allergic response, or other complication commensurate with a reasonable benefit/risk ratio. Also included may be an agent that modifies the effect of other agents and is useful in preparing a therapeutic compound or composition that is generally safe, non-toxic, and neither biologically nor otherwise undesirable. Such an agent may be added to a therapeutic composition or pharmaceutical composition to modify for example the cellular target, cellular localization, or cellular uptake of an inorganic metal composition as described herein. Such an agent may include any

excipient, diluent, carrier, or adjuvant that is acceptable for pharmaceutical use. Such an agent may be non-naturally occurring, or may be naturally occurring, but not naturally found in combination with other agents in the therapeutic or pharmaceutical composition.

[0062] As used herein, a "therapeutic compound" or "therapeutic composition" refers to a composition comprising an inorganic ion composition of the present disclosure. In some embodiments, a therapeutic composition has the activity of inducing osteoblast differentiation or chondrocyte differentiation in a subject as described herein. Such a compound or composition is meant to encompass a composition suitable for administration to a subject, such as a mammal, particularly a human subject. In general, a therapeutic composition is sterile, and preferably free of contaminants that are capable of eliciting an undesirable response within the subject (e.g., the compound(s) in the composition are pharmaceutical grade). Therapeutic compositions may be designed for administration to subjects in need thereof via a number of different routes of administration including oral, intravenous, intraarticular, intraarterial, buccal, rectal, parenteral, intraperitoneal, intradermal, intratracheal, intramuscular, subcutaneous, inhalation, vaginal, intraosseous, trans nasal, injection, microneedle, topical, and transdermal. The appropriate dosage of a composition, as described herein, may be determined based on the type of disease to be treated, the severity and course of the disease, the clinical condition of the individual, clinical history, response to the treatment, and the discretion of the attending physician. In some embodiments, therapeutic compositions provided by the present disclosure may include various "unit doses." A unit dose is defined as containing a predetermined quantity of the therapeutic composition. The quantity to be administered, and the particular route and formulation, is within the skill of determination of those in the clinical arts. A unit dose need not be administered as a single injection but may comprise continuous infusion over a set period of time. In some aspects, a unit dose comprises a single administrable dose.

[0063] Precise amounts of the therapeutic composition also depend on the judgment of the practitioner and are peculiar to each individual. Factors affecting dose include physical and clinical state of the patient, the route of administration, the intended goal of treatment (alleviation of symptoms versus cure) and the potency, stability and toxicity of the particular therapeutic substance or other therapies a subject may be undergoing.

[0064] As used herein, "subject" or "patient" refers to animals, including humans, who are treated with the therapeutic compounds or compositions or in accordance with the methods described herein. For diagnostic or research applications, a wide variety of mammals may be

suitable subjects, including rodents (e.g., mice, rats, hamsters), rabbits, primates, and swine, such as inbred pigs and the like. In particular embodiments, a subject in need of therapy may be any subject is afflicted with or at risk of developing a disease or condition associated with altered osteoblast or chondrocyte growth, differentiation, or function. Non-limiting examples of such diseases or conditions include a fracture, a bone injury, rheumatoid arthritis, spondylarthritis, osteoarthritis, osteoporosis, bone infections (osteomyelitis), congenital bone disorders, tumor-related bone defects, age-related bone loss, metabolic bone diseases, a cartilage injury, costochondritis, intervertebral disc herniation, polychondritis, osteoarthritis, rheumatoid arthritis, traumatic joint injuries such as ACL tears, cartilage lesions and defects, hip labral tears, osteonecrosis, juvenile idiopathic arthritis, avascular necrosis, chondromalacia patellae, post-traumatic osteoarthritis, cartilage tumors, and achondroplasia-like conditions.

[0065] A composition, as described herein, may include, in particular embodiments, a combination of therapeutic agents. In some embodiments, a composition as described here may be administered as a single composition or as more than one composition. Different compositions as provided herein, in certain embodiments, may be administered by the same route of administration or by different routes of administration.

[0066] A pharmaceutical composition of the present disclosure may comprise, in certain embodiments, a) a silver ion composition or copper ion composition as described herein; and b) a second osteogenic or chondrogenic therapeutic agent. Any osteogenic or chondrogenic therapeutic agent known in the art may be used in a pharmaceutical composition of the present disclosure. An osteogenic or chondrogenic therapeutic agent used according to the present disclosure may be any osteogenic or chondrogenic therapeutic agent known in the art to increase or preserve osteoblast or chondrocyte differentiation, growth, or function.

[0067] A pharmaceutical composition of the present disclosure may comprise, in some embodiments, a targeting molecule. In one embodiment, the targeting molecule may be cell-specific or tissue-specific. The targeting molecule, in certain embodiments, may be stem cell or mesenchymal stem cell specific. Numerous such targeting molecules are known in the art and any such targeting molecule may be used according to the present disclosure. In certain embodiments, an inorganic ion composition of the present disclosure may be modified with or conjugated to a peptide, a protein, a colloidal molecule, or a polymer to facilitate delivery or adsorption. The pharmaceutical composition of the present disclosure, in some embodiments, may be serum-free, endotoxin-free, or sterile.

[0068] A peptide or polynucleotide molecule for use according to the compositions of the present disclosure may, in some embodiments, be a recombinant peptide or nucleic acid. As used herein, the term "recombinant" refers to a polynucleotide molecule, protein, or cell that is not naturally present, or is not naturally present in the same form or structure and was created by human intervention. In one embodiment, a recombinant polynucleotide may be a DNA molecule or may be an RNA molecule. A recombinant polynucleotide molecule or a recombinant polypeptide molecule or protein may comprise, in certain embodiments, a combination of two or more polynucleotide or polypeptide sequences that do not naturally occur together in the same manner, such as a polynucleotide molecule or protein that comprises at least two polynucleotide or protein sequences that are operably linked but heterologous with respect to each other. As used herein the term "heterologous" refers to a polynucleotide molecule or protein that is not naturally present or is not naturally present in the same form or structure and was created by human intervention. For example, a heterologous polynucleotide molecule or protein may not naturally occur in the cell being transformed or may be expressed in a manner or genomic context that differs from the natural expression pattern or genomic context found in the cell being transformed. The heterologous polynucleotide molecule or protein, in some embodiments, may be overexpressed in the cell being transformed. In certain embodiments, a recombinant polynucleotide molecule, protein, construct, or vector may comprise any combination of two or more polynucleotide or protein sequences in the same molecule which are heterologous to one another, such that the combination is man-made and not normally found in nature. As used herein, the phrase "not normally found in nature" means not found in nature without human intervention. A recombinant polynucleotide or protein molecule, may comprise, for example, polynucleotide or protein sequences that are separated from other polynucleotide or protein sequences that exist in proximity to each other in nature. A recombinant polynucleotide or protein molecule may also comprise, for example, polynucleotide or protein sequences that are adjacent to or contiguous with other polynucleotide or protein sequences that are not naturally in proximity with each other. Such a recombinant polynucleotide molecule, protein, or expression construct may also refer to a polynucleotide or protein molecule or sequence that has been genetically engineered or constructed outside of a cell. For example, a recombinant polynucleotide molecule may comprise any engineered or man-made plasmid, vector, or expression construct, and may include a linear or circular DNA molecule. Such plasmids, vectors, and expression constructs may comprise, for example, various maintenance elements including, but not limited to, a heterologous promoter sequence, a prokaryotic origin of replication, or a selectable marker.

[0069] In certain aspects, a therapeutic composition of the present disclosure may comprise an inorganic ion composition of the present disclosure and a therapeutic agent or a detectable label. Non-limiting example of therapeutic agents that may be used according to the present disclosure include an osteogenic therapeutic agent or a chondrogenic therapeutic agent. Non-limiting examples of detectable labels that may be used according to embodiments of the present disclosure include a paramagnetic ion, a radioactive isotope, a fluorochrome, an NMR-detectable agent, and an X-ray imaging agent.

[0070] In certain embodiments, the compositions, and methods for treating an individual described herein may be combined with any other composition or method of treatment known in the art. The compositions and methods may be administered in any suitable manner known in the art. For example, a first and a second osteogenic or chondrogenic treatment may be administered sequentially (at different times) or concurrently (at the same time). In some aspects, a first and a second osteogenic or chondrogenic treatment may be administered in separate compositions. In certain embodiments, a first and a second treatment may be administered in the same composition.

[0071] Non-limiting examples of additional treatment modalities that may be included in combination with the compositions and methods provided herein include a therapeutic agent or surgery. In specific embodiments, the methods and compositions of the present disclosure may be combined with other therapies directed towards increasing or preserving osteoblast or chondrocyte differentiation, growth, or function as described herein.

[0072] The term "about" is used to indicate that a value includes the standard deviation of the mean for the device or method being employed to determine the value. The use of the term "or" in the claims is used to mean "and/or" unless explicitly indicated to refer to alternatives only or the alternatives are mutually exclusive. When used in conjunction with the word "comprising" or other open language in the claims, the words "a" and "an" denote "one or more," unless specifically noted otherwise. The terms "comprise," "have," and "include" are open-ended linking verbs. Any forms or tenses of one or more of these verbs, such as "comprises," "comprising," "has," "having," "includes," and "including," are also open-ended. For example, any method that "comprises," "has," or "includes" one or more steps is not limited to possessing only those one or more steps and also covers other unlisted steps. Similarly, any system or method that "comprises," "has," or "includes" one or more components is not limited to possessing only those components and covers other unlisted components.

[0073] Other objects, features, and advantages of the present disclosure are apparent from detailed description provided herein. It should be understood, however, that the detailed description and any specific examples provided, while indicating specific embodiments of the disclosure, are given by way of illustration only, since various changes and modifications within the spirit and scope of the disclosure will become apparent to those skilled in the art from this detailed description. Any embodiment of the present disclosure may be used in combination with any other embodiment described herein.

[0074] All references herein are incorporated herein by reference in their entirety.

EXAMPLES

[0075] The following examples are included to illustrate embodiments of the present disclosure. It should be appreciated by those of skill in the art that the techniques disclosed in the examples that follow represent techniques discovered by the inventor to function well in the practice of the invention. However, those of skill in the art should, in light of the present disclosure, appreciate that many changes can be made in the specific embodiments which are disclosed and still obtain a like or similar result without departing from the concept, spirit and scope of the invention. More specifically, it will be apparent that certain agents which are both chemically and physiologically related may be substituted for the agents described herein while the same or similar results would be achieved. All such similar substitutes and modifications apparent to those skilled in the art are deemed to be within the spirit, scope and concept of the invention as defined by the appended claims.

Example 1: Cellular Responses to Inorganic Ions

[0076] To determine basic cellular responses to inorganic ions (silver, copper, platinum, tantalum, and titanium), the metabolic activity of hMSCs was assessed following exposure to escalating concentrations of these inorganic ions. Cell viability was quantified relative to a control group of untreated cells using the metabolic activity marker 3-(4,5-dimethylthiazol-2-yl)-2,5-diphenyltetrazolium (MTT). hMSCs were exposed to varying inorganic ion concentrations under standard culture conditions for a duration of 48 hours. The results demonstrated that cell viability was dependent on the concentration for each specific inorganic ion. The ion concentration that led to a 20% reduction in cell viability is denoted (FIG. 1A). For long-term functional studies, it was crucial to ensure cell survival. Therefore, a non-inhibitory concentration was calculated for each ion, defined as the concentration resulting in less than 10% inhibition of cell viability (IC_{10}). A visual assessment of cell viability was

performed using the LIVE/DEAD assay using calcein-AM (green) and ethidium homodimer-1 (red) (FIG. 1B). Cells were then exposed to the IC_{10} concentration for 72 hours. Using fluorescent imaging, cell viability was confirmed to exceed 90% when exposed to ion concentrations of ~IC_{10}.

[0077] Cytocompatibility was further assessed by examining cell cycle shifts, which included an increase in apoptotic behavior and accumulation in the G0/G1 phase. Flow cytometric analysis of DNA content showed minimal perturbation in the cell cycle due to exposure to inorganic ions over a 48-hour period, when compared to untreated hMSC populations. Overall, silver led to the most significant shift towards apoptosis (14.4%), copper induced a slight cell cycle arrest in the G0/G1 phase (88.1%), while tantalum and platinum resulted in an increased presence in the G2/M phase (7.75% and 8.08%, respectively) (FIG. 1C). For all subsequent cell studies, concentrated solutions of inorganic ions were prepared in deionized water at ten times the IC_{10} treatment concentration (FIG. 2). These concentrated solutions were introduced to the cultured hMSCs by addition of 10% of the working stock (v/v) to the complete culture medium where final ion concentrations were 29.95 μM silver, 26.66 μM copper, 1.48 μM platinum, 41.45 μM tantalum, and 10.44 μM titanium. The addition of ions to culture media does not alter pH conditions (FIG. 2).

Example 2: Inorganic Ions Drive Transcriptomic Changes in Stem Cell

[0078] To explore the impact of ions on the transcriptomic landscape, hMSCs were subjected to the IC_{10} concentration of ions (29.95 μM silver, 26.66 μM copper, 1.48 μM platinum, 41.45 μM tantalum, 10.44 μM titanium) for a period of 7 days. Subsequently, these cells were harvested and lysed to extract RNA (FIG. 3A). The RNA-seq data was aligned to the human genome (hg38) and processed. A principal component analysis (PCA) of the expression values of 50% most variable genes further illustrated the variance between technical replicates, thereby validating the extensive ion-dependent effects (FIG. 3B). A high degree of separation along PC1 (45.23% of variance) was observed between untreated hMSC populations and silver-treated groups. Moreover, copper-treated groups were distinctly clustered away from other conditions such as silver (along PC2, 17.16% of variance), platinum (along PC1), and untreated hMSCs. The most minor profile shift was observed in titanium-treated populations, verifying that titanium is inert and induces negligible transcriptomic changes.

[0079] Generalized linear models (GLMs) were subsequently utilized to determine the differentially expressed genes (DEGs) induced by each inorganic ion in comparison with the untreated control hMSCs. The effect of silver upregulated 1,257 and downregulated 957 genes, the effect of copper upregulated 1,310 and downregulated 1,323 genes, the effect of platinum upregulated 609 and downregulated 706 genes, the effect of tantalum upregulated 393 and downregulated 337 genes, and the effect of titanium upregulated 8 and downregulated 1 gene compared to untreated control hMSCs (Padjust < 0.05, FIG. 3C). Compared to conservative significance cutoff of 0.01, the Padjust < 0.05 threshold reveals a slight increase in the total differential gene expression (both upregulated and downregulated) triggered by the ions (FIG. 3D). Thus, a significance threshold of Padjust < 0.05 was applied for downstream analyses.

[0080] Hierarchical clustering of DEGs for replicates provides a comprehensive depiction of the ion-dependent shifts in the cell expression profile (FIG. 3E). Specifically, untreated hMSC replicates exhibit a unique profile compared to ion-treated populations, with the exception of titanium-treated cells. These data suggest that silver, copper, and platinum induce substantial transcriptomic shifts, drastically altering the gene signature of hMSCs. On the other hand, tantalum ion treatment results in minor shifts that appear closely related to platinum profile. Upon comparing conserved DEGs among each inorganic ion, it was found that silver and copper shared the highest number of genes (1,414), followed by copper and platinum (818). Less than 20 total DEGs were shared between any given ion and titanium, further supporting the notion that titanium acts as an inert material (FIG. 4A). Given these outcomes, cells treated with titanium were omitted from subsequent analyses.

[0081] To further assess the effects of inorganic ions, hypergeometric over-representation testing was conducted against the gene ontology (GO) database. Semantically sorted biological processes (BP) ($P < 0.01$) shared between ion treatment conditions reveal that terms relating to the developmental processes and morphogenesis were the most highly enriched, particularly by silver and copper (FIG. 4B). Trends in BPs related to cell motility, adhesion, extracellular matrix remodeling, epithelial cell development, and reproductive processes were observed.

[0082] Gene set enrichment analysis (GSEA) was also utilized to analyze shared trends in cellular component (CC) and molecular function (MF) processes within similarity networks (FIG. 5). Significant enrichment of ribosomal CCs by silver, copper, and platinum was initially observed (FIG. 5A), indicating the impact of inorganic ions on protein synthesis.

Platinum was unique in enriching CCs associated with the electron transport chain (ETC), mitochondrial complex, and vesicle and enzymatic complexes. In contrast, silver regulated cell cycle components including the mitotic spindle, spliceosomal complex, chromosomal region, and nuclear replication fork. These findings demonstrate that silver plays a role in cell division. In terms of molecular functions, platinum significantly enriched MFs related to energy metabolism from the mitochondria (FIG. 5B). Subsequent analyses were next conducted individually for each ion to better understand their unique effects on hMSCs.

Example 3: Silver Drives Osteogenic Differentiation via the MAPK and Wnt Signaling Pathways

[0083] Analysis of GO related to BP terms enriched by silver reveals a strong association with osteogenic differentiation in hMSCs (FIG. 6A). Specifically, the processes of Skeletal System Development (GO:0001501) (FIG. 6B), Ossification (GO:0001503) (FIG. 6C), Osteoblast Differentiation (GO:0001649), and Bone Mineralization (GO:0030282) were highly enriched. To investigate the factors driving silver-induced osteogenesis, DEGs associated with the most statistically significant terms were examined. It was found that Alkaline phosphatase 1 (*ALP1*), platelet-derived growth factor C (*PDGFC*), and mitogen-activated protein kinase 4 (*MAPK4*) play key roles in promoting osteogenesis following treatment with silver. Interestingly, an upregulation of SMAD family member 6 (*SMAD6*), a known negative regulator of BMP signaling, was also observed. This demonstrates that silver may stimulate osteogenesis via a non-traditional pathway. The upregulation of Leptin (*LEP*) further points to the potential involvement of p38 MAPK signaling in this process.

[0084] Functional validation of osteogenic differentiation was carried out through lineage-specific staining for osteogenic markers at 7, 14, and 21 days following silver treatment. Initially, hMSCs were cultured in a 2D monolayer in both normal and osteoconductive (OC) media. After a 7-day period, the production of alkaline phosphatase (ALP) was evaluated and compared to untreated hMSCs and those treated with dexamethasone, a known inducer of osteogenic differentiation. While ALP staining indicated a slight increase in activity in silver-treated cells, quantitative assessment suggested this change was not significant (FIG. 6D, FIG. 6E). As the differentiation process continued, transitioning the hMSCs to osteoblast lineage, calcium deposition in the extracellular matrix (ECM), become evident. After 14 and 21 days of silver treatment, a significant increase in ECM-bound calcium nodules was observed, particularly evident at the later time point (FIG. 6F). This further substantiates the role of silver in promoting osteogenic differentiation.

[0085] Recent research suggests that the osteogenic potential of cells can be better evaluated in 3D culture systems compared to traditional 2D monolayers. Therefore, a 3D spheroid model of hMSCs to provide a more rigorous validation of osteogenic differentiation induced by silver treatment was utilized. Following 10 and 21 days of treatment, histological assessment of ALP activity and matrix mineralization showed a high degree of osteogenic commitment in silver-treated spheroids. The observed osteogenic commitment in silver treated spheroids was visually comparable to the positive control group treated with dexamethasone, a known inducer of osteogenesis (FIG. 6G). In addition, the protein expression of osteopontin (OPN), an important biomarker of osteogenesis, was examined via Western blot analysis after 21 days of treatment. The results demonstrated a significant increase in OPN expression following silver treatment (4.53 ± 0.35-fold), when compared to untreated hMSCs (FIG. 6H). In summary, these findings demonstrate that silver treatment induces osteogenic differentiation in hMSCs. To understand the underlying mechanism by silver influences this process, the associated signaling pathways were further explored.

[0086] To uncover the osteogenic signaling pathways influenced by silver treatment, GO terms related to well-known osteogenic signaling mechanisms were compiled. These included Positive Regulation of MAPK Cascade (GO:0043410), Response to BMP (GO:0071772), and Regulation of Non-Canonical Wnt Signaling Pathway (GO:2000050), all of which are significantly enriched in silver-treated hMSCs (FIG. 7A, FIG. 7B, FIG. 7C). The roles of these pathways in driving osteogenesis were analyzed by examining DEGs conserved between these signaling terms and those associated with previously identified osteogenic differentiation terms (Skeletal System Development (GO:0001501) and Ossification (GO:0001503)). The intersection of these gene sets was visualized using an UpSet plot (FIG. 7D). Interestingly, while BMP signaling also highly overlapped with the osteogenic differentiation terms (17 conserved DEGs), the analysis revealed that silver upregulated BMP inhibitor genes and downregulated the classical BMP signaling mediator, BMP4. This demonstrates that BMP signaling may not be a primary driver of silver's osteogenic effect. Key DEGs found to regulate MAPK cascade and influence osteogenesis includes gremlin (*GREM1*), fibroblast growth factor 2 (*FGFR2*), and mitogen-activated protein kinase 3 (*MAP2K3*) (FIG. 7E). Notably, *GREM1* is also an antagonist of bone morphogenetic protein (BMP), further demonstrating that BMP signaling is attenuated following silver treatment to allow propagation of alternative signaling pathways.

[0087] Additionally, DEGs associated with MAPK signaling suggested that stress-mediated signaling is occurring. These DEGs include Wnt family member 5a (*WNT5A*), ROS proto-oncogene 1 (*ROS1*), peroxiredoxin 2 (*PRDX2*), receptor tyrosine kinase-like orphan receptor 1 (*ROR1*), and tumor necrosis factor associated factor 5 (*TRAF5*). Further GO analysis and exploration of enriched terms from the Hallmark GSEA database revealed that silver promotes ROS Metabolic Process and Hypoxia (FIG. 8A, FIG. 8B), suggesting that silver promotes the generation of reactive oxygen species (FIG. 8C), leading to stress signaling through the MAPK and Wnt pathways. To test this pathway inhibition studies were preformed using known attenuators of each potential cascade. Examination of RUNX2 protein production after 7 days of silver treatment with and without each pathway inhibitor, revealed that both MAPK and Wnt signaling pathways are triggered by silver treatment (FIG. 7F). These findings demonstrate a mechanism illustrating the interplay between ROS generation, Wnt signaling, and MAPK cascade in promoting osteogenic differentiation (FIG. 7G, FIG. 9). All components of the proposed pathway represent DEGs regulated by silver treatment, and the connections were validated using Cytoscape GeneMania and literature.

Example 4: Copper Promotes Chondrogenic Differentiation in hMSCs

[0088] RNA-seq data demonstrate that hMSCs treated with copper undergo chondrogenic differentiation. GO terms significantly ($P < 0.05$) enriched due to treatment with copper include Cartilage Development (GO:0051216) and Glycosaminoglycan Biosynthetic Process (GO:0006024) (FIG. 10A, FIG. 10B). Compared to untreated hMSCs, copper induces differential regulation of nearly 100 genes associated with chondrogenic differentiation, as demonstrated by heatmap hierarchical clustering (FIG. 10C). Particularly, the upregulated DEGs contributing to chondrogenesis include aggrecan (*ACAN*), cartilage oligomeric matrix protein (*COMP*), and transforming growth factor beta 1 (*TGFB1*) (FIG. 10D), all of which are well-recognized markers of differentiating chondrocytes. Intriguingly, the expression of marker matrix metalloproteinase 13 (*MMP13*), a known marker of cartilage degradation, decreases in response to copper treatment (FIG. 11A). While MMP13 is a natural catabolic factor in healthy joints, its overexpression is linked to pathological cartilage degeneration, including osteoarthritis (OA). During OA progression, chondrocytes exhibit increased superoxide production which leads to impaired mitochondrial function, activation of inflammatory cytokines and MMPs, and cell death. Notably, copper treatment suppresses superoxide generation in hMSCs (FIG. 11B). These findings demonstrate that copper is a

promising material not only for supporting cartilage regeneration but also for combating degeneration in pathological conditions such as OA.

[0089] To substantiate the enduring commitment to the chondrocyte phenotype resulting from copper treatment, protein levels were analyzed after 7 and 21 days. Western blotting confirmed that the key chondrogenic genes identified in the RNA-seq were functionally translated, leading to increased expression of ACAN and COMP after 7 and 21 days, respectively (FIG. 10E, FIG. 10F). The production of key ECM components by mature chondrocytes such as glycosaminoglycans (GAGs), were assessed using histochemical staining in 2D and 3D microenvironment. The detection of significant levels of Safranin O and Alcian Blue staining in hMSCs treated with copper for 21 days confirms the presence of chondro-specific ECM similar to positive controls (cells treated with chondro-inductive TGFβ) (FIG. 10G, FIG. 10H, FIG. 12A). Additionally, ALP activity significantly decreases after 7 days of copper treatment (FIG. 12B, FIG. 12C), indicative of inhibited osteogenic differentiation and loss of hMSC pluripotency as copper fosters commitment towards chondrogenic lineage. These data collectively demonstrate the capacity of copper to induce chondrogenic differentiation in hMSCs.

[0090] The biochemical signaling mechanism underpinning the chondrogenic effects of copper were explored. A manual compilation of GO terms from the list of significantly enriched biological processes ($P < 0.05$) revealed activation of several key signaling pathways in response to copper (FIG. 10I, FIG. 10J). Two major GO terms, Transforming Growth Factor Beta Receptor Signaling (GO:0007179) and Response to Transforming Growth Factor Beta (GO:0071559), are notably influenced. The key DEGs contributing to TGFβ-mediated chondrogenesis by copper include Cbp/P300 interacting transactivator with Glu/Asp rich carboxy-terminal domain 2 (*CITED2*) and Cellular communication network factor 2 (*CCN2*). These genes play crucial roles in propagating the TGFβ cascade via the SMAD/p300/Cbp activator complex and promoting chondrocyte differentiation and growth, respectively. Also, Integrin Mediated Signaling Pathway (GO:0007229) was significantly enriched. This pathway is particularly important as integrin-mediated surface interactions foster necessary cell-ECM connections during condensation. The RNA-seq data further supports the interplay between TGFβ receptor pathway and integrins (FIG. 13). TGFβ signaling, widely known to promote chondrogenesis through the stimulation of the Notch and Fibroblast Growth Factor (FGF) pathways, is increased by copper treatment. Copper's effect also involves downregulating GLI3, a repressor of Notch-Shh signaling, demonstrating its role in promoting

chondrogenesis by suppressing pathway inhibitors. Moreover, the copper treatment induces an upregulation of FERM domain containing kindlin 2 (*FERMT2*), which facilitates phosphatidylinositol-3,4,5-triphosphate (PIP3) and TGFβ binding activity and in turn supports chondrocyte differentiation. In summary, the data demonstrate the biochemical role of copper in stimulating TGFβ signaling, thereby guiding hMSCs toward chondrogenic lineage commitment (FIG. 14).

Example 5: Copper Enhances hMSC Pro-Regenerative Immune Modulation

[0091] During pathway analysis following copper treatment, RNA-seq data also pointed to immunomodulatory activity. It is well documented that hMSCs possess immunomodulatory characteristics (FIG. 15A). Interestingly, RNA-seq data demonstrate that copper controls numerous immune-related processes in hMSCs, including T Cell Activation (GO:0030217), Immune System Process (GO:0002376), Regulation of Leukocyte Activation (GO:0043122), B Cell Activation (GO:0042113), and Regulation of I-kappaβ Kinase/NF-kappaβ Signaling (GO:0043123) (FIG. 15B). Numerous relevant DEGs contributing to these enriched terms have been identified, including several genes encoding for interferon molecules (*IF130*, *IF135*, *IF144*), interleukins (*IL1B*, *IL6ST*, *IL7*), and tumor necrosis factors (*TNFRSF1B*, *TNFSF13B*, *TNFSF9*) (FIG. 15B, FIG. 16B). All of these are significantly ($P < 0.05$) downregulated in response to copper treatment. Additionally, evaluation using the GSEA against the curated *Hallmark* MSigDB database reveals significant (false discovery rate (FDR) < 0.05) negative enrichment of terms including Interferon Alpha Response, IL6 JAK STAT3 Signaling, Interferon Gamma Response, Inflammatory Response, and Apoptosis (FIG. 16A). Gene validation via qRT-PCR shows that as early as 3 days after copper treatment, hMSCs downregulate inflammatory immune markers including *IL1B*, *IL7*, *IRF1*, and *STAT2*. Similarly, both *JAK2* and *STAT2* are downregulated after 7 days (FIG. 16C, FIG. 15C). These findings demonstrate that copper promotes immunosuppressive activity by activating several key immune signaling pathways.

[0092] To validate the immunomodulatory effect of copper, hMSCs treated with and without copper, were co-cultured with THP-1 macrophages. Cytokines secreted by the cells were extracted at 24, 48, and 72 hours. Compared to M1 macrophages, which were pharmacologically induced to the inflammatory phenotype using LPS and IFNγ, the hMSCs treated with copper significantly reduced IL1β production (3.81±0.89 pg/mL, $P < 0.0001$, 24 hours). After 72 hours, IL1β activity decreased even further to 2.72±0.36 ($P < 0.0001$), demonstrating a sustained anti-inflammatory macrophage phenotype due to exposure to

copper (FIG. 16D). Indirect ELISA was also performed to determine the relative expression of M2 marker (IL10) (FIG. 16E). While hMSCs alone were not effective in stimulating IL10 activity, the introduction of copper resulted in IL10 expression on par with the M2 control population. This provides confirmation that copper treatment drives macrophage polarization toward M2 phenotype.

Example 6: Platinum Regulates hMSC Energy Metabolism via Pathological Oxidative Phosphorylation

[0093] Another important property of hMSCs is their metabolic plasticity. Platinum, a core component of chemotherapeutics such as cisplatin ($Pt(NH_3)_2Cl_2$), carboplatin ($Pt(C_6H_6O_4)(NH_3)_2$), and oxaliplatin ($PtC_8H_{14}N_2O_4$), is known to act through altering energy metabolism in cancer cells. These responses have mainly been studied in the context of cancer biology, while the behavior of hMSCs is less well understood. Following 7 days of treatment with platinum, a significant perturbation in energy metabolism was identified in hMSCs. Specifically, analysis of GO biological processes identify Oxidative Phosphorylation (GO:006119), Respiratory Electron Transport Chain (GO:0022904), and Mitochondrial Electron Transport Ubiquinol to Cytochrome C (GO:006122), among others involved in ATP production, being significantly (FDR < 0.05) affected by platinum treatment (FIG. 17A).

[0094] To further investigate the metabolic pathways influenced by platinum, GSEA against *Hallmark* and *Reactome* databases was utilized. Consistent with our GO analysis, *Hallmark* Oxidative Phosphorylation and Fatty Acid Metabolism were significantly enriched ($P < 0.05$), demonstrating the role of platinum in modulating cellular processes for fatty acid degradation (FIG. 17B). Analysis of *Reactome* database further affirmed the enrichment of Citric Acid TCA Cycle and Respiratory Electron Transport. Collectively, these results demonstrate platinum disrupts hMSC energy production by regulating genes associated with the mitochondrial electron transport chain.

[0095] The genes differentially regulated by platinum that mediate metabolic changes were investigated further. Platinum treatment led to the upregulation of genes across all components of the electron transport chain (FIG. 18). Key genes such as cytochrome C1 (*CYC1*) and its enzymatic co-factor, cytochrome C oxidase subunit 6A1 (*COX6A1*), were upregulated, facilitating oxidative phosphorylation and electron transport in the mitochondrial ETC. Interestingly, genes linked with mitochondrial membrane uncoupling, including voltage dependent anion channel 2 (*VDAC2*) and solute carrier family 25 member 4 (*SLC25A4*), were

similarly upregulated (FIG. 17C). *VDAC2* regulates the mitochondrial apoptosis pathway via the activation of B-cell lymphoma 2 (BCL-2) proteins BCL2 and BAX, while SLC25A4 engages in mitophagy through interaction with membrane transporter enzymes. Lastly, an upregulation of enoyl-CoA isomerase 1 (*ECI1*), an enzyme involved in unsaturated fatty acid beta-oxidation within the canonical Wnt/beta-catenin pathway, and of 6-pyruvoyltetrahydropterin synthase (*PTS*)(46, 47), a biosynthesis cofactor, was observed in response to platinum. The modulation of these genes provides insight into platinum's effect on cellular metabolism.

[0096] The RNA-seq data suggests that platinum treatment may disrupt mitochondrial function, a hypothesis supported by previous studies linking platinating agents with endoplasmic reticulum stress, cytosolic calcium accumulation, mitochondrial membrane potential loss, and DNA damage. This idea of calcium perturbation by platinum is bolstered by the significant enrichment of GO terms such as Positive Regulation of Cytosolic Calcium Ion Concentration (GO:0007204) and Response to Calcium Ion (GO:0051592) (FIG. 19). To evaluate the effect of platinum on mitochondrial biogenesis and energy production, mitochondrial copy number was assessed via qRT-PCR, which revealed a significant decrease in mitochondrial count in platinum-treated hMSCs after 3 days (FIG. 17D). This finding suggests compromised mitochondrial replication efficiency. Furthermore, MitoView™ Green, a fluorescent dye that targets the inner mitochondrial membrane, was employed to visualize mitochondrial mass. Fluorescent tracking over 7 days demonstrated platinum-induced mitochondrial morphological changes, evidenced by dye aggregation indicative of swelling (FIG. 17E). Quantifying the green fluorescent intensity confirmed a significant decrease in mitochondrial mass in platinum-treated cells. Collectively, these data demonstrate that platinum treatment impairs mitochondrial function in hMSCs (FIG. 17F).

[0097] Mitochondrial dysfunction can lead to decreased bioenergetic efficiency by affecting the respiratory transport chain (RTC), the primary cellular energy production method located across the mitochondria's double membrane. To understand the effect of platinum-induced dysfunction on RTC, mitochondrial membrane polarization changes were assessed following platinum treatment using a JC-1 assay. JC-1 (Tetraethylbenzimidazolylcarbocyanine iodide), a cationic dye, measures mitochondrial membrane potential by shifting its color from green monomer (emission ~530 nm) to red aggregate (emission ~590 nm). Therefore, analyzing the ratio of accumulated to monomeric dye provides insight into the treatment-induced shifts towards depolarization or hyperpolarization in the mitochondria. In mitochondria under acute

oxidative stress, a shift towards membrane depolarization is expected. For instance, when treated with the positive control carbonyl cyanide 3-chlorophenylhydrazone (CCCP), a membrane potential disrupter, significantly lower red:green fluorescence is observed compared to untreated hMSCs. This analysis showed that platinum treatment resulted in mitochondrial membrane depolarization, demonstrating that this ion interferes with the energy metabolism in hMSCs by affecting electron transport chain function (FIG. 17G, FIG. 17H). These findings demonstrate that platinum-induced endoplasmic reticulum stress and subsequent mitochondrial DNA damage lead to mitochondrial membrane depolarization and hMSC apoptosis (FIG. 17I)

Example 7: Materials and Methods

[0098] Materials: Ion solutions of silver acetate (Ag), copper (II) nitrate (Cu), platinum (IV) chloride (Pt), tantalum (V) chloride (Ta), and titanium (IV) iodide (Ti) were purchased from VWR, prepared in DI water, and sterilized via 0.2 μm filtration for cell studies. All chemicals were directly used without further purification. hMSCs (ATCC, passage < 5) were cultured in MEM-α modification media completed with 16.5% fetal bovine serum (FBS, Atlanta Biologics) and 1% penicillin-streptomycin (P/S), referred throughout as normal media.

[0099] Cytocompatibility: Cell viability was determined using standard MTT assay protocol (Zhong ZY, *et al. BIOACTIVE MATERIALS* 10:195-206 (2022)). Briefly, hMSCs were seeded at 10^4 cells/mL in 96-well tissue culture plates. After 12 hours, cells were treated with inorganic ion solutions (1:10 working stock) in normal media for final concentrations ranging from 0 to 1000 μg/mL (n = 4, with respect to total compound mass) and incubated for 48 hours. Media was removed and cells washed twice with phosphate buffered saline (PBS, VWR). Then, 5 μg/mL 3-(4,5-Dimethylthiazol-2-yl)-2,5-Diphenyltetrazolium Bromide (MTT) (Thermo Fisher Scientific) in media was added and incubated for an additional 3 hours. MTT was removed and dimethyl sulfoxide (DMSO, The Lab Depot, Inc.) added for 20 minutes. The absorbance was read on an Infinite 200pro Microplate Reader (Tecan) at 565 nm. The inhibitory concentration for 90% viability (IC_{10}) was determined from the resulting viability plot and reported with respect to target ion molar mass (μM).

[00100] Cell cycle: To evaluate the impact of inorganic ions on cell cycle, flow cytometric analysis was used to quantitate DNA content with propidium iodide (PI) staining. After 10-12 hours serum starvation to induce cycle synchronization, cells were treated with ion solutions for 48 hours. Cells were fixed and permeabilized via drop-wise ethanol addition during vortex,

then treated with a combination of PI and ribonuclease, to prepare for single parameter DNA analysis.

[00101] Reactive oxygen species generation: To monitor intracellular reactive oxygen species (ROS) superoxide generation, cells at 70% confluency were pre-treated with dihydroethidium (DHE, 25 μM) for 10 minutes and subsequently incubated with ion solutions (IC_{10}) or hydrogen peroxide (H_2O_2, 10 μM) in phenol red-free basal medium for 2 hours at 37°C. Fluorescence imaging was obtained using a Zeiss Axio Vert.A1 fluorescent microscope.

[00102] Stem cells differentiation assays: hMSCs were seeded at $2x10^4$ cells/mL in 24-well plates. For osteogenic studies, cells were cultured in both normal and osteoconductive (OC) media (complete MEM-α supplemented with 10 mM β-glycerophosphate (Sigma), 50 μM ascorbic acid (VWR)). Osteoinductive (OI) media (OC media supplemented with 100 nM dexamethasone (Sigma)) was used for positive control samples. For chondrogenic studies, cells were cultured in chondroconductive (CC) media (DMEM supplemented with 1% insulin transferrin sodium selenite, 10^{-7} M dexamethasone, 1 mM sodium pyruvate), and chondroinductive (CI) media (CC supplemented with 10 ng/mL TGF β-1) for positive control samples. For ALP staining, hMSCs were cultured in normal media with and without inorganic ions (IC_{10}) for Day 7. At time point, media was removed, and cells were fixed with 2.5% glutaraldehyde (VWR) for 20 minutes. Cells were washed once with PBS and ALP (Thermo Fisher Scientific) stain was added for 6 hours. Stain was removed and cells washed twice with DI water. ALP quantification was performed using 1-step *p*-nitrophenyl phosphate (pNPP) assay (Thermo Fisher), corrected by DNA content. For matrix mineralization assessment, hMSCs were cultured in OC media with and without ions for Day 14 and 21. At time points, cells were fixed and washed as previously described, and Alizarin Red S (ARS, pH 4.2) (Sigma) stain was added for 5 min. ARS was removed and cells washed twice with DI water. ARS stain was dissolved and quantified with spectrophotometry. For glycosaminoglycan evaluation, cells cultured in CC and CI media for Day 21 were fixed as previously described and washed with PBS. Briefly, fixed cells were rinsed with 1% acetic acid, then stained with Safranin O and Alcian Blue for 5 minutes. Stains were dissolved overnight with 10% acetic acid and quantified by spectrophotometry. Bright field images of hMSCs following staining were collected using a Zeiss microscope.

[00103] RNA extraction: hMSCs were cultured in T-75 tissue culture flasks (Corning) with and without inorganic ions (IC_{10}) until Day 7, 14, and 21. At time points, media was removed, and cells were washed with PBS and gently scraped for collection. Cell pellets were obtained

via centrifugation at 1,000 rpm for 5 minutes, then placed on ice. Total RNA was extracted according to Quick-RNA™ MiniPrep kit (Zymo Research) following cell lysis. RNA quality was determined by spectrophotometry absorbance readings between 280/260 nm, with acceptable samples yielding a ratio of 2.0. Samples were stored at -80°C until further use.

[00104] DNA extraction: hMSCs were cultured in 6-well tissue culture treated polystyrene dishes with and without Pt ion until Day 3. At time point, media was removed, and cells were washed with PBS and gently scraped for collection. Cell pellets were obtained via centrifugation at 1,000 rpm for 5 minutes, then placed on ice. Total DNA was extracted according to Quick-DNA Miniprep Kit (Zymo Research). DNA quality was determined by spectrophotometry absorbance readings between 280/260 nm, with acceptable samples yielding a ratio of 2.0. Samples were stored at -80°C until further use.

[00105] Whole transcriptome sequencing: Extracted Day 7 RNA samples were sequenced on the Illumina NovaSeq 6000 platform to provide 20-30 million reads per sample of 75 paired ends. Following sequencing, the reads underwent trimming and alignment to the human genome (hg38, GRCh37 Genome Reference Consortium Human Reference 37, obtained from University of California, Santa Cruz (Kent WJ, *et al. Genome research* 12(6):996-1006 (2002)) using the R-Bioconductor (Gentleman RC, *et al. Genome biology* 5(10):1-16 (2004)) package Spliced Transcripts Aligned to a Reference (STAR) (Dobin A, *et al. Bioinformatics* 29(1):15-21 (2013)). mRNA levels of hMSCs treated with each inorganic ion (Ag, Cu, Pt, Ta, and Ti) were compared to untreated hMSCs sample group to determine ion-induced differential gene expression (DEG). For untreated negative control hMSC sample group, 67,075,620 (59,739,563 uniquely mapped), 63,266,001 (58,425,331 uniquely mapped) reads were aligned to the genome for the two replicates. For the Ag ion sample group, 42,402,909 (37,676,502 uniquely mapped), 44,354,751 (40,834,843 uniquely mapped), 68,174,829 (63,874,158 uniquely mapped) reads were aligned to the genome for the three replicates. For the Cu ion sample group, 61,158,998 (56,238,338 uniquely mapped), 55850674 (51,179,202 uniquely mapped), 43,025,166 (39,131,823 uniquely mapped) reads were aligned to the genome for the three replicates. For the Pt ion sample group, 53,224,055 (47,895,246 uniquely mapped), 47,770,626 (43,621,898 uniquely mapped) reads were aligned to the genome for the two replicates. For the Ta ion sample group, 47,610,853 (45,339,821 uniquely mapped), 61,312,473 (58,061,992 uniquely mapped), 65,713,599 (62,011,963 uniquely mapped) reads were aligned to the genome for the three replicates. For the Ti ion sample group, 57,006,741

(52,529,077 uniquely mapped), 52,876,986 (48,698,294 uniquely mapped) reads were aligned to the genome for the two replicates.

[00106] In further analysis, only uniquely mapped reads were used. RefSeq gene models were retrieved from UCSC using Bioconductor package GenomicFeatures and expression was quantified to read counts using the uniquely mapped reads of the coding exons, normalized by gene length using reads per kilobase of transcript per million mapped reads (RPKM) factor. Minimal to no expression genes were removed with RPKM less than 1. Genes with RPKM greater than 1 in at least half (0.5) of replicates for each condition were considered expressed. Bioconductor package DESeq2 was used to model genes expressed in distinct conditions using negative binomial distribution with subsequent statistical thresholding of P value < 0.05 (Benjamini-Hochberg false discovery rate (FDR) adjust) used for downstream analysis. High dimensional clustering (HDC) was performed using Log2-adjusted RPKM. The Bioconductor package Gvis was used to generate gene tracks.

[00107] Statistically significant DEGs were used to calculate functional annotation enrichment of gene ontology (GO) terms belonging to Biological Processes (BP), Cellular Components (CC), and Molecular Functions (MF) ontologies using Bioconductor package GoStats conditional hyperGTest of overrepresentation. Gene set enrichment analysis (GSEA) was performed using the GSEA java desktop application against the current Molecular Signatures Database (v7.4 MSigDB). DEGs rank lists were constructed according to the following function: Rank = -Log10(Pvalue)*sign(FoldChange). Ranked lists were uploaded to the GSEA desktop application and used in performing GSEAPreranked analysis where test parameters were default against the Chip platform "Human_ENSEMBL_Gene_ID_MSigDB.v7.5.chip" as described in Subramanian A, *et al. Proceedings of the National Academy of Sciences* 102(43):15545-15550 (2005). Probed databases included current releases of curated Hallmarks (h.all.v7.5.symbols.gmt), Reactome (c2.cp.reactome.v7.5.symbols.gmt), Wikipathways (c2.cp.wikipathways.v7.5.symbols.gmt), and GO (c5.all.v7.5.symbols.gmt). Enriched GSEA terms are represented using Log10 transformation of FDR-adjusted P value (i.e., Q value) and normalized enrichment score (NES). DEGs comprising the leading edge of an enriched term (i.e., core enrichments) were selected for further analysis. Organization and network visualization of enriched GO and GSEA terms was performed using available online software including Cytoscape (version 3.8.0). Gene set networks were generated using significant DEGs contributing to enrichment of GO processes and GSEA clusters. Edges were

generated using the GeneMANIA plugin. GOplot package was used to generate GOBubble and GOCircle plots. Z-scoring was calculated as:

$$Z - score = \frac{(Up - Down)}{\sqrt{Count}},$$

where *Up* and *Down* correspond to the number of DEGs (*P*adjust < 0.05) belonging to a GO term that were upregulated and downregulated, and *Count* was the total number of DEGs (*P*adjust < 0.05).

[00108] Gene expression analysis: Extracted RNA from Day 7, 14, and 21 was used to prepare cDNA was synthesized from 1 µg of RNA using qScript® cDNA Synthesis Kit (Quantabio), following manufacturer's protocol. Amplification of primers was initiated with SYBR Green reagent (BioRad). Expression fold change was determined from output cycle threshold data referencing normal media control and GAPDH housekeeping amplification. qRT-PCR (Applied Biosciences) was performed accordingly: Total 40 cycles passed through Hold (2 minutes 50 °C, 10 minutes 95 °C), PCR (15 seconds 95 °C, 1 minute 60 °C), and Melt Curve (15 seconds 95 °C, 1 minute 60 °C, 15 seconds 95 °C) stages. Total volume per well was 20 µL. The following primers (Invitrogen) were used:

[00109] *ALP:* (F) ACCATTCCCACGTCTTCACATTT (SEQ ID NO:1),

[00110] (R) AGACATTCTGTTCACCGCC (SEQ ID NO:2);

[00111] *OCN:* (F) ATGAGAGCCCTCACACTCCTCG (SEQ ID NO:3),

[00112] (R) GTCAGCCAACTCGTCACAGTCC (SEQ ID NO:4);

[00113] *OPN:* (F) CTAGGCATCACCTGTGCCATACC (SEQ ID NO:5),

[00114] (R) CTACTTAGACTACTTGACCAGTGAC (SEQ ID NO:6);

[00115] *IBSP*: (F) CAATCCAGCTTCCCAAGAAG (SEQ ID NO:7),

[00116] (R) CTTCTGCTTCGCTTTCTTCG (SEQ ID NO:8);

[00117] *Runx2:* (F) AGATGATGACACTGCCACCTCTG (SEQ ID NO:9),

[00118] (R) GGGATGAAATGCTTGGGAACT (SEQ ID NO:10);

[00119] *Col1a1:* (F) GATTCCCTGGACCTAAAGGTGC (SEQ ID NO:11),

[00120] (R) AGCCTCTCCATCTTTGCCAGCA (SEQ ID NO:12);

[00121] *TNFα:* (F) CTCTTCTGCCTGVTGCACTTTG (SEQ ID NO:13),

[00122] (R) ATGGGCTACAGGCTTGTCACTC (SEQ ID NO:14)

[00123] *IL6:* (F) AGACAGCCACTCACCTCTTCAG (SEQ ID NO:15),

[00124] (R) TTCTGCCAGTGCCTCTTTGCTG (SEQ ID NO:16);

[00125] *MEK1:* (F) GGTGTTCAAGGTCTCCCACAAG (SEQ ID NO:17),

[00126] (R) CCACGATGTACGGAGAGTTGCA (SEQ ID NO:18);

[00127] *ERK1:* (F) TGGCAAGCACTACCTGGATCAG (SEQ ID NO:19),

[00128] (R) GCAGAGACTGTAGGTAGTTTCGG (SEQ ID NO:20);

[00129] *Sox9:* (F) AGGAAGCTCGCGGACCAGTAC (SEQ ID NO:21),

[00130] (R) GGTGGTCCTTCTTGTGCTGCAC (SEQ ID NO:22);

[00131] *ACAN:* (F) CTACACGCTACACCCTCGAC (SEQ ID NO:23),

[00132] (R) ACGTCCTCACACCAGGAAAC (SEQ ID NO:24);

[00133] *GAPDH:* (F) CTATAAATTGAGCCCGCAGC (SEQ ID NO:25),

[00134] (R) GACCAAATCCGTTGACTCCG (SEQ ID NO:26).

[00135] Extracted total DNA for each condition was aliquoted for final concentration of 1 µg per reaction and used in amplification of mitochondrial gene Nidogen 2 (mtND2) using SYBR Green reagent (BioRad). Expression fold change was determined from output cycle threshold data referencing normal media control and *GAPDH* housekeeping amplification. qRT-PCR was performed as described above with human MT-ND2 primer (Hs02596874_g1, Invitrogen).

[00136] Macrophage polarization: Human monocytic THP-1 cells were cultured in Roswell Park Memorial Institute (RPMI) medium supplemented with 10% heat-inactivated FBS and 1% P/S. THP-1 cells were differentiated to M0 macrophages via 72-hour incubation with 100 nM phorbol 12-myristate 13-acetate (PMA). For M1 polarization, M0 cells were incubated with 10 pg/mL lipopolysaccharide (LPS) and 20 ng/mL IFNγ for 24 hours. For M2 polarization, M0 cells were incubated with 20 ng/mL of interleukin 4 (IL4) and 20 ng/mL interleukin 13 (IL13) for 72 hours. Cell culture medium was sampled from M0, M1, and M2 populations following differentiation, centrifuged at 14,000 RPI for 5 minutes to pellet debris, and stored at -80°C until further use.

[00137] Co-culture design: Tissue culture treated polystyrene 6-well plates with transwell inserts (0.4 µm pores, Corning) were used to culture hMSCs (TCPS) and M0 macrophages (transwell). Briefly, THP-1 monocytes were suspended in supplemented RPMI media in sterile inserts and differentiated to M0 macrophages as described above. After differentiation was complete, RPMI was replaced with normal hMSC growth media and inserts were transferred to 6-well plate with cultured hMSCs. To test macrophage polarization in response to inorganic ion treatment, hMSCs were treated with and without Cu ion and cell culture medium was sampled from transwell inserts at 24, 48, and 72 hours. After 72 hours, intracellular proteins were extracted from macrophages via RIPA buffer extraction. Samples were stored at -80°C until further use.

[00138] Protein quantification: Cytokine secretion was assayed using a direct ELISA kit (Human IL1β, Invitrogen) according to manufacturer's instructions. Indirect ELISA was performed in Nunc MaxiSorp™ flat-bottom plates where 20 μg/mL total protein was loaded per well and allowed to attach during overnight incubation at 4 °C. After washing, primary antibody IL10 (1:500, #PA5-85660, Invitrogen) or GAPDH (1:1000, #X2412P, Invitrogen) was applied. Following primary antibody overnight incubation at 4 °C, H&L-conjugated goat anti-rabbit polyclonal secondary antibody was applied to each well and incubated at room temperature for 2 hours. 1-Step TMB ELISA substrate (Invitrogen) was then applied for 25 minutes for HRP detection, followed by reaction quenching with 0.16 M sulfuric acid. Absorbance was measured via spectrophotometer at 450 nm immediately after quenching.

[00139] Mitochondria function: After 7 days of culture with Pt, hMSCs were stained for 15 minutes with MitoView™ Green, counterstained with DAPI nuclear stain for 5 minutes, then imaged on a Zeiss Axio Vert.A1 fluorescent microscope. Fluorescent intensity was quantified, and data were normalized to nuclear content to yield relative mitochondria content between hMSCs and Pt-treated hMSCs. To investigate mitochondria membrane polarization, 2D seeded hMSCs cultured for 48 hours with Pt ion were washed briefly with PBS, then incubated for 30 minutes with JC-1 dye. Cells were washed again and counterstained with DAPI nuclear stain as previously described. The ratio of red:green fluorescence was determined using a plate reader (green: excitation 475 nm emission 530 nm, red: excitation 525 nm emission 590 nm), where mean red and green fluorescent intensities were normalized to DAPI content.

[00140] Data analysis and statistics: All quantitative data were analyzed via GraphPad Prism software. Sample sizes were maintained at n = 3 technical replicates for each assay and transcriptomic analysis. Student t-test and ANOVA were used to compare samples and determine significance, where $P < 0.05$ was used as threshold for significant difference.

* * *

[00141] All of the methods disclosed and claimed herein can be made and executed without undue experimentation in light of the present disclosure. While the compositions and methods of this invention have been described in terms of preferred embodiments or aspects, it will be apparent to those of skill in the art that variations may be applied to the methods and in the steps or in the sequence of steps of the method described herein without departing from the concept, spirit, and scope of the invention. More specifically, it will be apparent that certain agents which are both chemically and physiologically related may be substituted for the agents

described herein while the same or similar results would be achieved. All such similar substitutes and modifications apparent to those skilled in the art are deemed to be within the spirit, scope and concept of the invention as defined by the appended claims.

CLAIMS

What is claimed is:

1. A method of inducing osteoblast differentiation of a stem cell in a subject in need thereof, the method comprising administering to the subject an effective amount of a silver ion composition to induce osteoblast differentiation.

2. The method of claim 1, wherein the silver ion composition is defined as a silver salt composition.

3. The method of claim 2, wherein the silver salt composition comprises a silver salt selected from the group consisting of silver acetate, silver nitrate, silver chloride, silver bromide, silver iodide, silver fluoride, silver sulfide, silver phosphate, silver chromate, and silver sulfate.

4. The method of claim 2, wherein the silver salt composition is defined as an aqueous solution comprising the silver salt.

5. The method of claim 1, wherein the silver ion composition is defined as a silver biomaterial composition.

6. The method of claim 5, wherein the silver biomaterial composition is defined as a silver nanoparticle composition, a silver microparticle composition, a silver hydrogel composition, a silver microgel composition, a silver nanofiber composition, a silver microfiber composition, a silver polymer composition, a silver biomaterial coating, a silver depot, or a silver microneedle composition.

7. The method of claim 1, wherein the effective amount of silver ions in the silver ion composition is a concentration sufficient to produce a local effective concentration of about 0.1 μM to about 100 μM or about 0.1 μM to about 29.95 μM.

8. The method of claim 1, wherein the silver ion composition further comprises a targeting molecule.

9. The method of claim 1, wherein the stem cell is a mesenchymal stem cell.

10. The method of claim 1, wherein the subject is afflicted with or at risk of developing a disease or condition associated with altered osteoblast growth, differentiation, or function.

11. The method of claim 1, wherein the subject is afflicted with or at risk of developing a disease or condition selected from the group consisting of: a fracture, a bone injury, rheumatoid arthritis, spondylarthritis, osteoarthritis, osteoporosis, a bone infection (osteomyelitis), a congenital bone disorder, a tumor-related bone defect, age-related bone loss, and a metabolic bone disease.

12. The method of claim 1, wherein said administering comprises injection, microneedle administration, oral administration, buccal administration, vaginal administration, inhalation, intraosseous administration, trans nasal application, topical administration, transdermal application, or rectal administration.

13. The method of claim 1, the method comprising administering a pharmaceutical composition comprising the effective amount of the silver ion composition to the subject.

14. A method of inducing chondrocyte differentiation of a stem cell in a subject in need thereof, the method comprising administering to the subject an effective amount of a copper ion composition to induce chondrocyte differentiation.

15. The method of claim 14, wherein the copper ion composition is defined as a copper salt composition.

16. The method of claim 15, wherein the copper salt composition comprises a copper salt selected from the group consisting of copper acetate, copper nitrate, copper sulfate, copper chloride, copper carbonate, copper oxide, copper hydroxide, copper bromide, copper iodide, copper chloride, and copper oxide.

17. The method of claim 16, wherein the copper salt composition is defined as an aqueous solution comprising the copper salt.

18. The method of claim 14, wherein the copper ion composition is defined as a copper biomaterial composition.

19. The method of claim 18, wherein the copper biomaterial composition is defined as a copper nanoparticle composition, a copper microparticle composition, a copper hydrogel composition, a copper microgel composition, a copper nanofiber composition, a copper microfiber composition, a copper polymer composition, a copper biomaterial coating, a copper depot, or a copper microneedle composition.

20. The method of claim 14, wherein the effective amount of copper ions in the copper ion composition is a concentration sufficient to produce a local effective concentration of about 0.1 μM to about 100 μM or about 0.1 μM to about 26.66 μM.

21. The method of claim 14, wherein the copper ion composition further comprises a targeting molecule.

22. The method of claim 14, wherein the stem cell is a mesenchymal stem cell.

23. The method of claim 14, wherein the subject is afflicted with or at risk of developing a disease or condition associated with altered chondrocyte growth, differentiation, or function.

24. The method of claim 14, wherein the subject is afflicted with or at risk of developing a disease or condition selected from the group consisting of: a cartilage injury, costochondritis, intervertebral disc herniation, polychondritis, osteoarthritis, rheumatoid arthritis, a traumatic joint injury, an ACL tear, a cartilage lesion or defect, a hip labral tear, osteonecrosis, juvenile idiopathic arthritis, avascular necrosis, chondromalacia patellae, post-traumatic osteoarthritis, a cartilage tumor, and an achondroplasia-like condition.

25. The method of claim 14, wherein said administering comprises injection, microneedle administration, oral administration, buccal administration, vaginal administration, inhalation, intraosseous administration, trans nasal application, topical administration, transdermal application, or rectal administration.

26. The method of claim 14, the method comprising administering a pharmaceutical composition comprising the effective amount of the copper ion composition to the subject.

27. A pharmaceutical composition comprising:

a) a silver ion composition capable of producing a local effective silver ion concentration of about 0.1 μM to about100 μM or about 0.1 μM to about 29.95 μM; or

b) a copper ion composition capable of producing a local effective copper ion concentration of about 0.1 μM to about 100 μM or about 0.1 μM to about 26.66 μM.

28. The pharmaceutical composition of claim 27, wherein the silver ion composition is defined as a silver salt composition, or wherein the copper ion composition is defined as a copper salt composition.

29. The pharmaceutical composition of claim 28, wherein the silver salt composition comprises a silver salt selected from the group consisting of silver acetate, silver nitrate, silver chloride, silver bromide, silver iodide, silver fluoride, silver sulfide, silver phosphate, silver chromate, and silver sulfate, or wherein the copper salt composition comprises a copper salt selected from the group consisting of copper acetate, copper nitrate, copper sulfate, copper chloride, copper carbonate, copper oxide, copper hydroxide, copper bromide, copper iodide, copper chloride, and copper oxide.

30. The pharmaceutical composition of claim 29, wherein the silver salt composition is defined as an aqueous solution comprising the silver salt, or wherein the copper salt composition is defined as an aqueous solution comprising the copper salt.

31. The pharmaceutical composition of claim 27, wherein the silver ion composition is defined as a silver biomaterial composition, or wherein the copper ion composition is defined as a copper biomaterial composition.

32. The pharmaceutical composition of claim 31, wherein the silver biomaterial composition is defined as a silver nanoparticle composition, a silver microparticle composition, a silver hydrogel composition, a silver microgel composition, a silver nanofiber composition, a silver microfiber composition, a silver polymer composition, a silver biomaterial coating, a silver depot, or a silver microneedle composition, or wherein the copper biomaterial composition is defined as a copper nanoparticle composition, a copper microparticle composition, a copper hydrogel composition, a copper microgel composition, a copper nanofiber composition, a copper microfiber composition, a copper polymer composition, a copper biomaterial coating, a copper depot, or a copper microneedle composition.

33. The pharmaceutical composition of claim 27, wherein the silver ion composition further comprises a targeting molecule, or wherein the copper ion composition further comprises a targeting molecule.

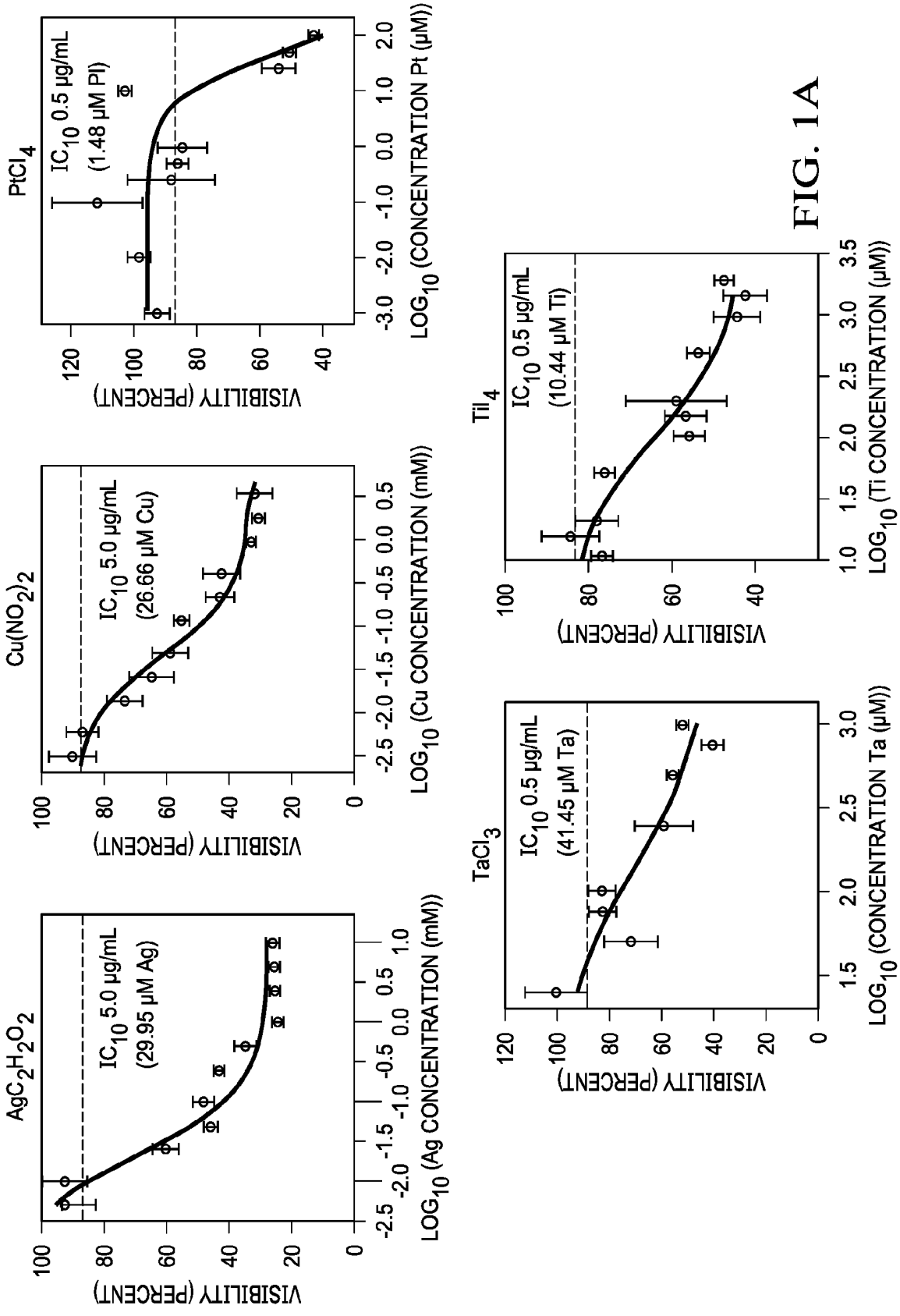
AgC2H2O2
IC10 5.0 µg/mL
(29.95 µM Ag)
VISIBILITY (PERCENT)
LOG10 (Ag CONCENTRATION (mM))
Cu(NO2)2
IC10 5.0 µg/mL
(26.66 µM Cu)
VISIBILITY (PERCENT)
LOG10 (Cu CONCENTRATION (mM))
PtCl4
IC10 0.5 µg/mL
(1.48 µM Pt)
VISIBILITY (PERCENT)
LOG10 (CONCENTRATION Pt (µM))
TaCl5
IC10 0.5 µg/mL
(41.45 µM Ta)
VISIBILITY (PERCENT)
LOG10 (CONCENTRATION Ta (µM))
TiI4
IC10 0.5 µg/mL
(10.44 µM Ti)
VISIBILITY (PERCENT)
LOG10 (Ti CONCENTRATION (µM))

FIG. 1A

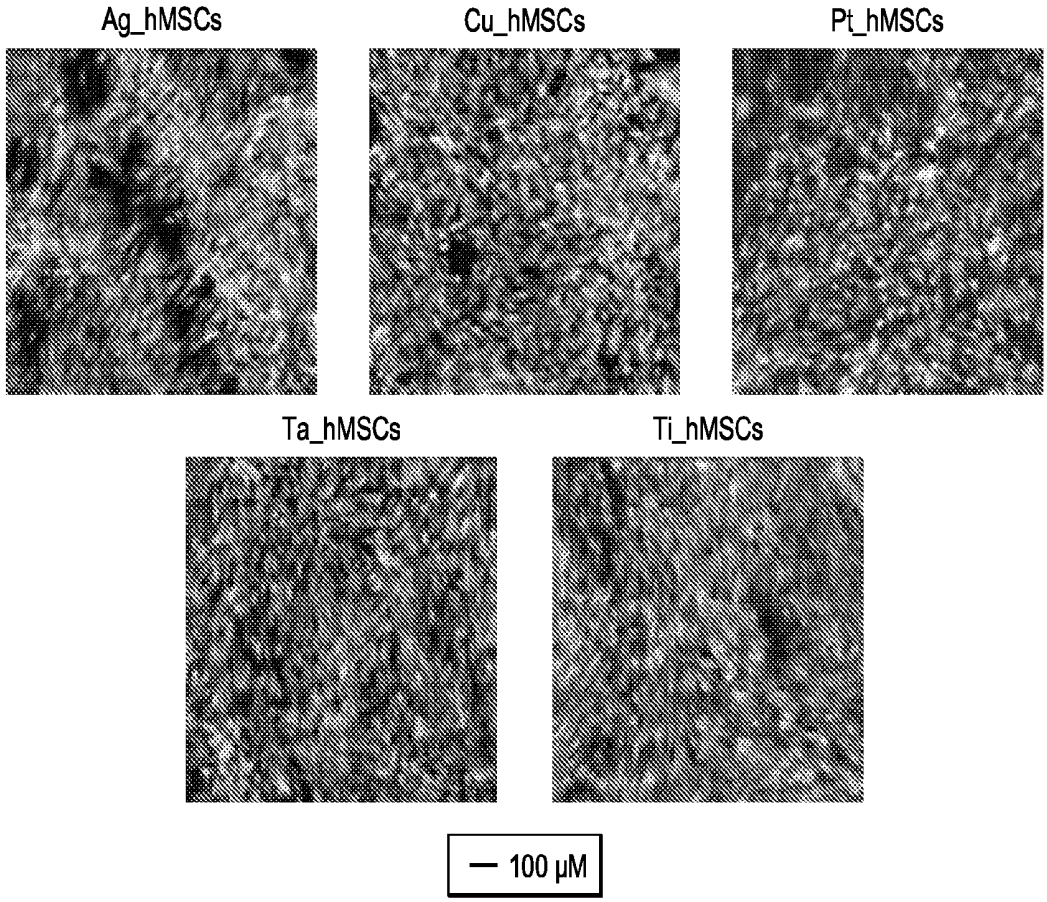
Ag_hMSCs
Cu_hMSCs
Pt_hMSCs
Ta_hMSCs
Ti_hMSCs
— 100 μM

FIG. 1B

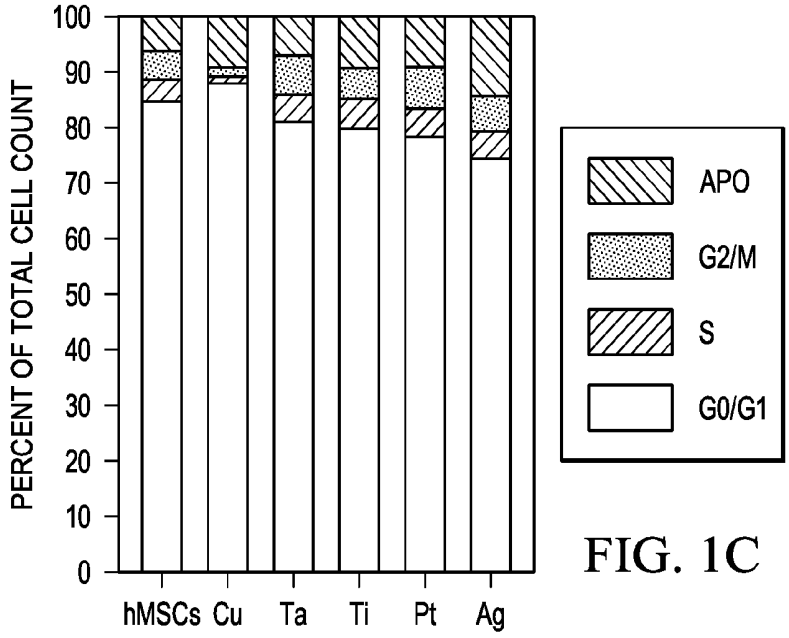
PERCENT OF TOTAL CELL COUNT
100
90
80
70
60
50
40
30
20
10
0
hMSCs
Cu
Ta
Ti
Pt
Ag
APO
G2/M
S
G0/G1

FIG. 1C

		pH	
SAMPLE	STOCK SOLUTION CONCENTRATION (10x, μM)	STOCK SOLUTION IN Di WATER, 21C	1:10 IN MEM ALPHA, 37C
Ag	299.5	7.5	8.0
Cu	266.6	6.0	8.0
Pt	14.8	4.5	8.0
Ta	415.5	4.5	8.0
Ti	104.4	9.5	8.0

FIG. 2

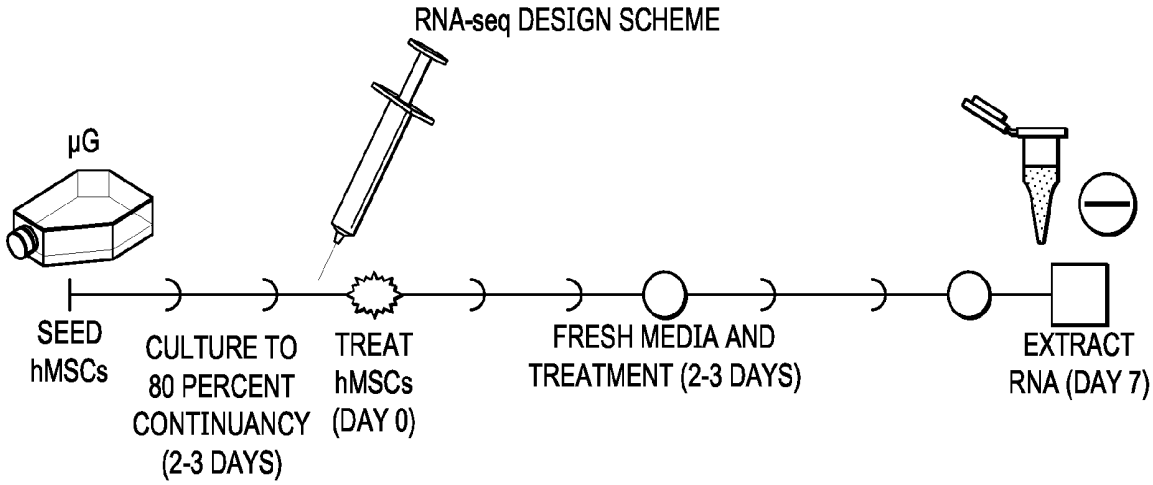
RNA-seq DESIGN SCHEME
μG
SEED hMSCs
CULTURE TO 80 PERCENT CONTINUANCY (2-3 DAYS)
TREAT hMSCs (DAY 0)
FRESH MEDIA AND TREATMENT (2-3 DAYS)
EXTRACT RNA (DAY 7)

FIG. 3A

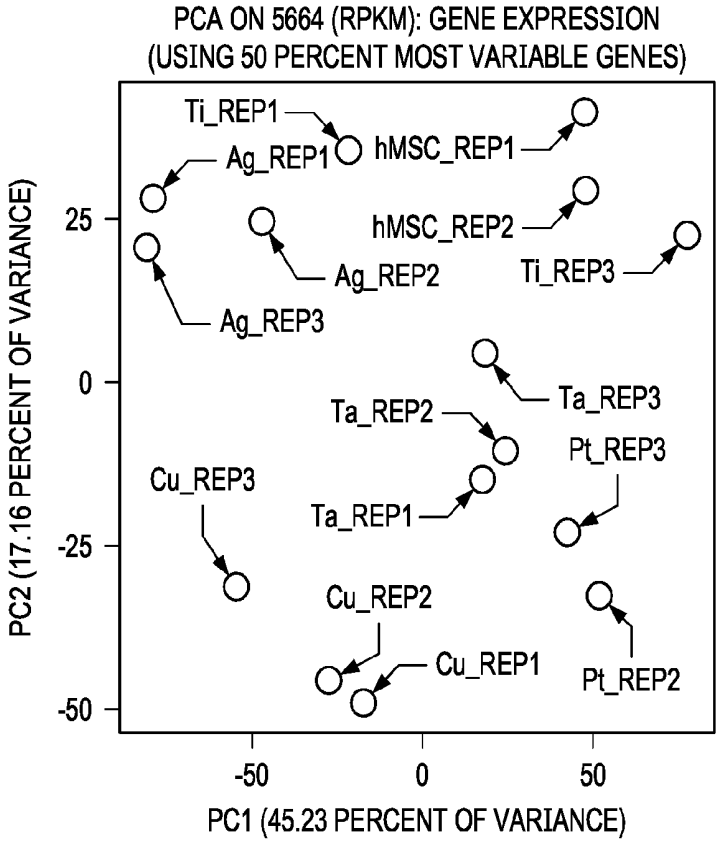
PCA ON 5664 (RPKM): GENE EXPRESSION
(USING 50 PERCENT MOST VARIABLE GENES)
Ti_REP1
Ag_REP1
hMSC_REP1
hMSC_REP2
Ag_REP2
Ti_REP3
Ag_REP3
Ta_REP3
Ta_REP2
Pt_REP3
Cu_REP3
Ta_REP1
Cu_REP2
Cu_REP1
Pt_REP2
25
0
-25
-50
-50
0
50
PC2 (17.16 PERCENT OF VARIANCE)
PC1 (45.23 PERCENT OF VARIANCE)

FIG. 3B

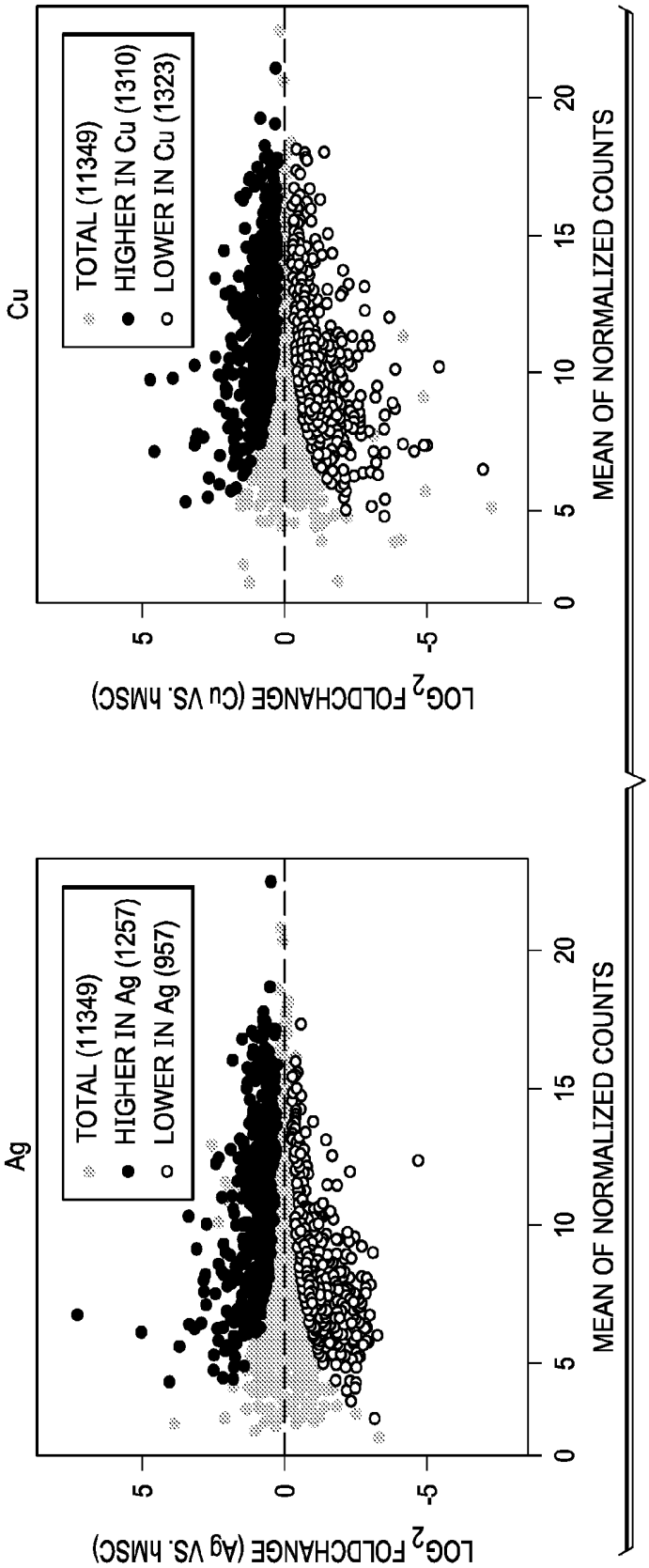
Ag
TOTAL (11349)
HIGHER IN Ag (1257)
LOWER IN Ag (957)
LOG2 FOLDCHANGE (Ag VS. hMSC)
MEAN OF NORMALIZED COUNTS
Cu
TOTAL (11349)
HIGHER IN Cu (1310)
LOWER IN Cu (1323)
LOG2 FOLDCHANGE (Cu VS. hMSC)
MEAN OF NORMALIZED COUNTS

FIG. 3C-1

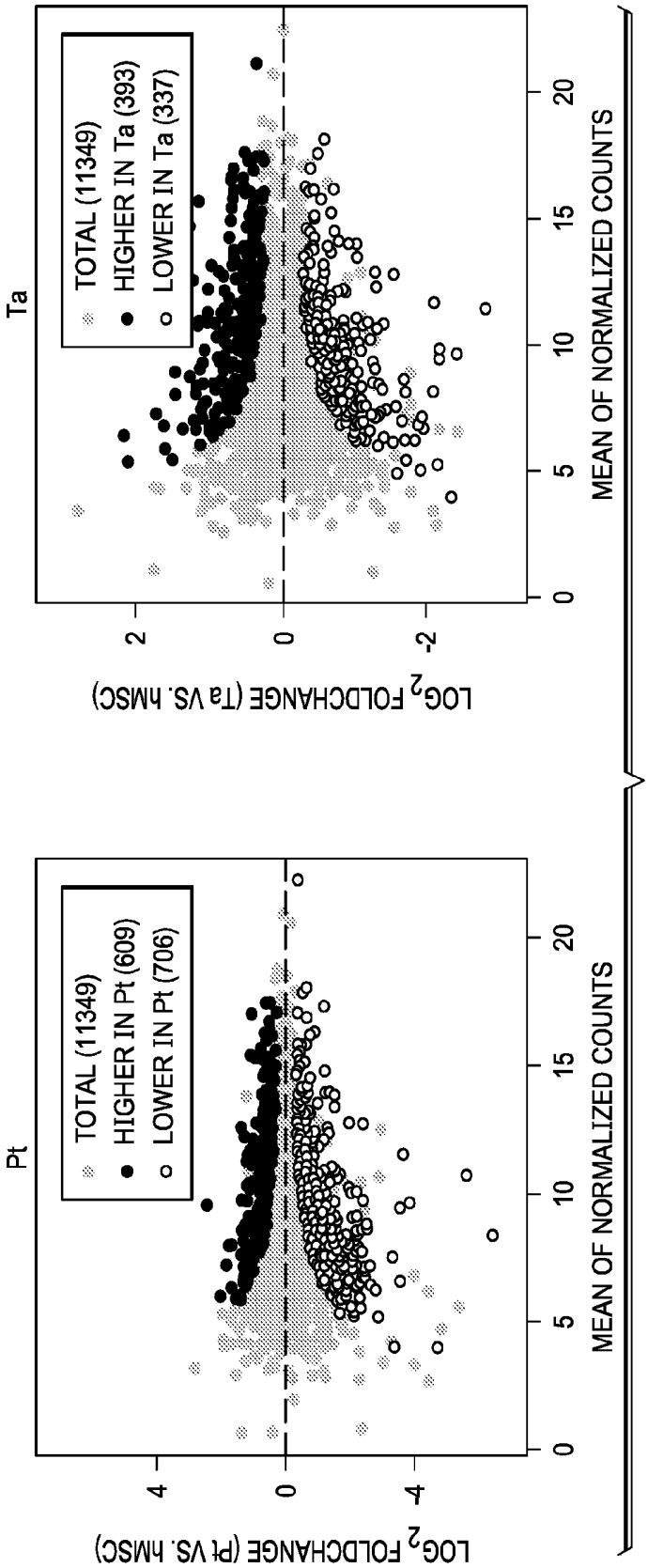
Ta
TOTAL (11349)
HIGHER IN Ta (393)
LOWER IN Ta (337)
LOG2 FOLDCHANGE (Ta VS. hMSC)
MEAN OF NORMALIZED COUNTS
Pt
TOTAL (11349)
HIGHER IN Pt (609)
LOWER IN Pt (706)
LOG2 FOLDCHANGE (Pt VS. hMSC)
MEAN OF NORMALIZED COUNTS

FIG. 3C-2

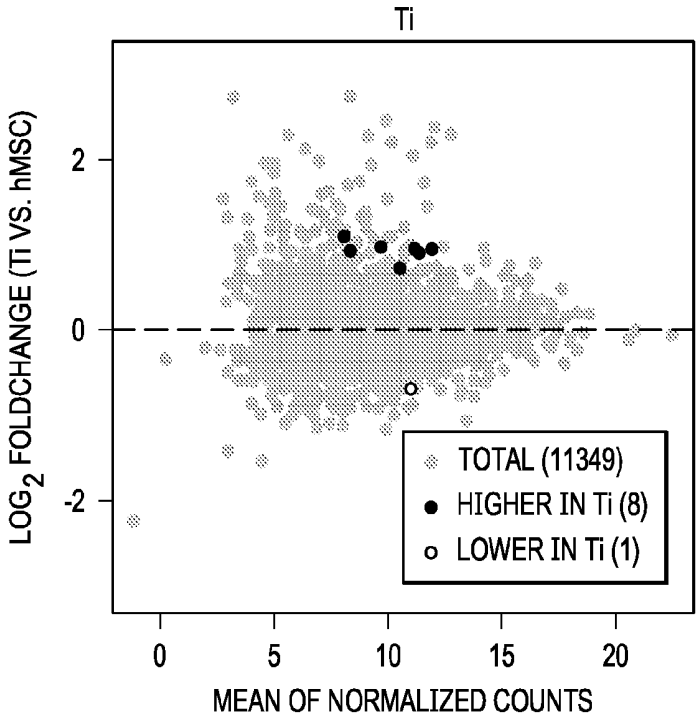

FIG. 3C-3

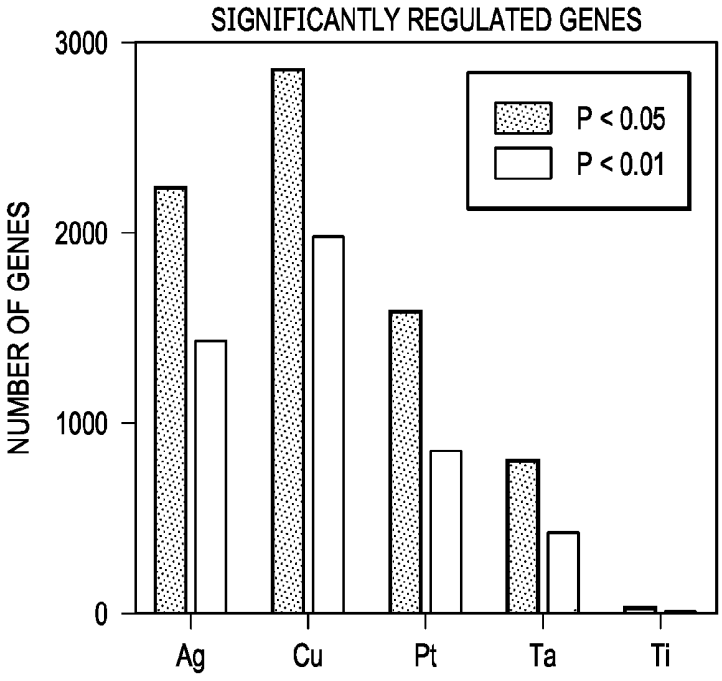

FIG. 3D

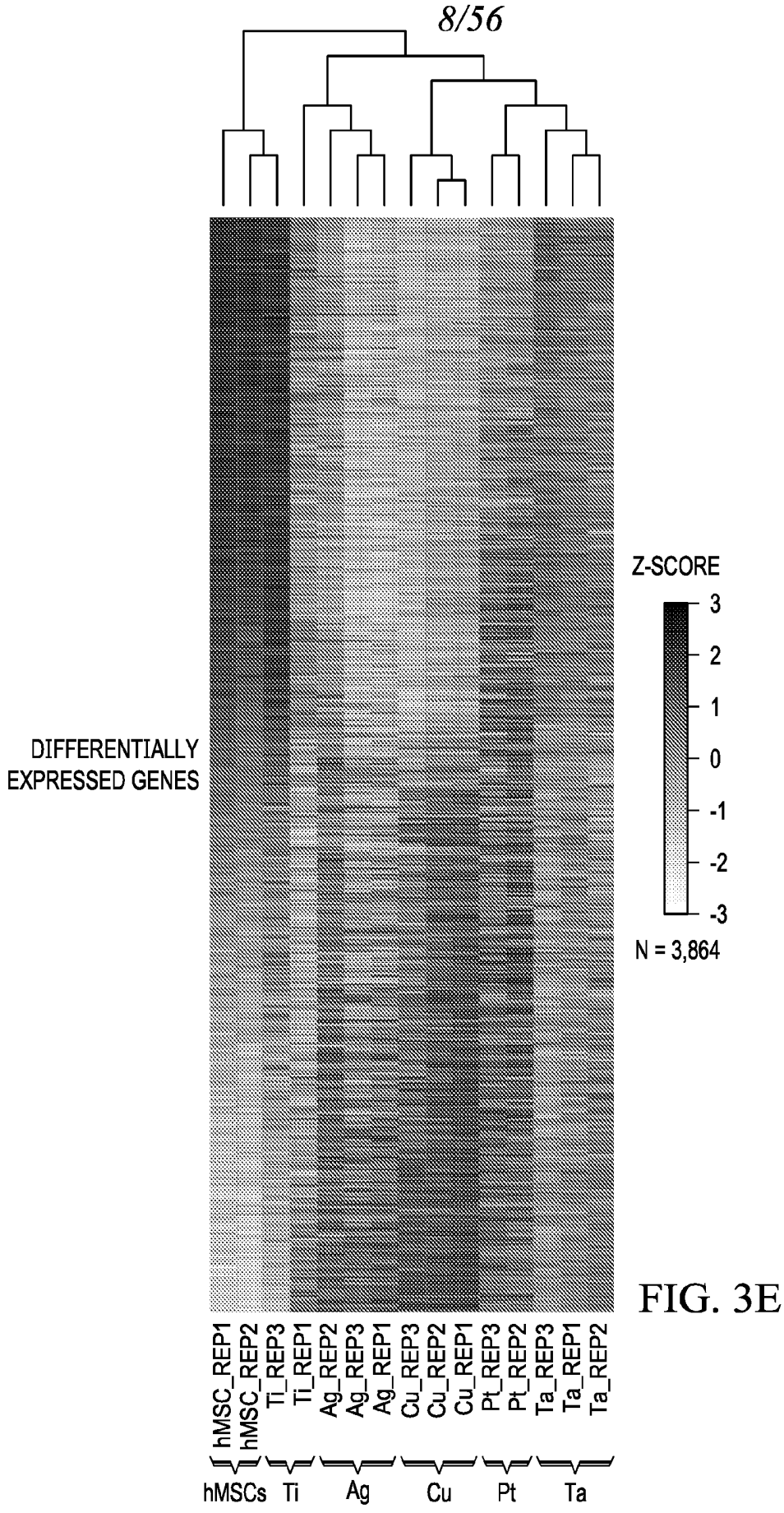
DIFFERENTIALLY EXPRESSED GENES
Z-SCORE
3
2
1
0
-1
-2
-3
N = 3,864
hMSC_REP1
hMSC_REP2
Ti_REP3
Ti_REP1
Ag_REP2
Ag_REP3
Ag_REP1
Cu_REP3
Cu_REP2
Cu_REP1
Pt_REP3
Pt_REP2
Ta_REP3
Ta_REP1
Ta_REP2
hMSCs
Ti
Ag
Cu
Pt
Ta

FIG. 3E

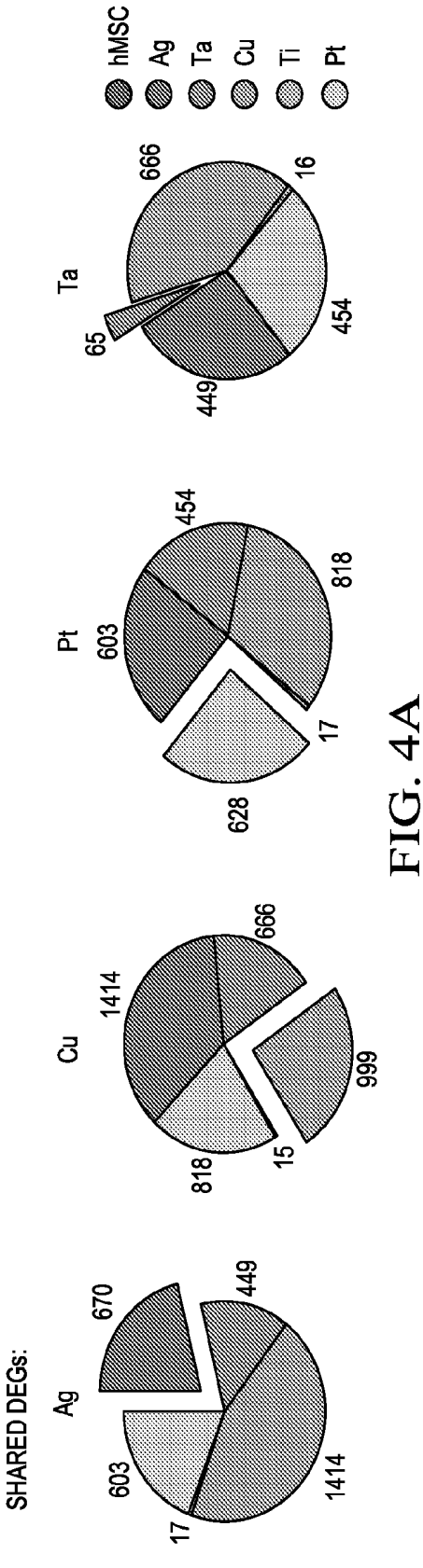
hMSC
Ag
Ta
Cu
Ti
Pt
Ta
666
16
65
454
449
Pt
454
603
818
17
628
Cu
1414
666
999
818
15
SHARED DEGs:
Ag
670
449
603
17
1414

FIG. 4A

FIG. 4B-1

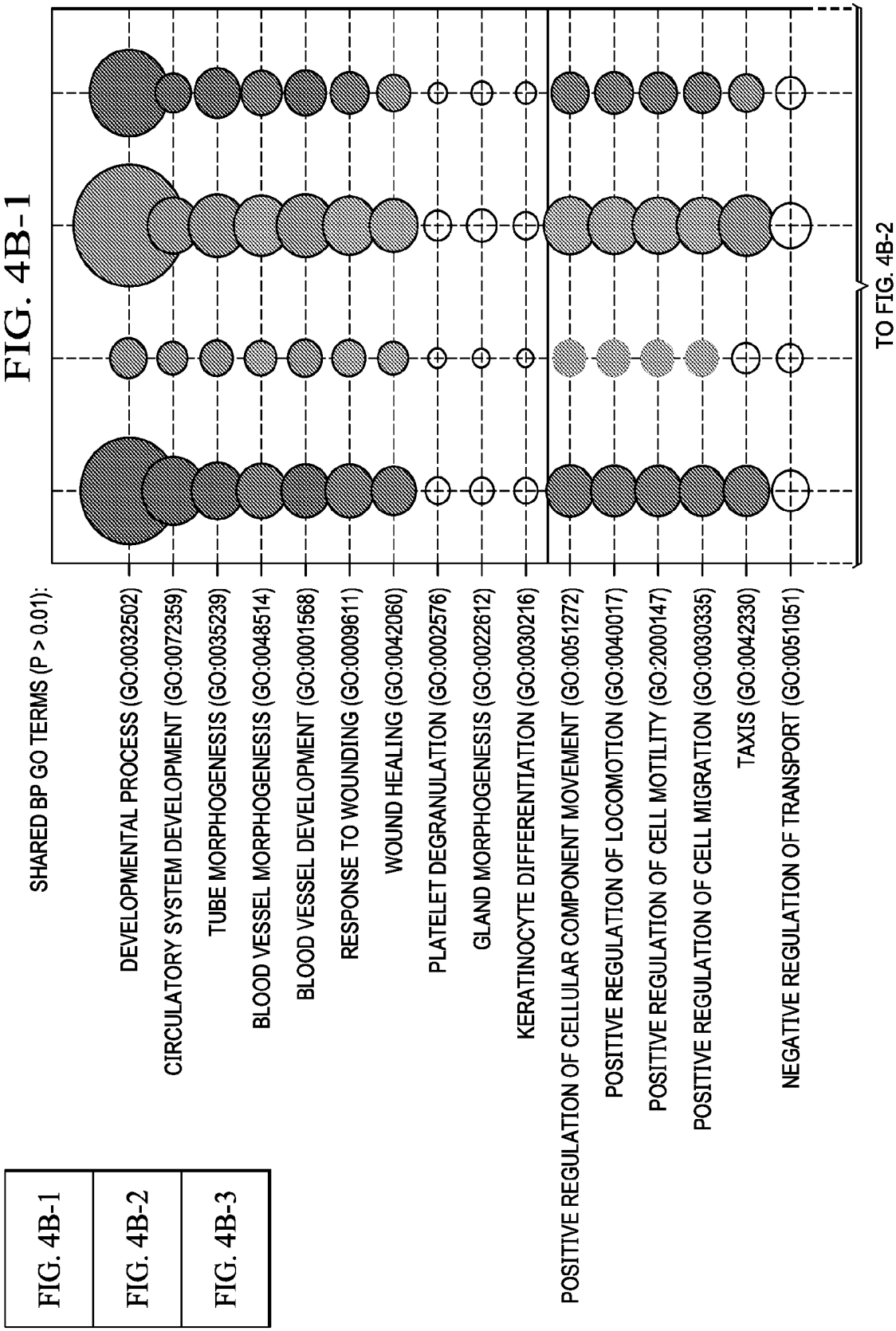

FIG. 4B-1
FIG. 4B-2
FIG. 4B-3

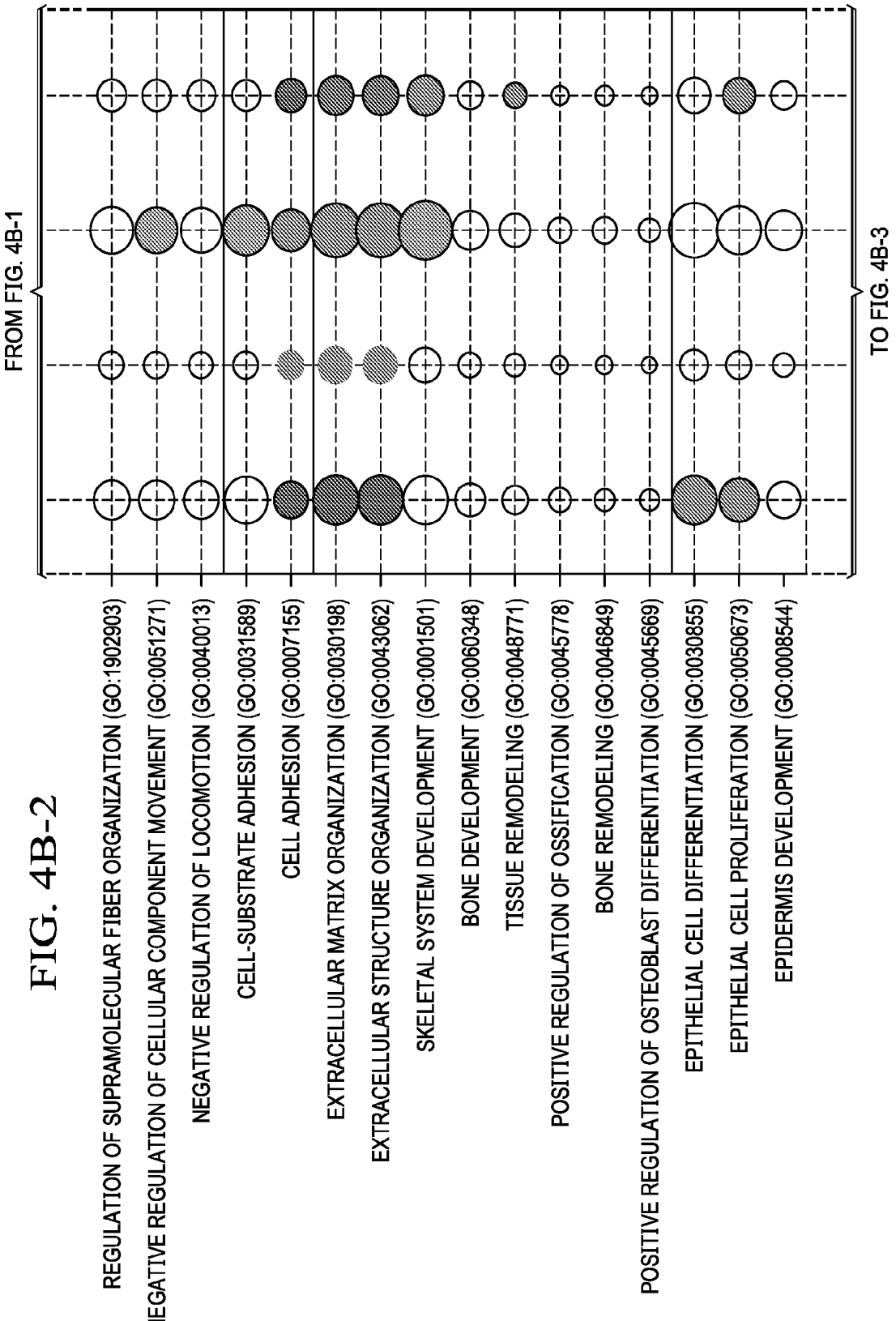
FROM FIG. 4B-1
TO FIG. 4B-3
REGULATION OF SUPRAMOLECULAR FIBER ORGANIZATION (GO:1902903)
NEGATIVE REGULATION OF CELLULAR COMPONENT MOVEMENT (GO:0051271)
NEGATIVE REGULATION OF LOCOMOTION (GO:0040013)
CELL-SUBSTRATE ADHESION (GO:0031589)
CELL ADHESION (GO:0007155)
EXTRACELLULAR MATRIX ORGANIZATION (GO:0030198)
EXTRACELLULAR STRUCTURE ORGANIZATION (GO:0043062)
SKELETAL SYSTEM DEVELOPMENT (GO:0001501)
BONE DEVELOPMENT (GO:0060348)
TISSUE REMODELING (GO:0048771)
POSITIVE REGULATION OF OSSIFICATION (GO:0045778)
BONE REMODELING (GO:0046849)
POSITIVE REGULATION OF OSTEOBLAST DIFFERENTIATION (GO:0045669)
EPITHELIAL CELL DIFFERENTIATION (GO:0030855)
EPITHELIAL CELL PROLIFERATION (GO:0050673)
EPIDERMIS DEVELOPMENT (GO:0008544)

FIG. 4B-2

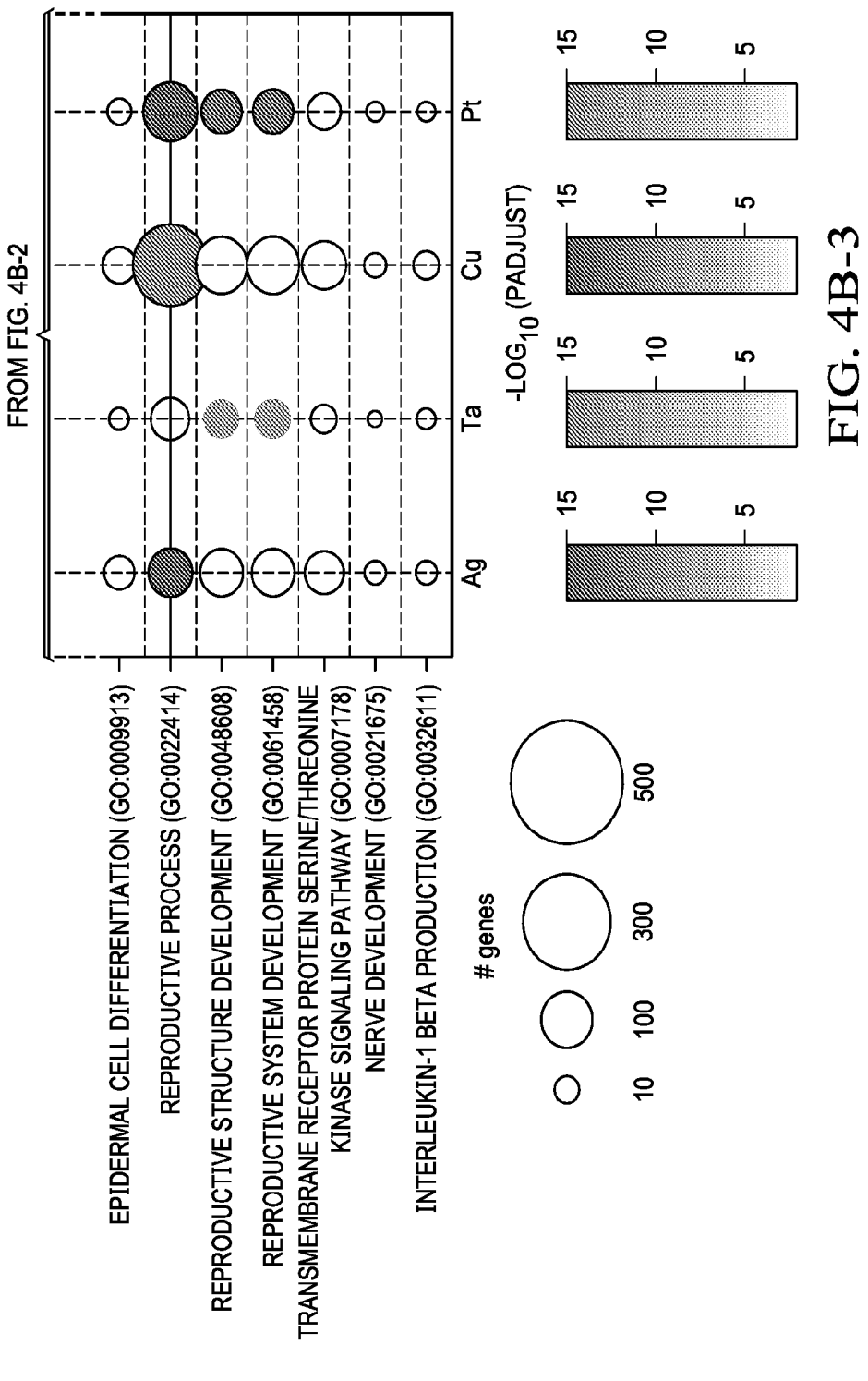
FROM FIG. 4B-2
EPIDERMAL CELL DIFFERENTIATION (GO:0009913)
REPRODUCTIVE PROCESS (GO:0022414)
REPRODUCTIVE STRUCTURE DEVELOPMENT (GO:0048608)
REPRODUCTIVE SYSTEM DEVELOPMENT (GO:0061458)
TRANSMEMBRANE RECEPTOR PROTEIN SERINE/THREONINE KINASE SIGNALING PATHWAY (GO:0007178)
NERVE DEVELOPMENT (GO:0021675)
INTERLEUKIN-1 BETA PRODUCTION (GO:0032611)
Ag
Ta
Cu
Pt
genes
10
100
300
500
-LOG10 (PADJUST)
15
10
5

FIG. 4B-3

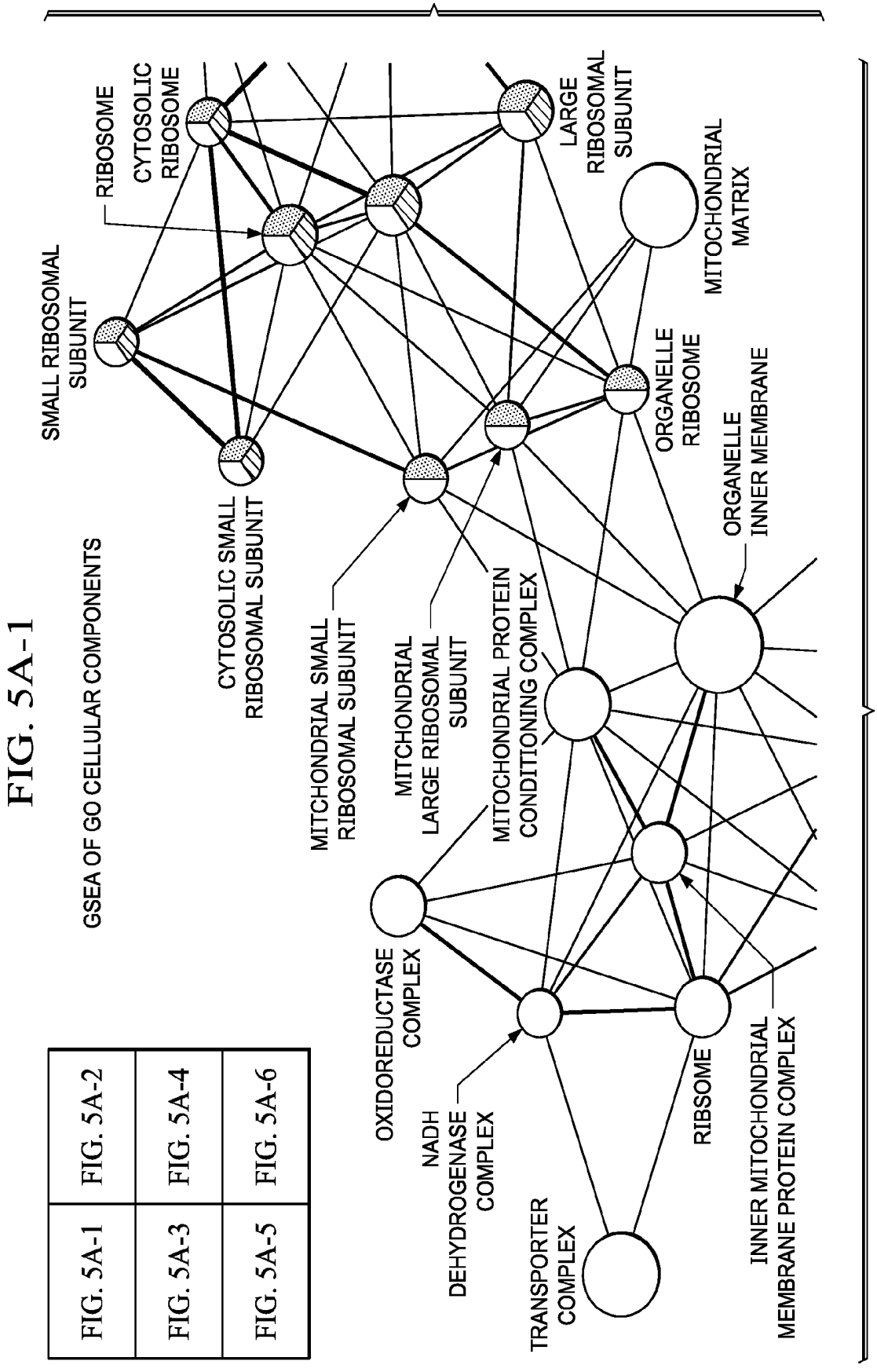

FIG. 5A-1

FIG. 5A-1	FIG. 5A-2
FIG. 5A-3	FIG. 5A-4
FIG. 5A-5	FIG. 5A-6

FIG. 5A-2

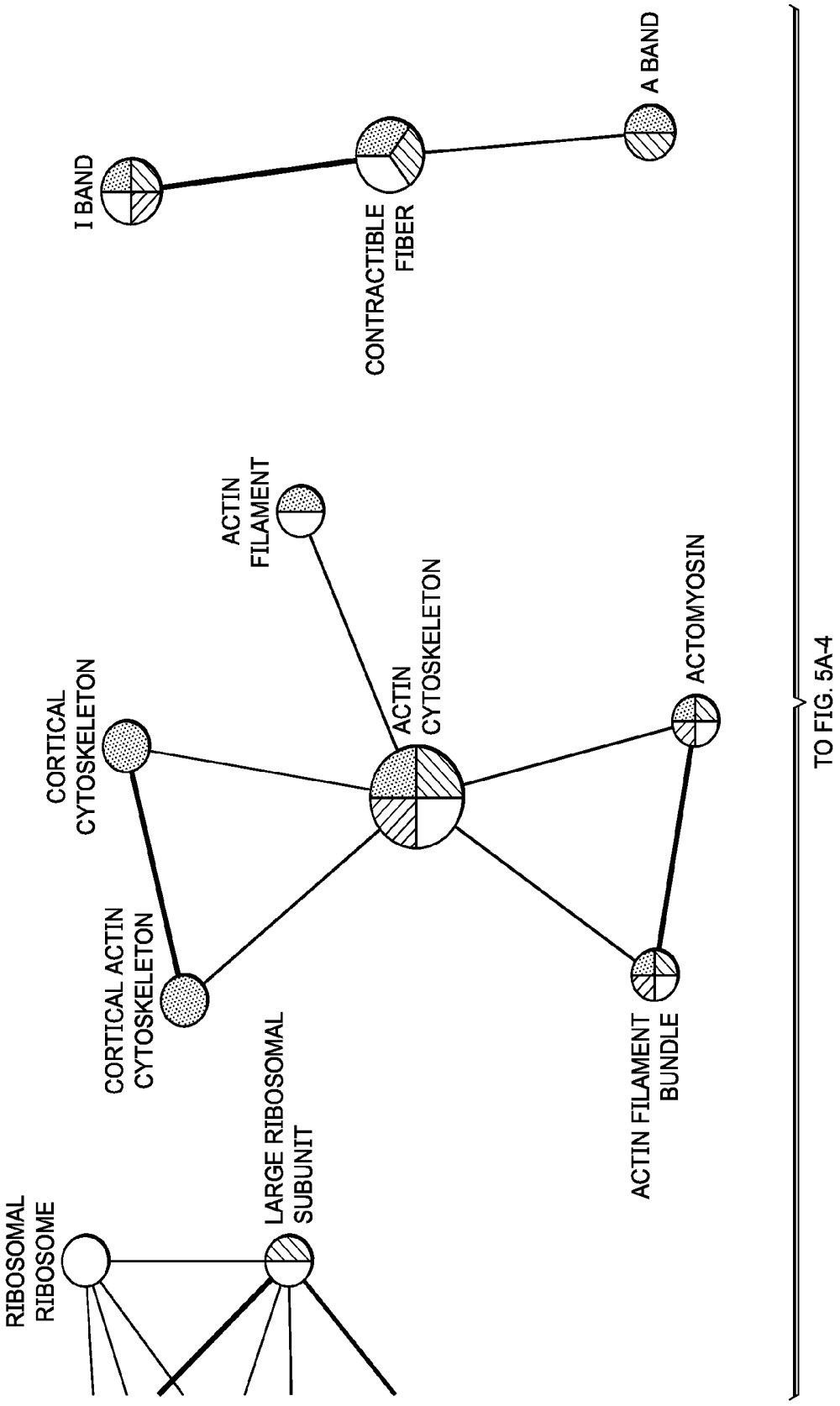
I BAND
CONTRACTIBLE FIBER
A BAND
ACTIN FILAMENT
CORTICAL CYTOSKELETON
ACTIN CYTOSKELETON
ACTOMYOSIN
CORTICAL ACTIN CYTOSKELETON
ACTIN FILAMENT BUNDLE
LARGE RIBOSOMAL SUBUNIT
RIBOSOMAL RIBOSOME
TO FIG. 5A-4
FROM FIG. 5A-1

TO FIG. 5A-4

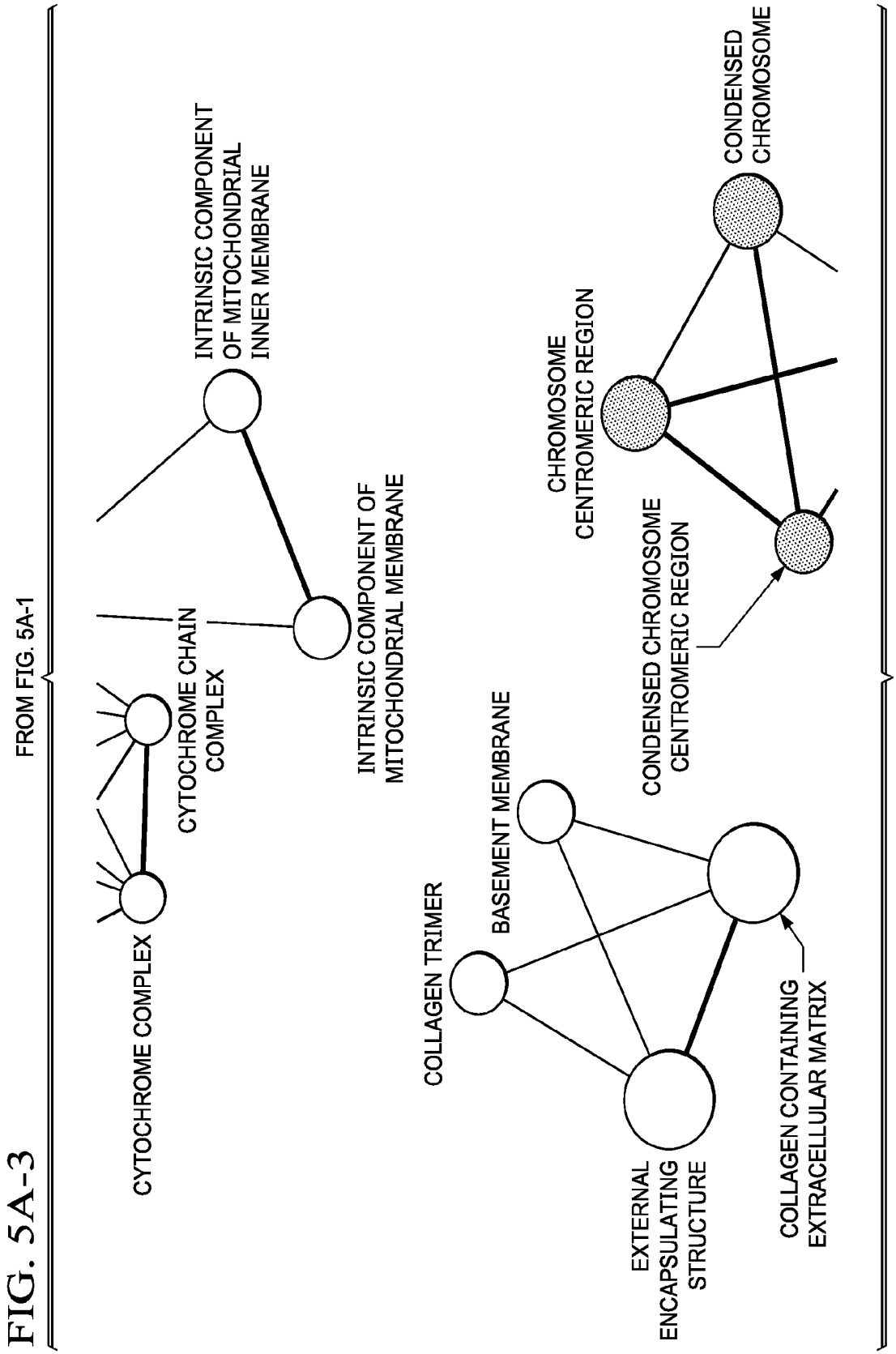

FIG. 5A-3

FIG. 5A-4

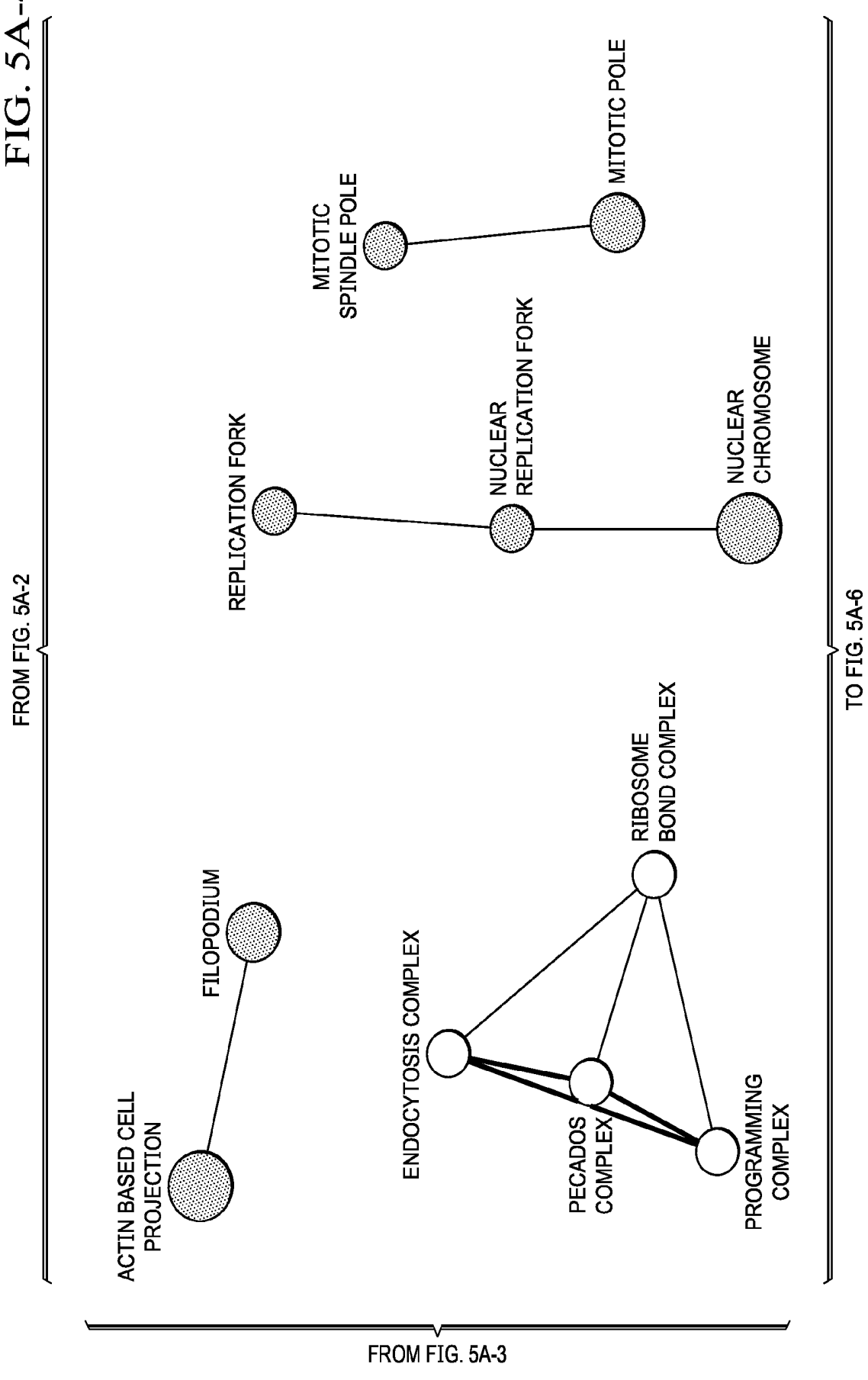
FROM FIG. 5A-2
TO FIG. 5A-6
FROM FIG. 5A-3
ACTIN BASED CELL PROJECTION
FILOPODIUM
REPLICATION FORK
NUCLEAR REPLICATION FORK
NUCLEAR CHROMOSOME
MITOTIC SPINDLE POLE
MITOTIC POLE
ENDOCYTOSIS COMPLEX
PECADOS COMPLEX
RIBOSOME BOND COMPLEX
PROGRAMMING COMPLEX

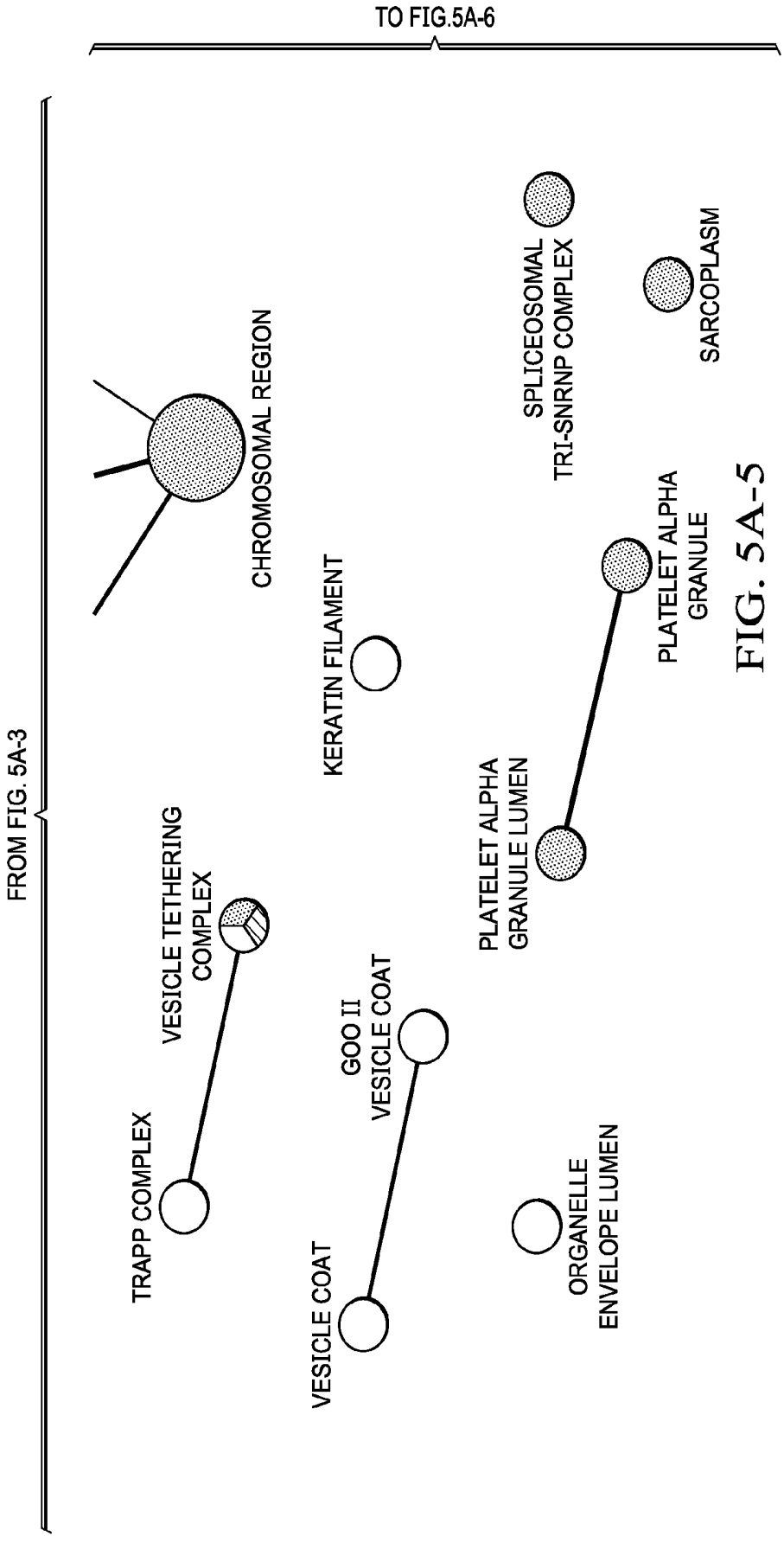
TO FIG.5A-6
FROM FIG. 5A-3
CHROMOSOMAL REGION
KERATIN FILAMENT
SPLICEOSOMAL TRI-SNRNP COMPLEX
SARCOPLASM
PLATELET ALPHA GRANULE
PLATELET ALPHA GRANULE LUMEN
VESICLE TETHERING COMPLEX
GOO II VESICLE COAT
TRAPP COMPLEX
VESICLE COAT
ORGANELLE ENVELOPE LUMEN

FIG. 5A-5

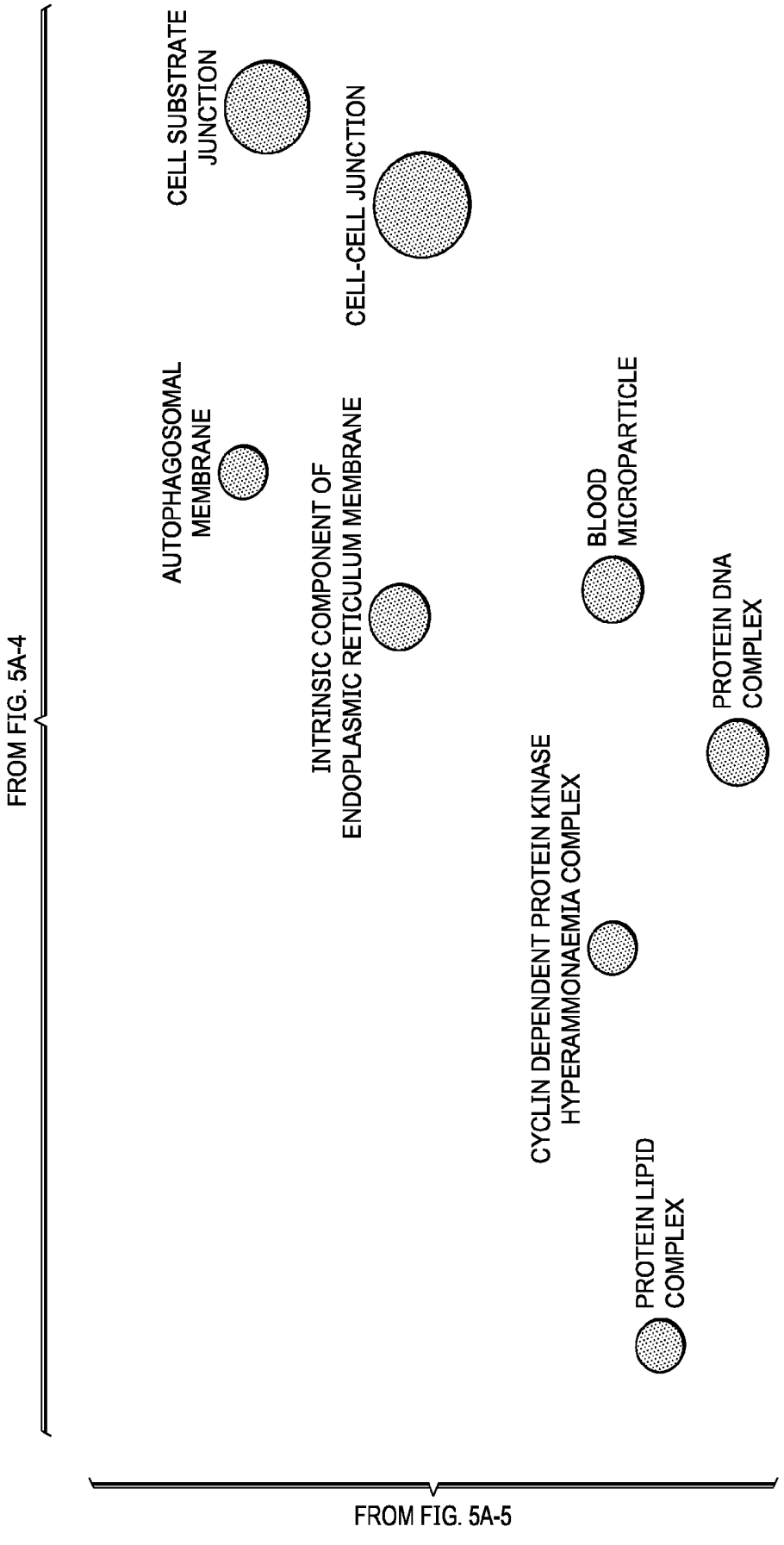
FROM FIG. 5A-4
CELL SUBSTRATE JUNCTION
CELL-CELL JUNCTION
AUTOPHAGOSOMAL MEMBRANE
INTRINSIC COMPONENT OF ENDOPLASMIC RETICULUM MEMBRANE
BLOOD MICROPARTICLE
PROTEIN DNA COMPLEX
CYCLIN DEPENDENT PROTEIN KINASE HYPERAMMONAEMIA COMPLEX
PROTEIN LIPID COMPLEX
FROM FIG. 5A-5

FIG. 5A-6

TO FIG. 5B-2

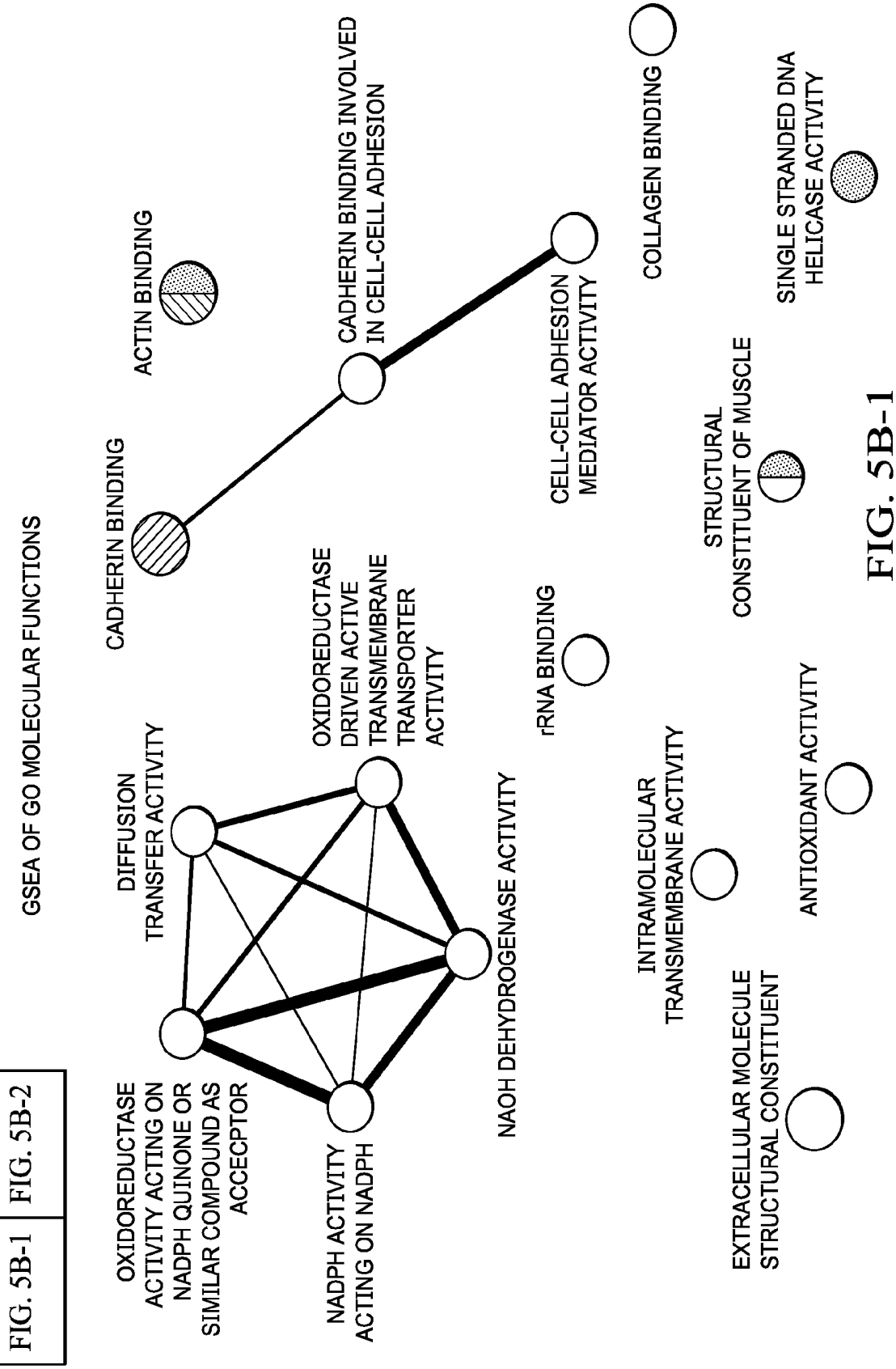

FIG. 5B-1

FIG. 5B-1 | FIG. 5B-2

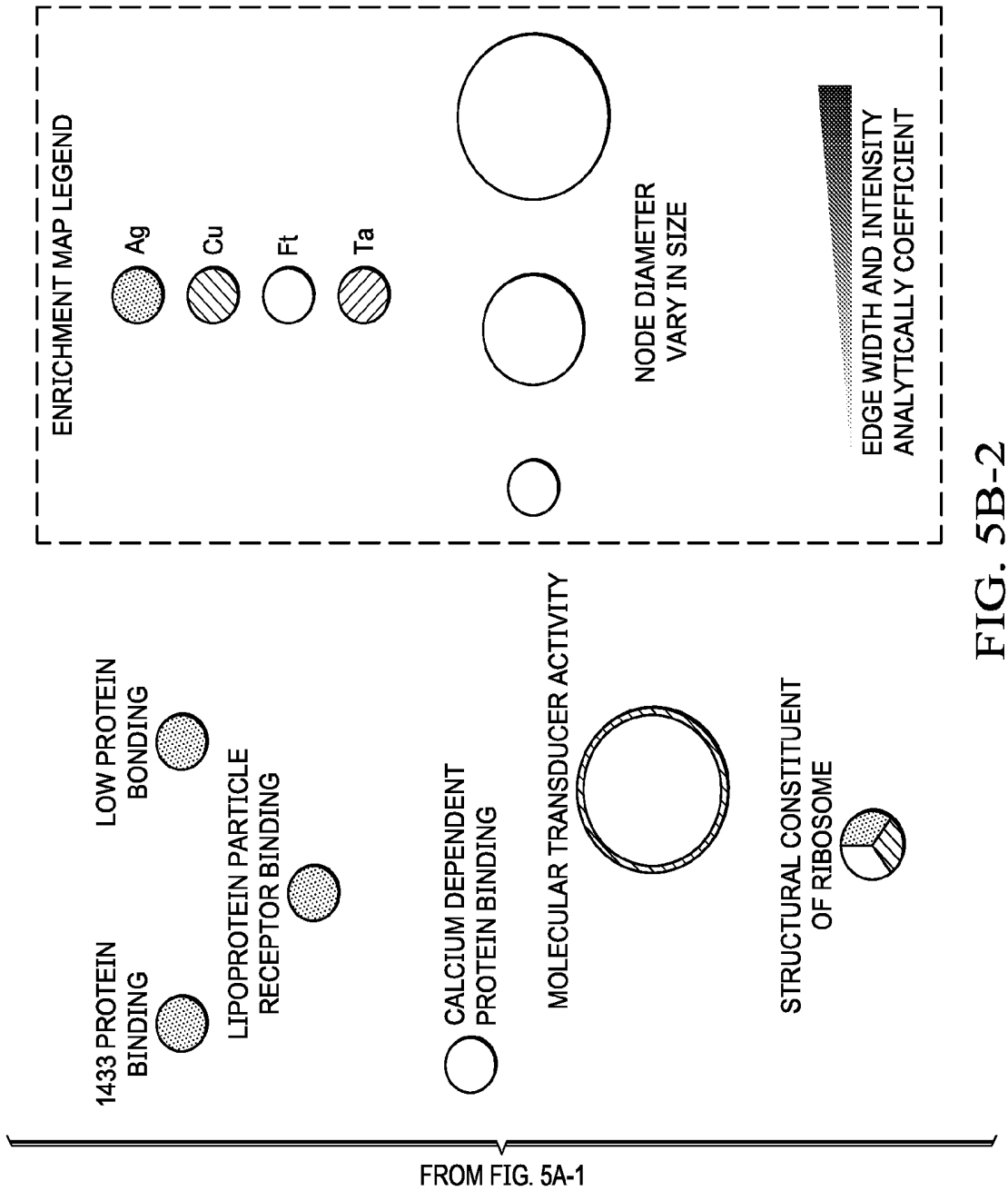
ENRICHMENT MAP LEGEND
Ag
Cu
Ft
Ta
NODE DIAMETER
VARY IN SIZE
EDGE WIDTH AND INTENSITY
ANALYTICALLY COEFFICIENT
1433 PROTEIN
BINDING
LOW PROTEIN
BONDING
LIPOPROTEIN PARTICLE
RECEPTOR BINDING
CALCIUM DEPENDENT
PROTEIN BINDING
MOLECULAR TRANSDUCER ACTIVITY
STRUCTURAL CONSTITUENT
OF RIBOSOME
FROM FIG. 5A-1

FIG. 5B-2

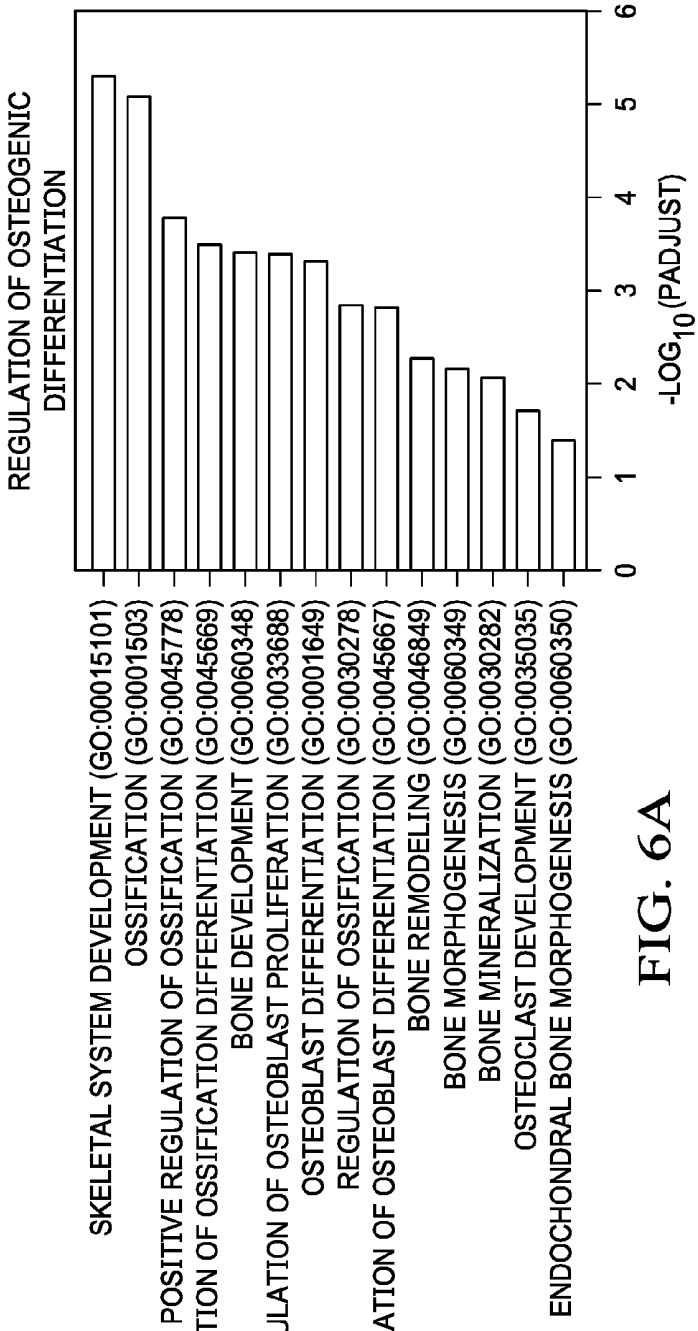
REGULATION OF OSTEOGENIC DIFFERENTIATION
SKELETAL SYSTEM DEVELOPMENT (GO:00015101)
OSSIFICATION (GO:0001503)
POSITIVE REGULATION OF OSSIFICATION (GO:0045778)
POSITIVE REGULATION OF OSSIFICATION DIFFERENTIATION (GO:0045669)
BONE DEVELOPMENT (GO:0060348)
REGULATION OF OSTEOBLAST PROLIFERATION (GO:0033688)
OSTEOBLAST DIFFERENTIATION (GO:0001649)
REGULATION OF OSSIFICATION (GO:0030278)
REGULATION OF OSTEOBLAST DIFFERENTIATION (GO:0045667)
BONE REMODELING (GO:0046849)
BONE MORPHOGENESIS (GO:0060349)
BONE MINERALIZATION (GO:0030282)
OSTEOCLAST DEVELOPMENT (GO:0035035)
ENDOCHONDRAL BONE MORPHOGENESIS (GO:0060350)
0
1
2
3
4
5
6
-LOG10(PADJUST)

FIG. 6A

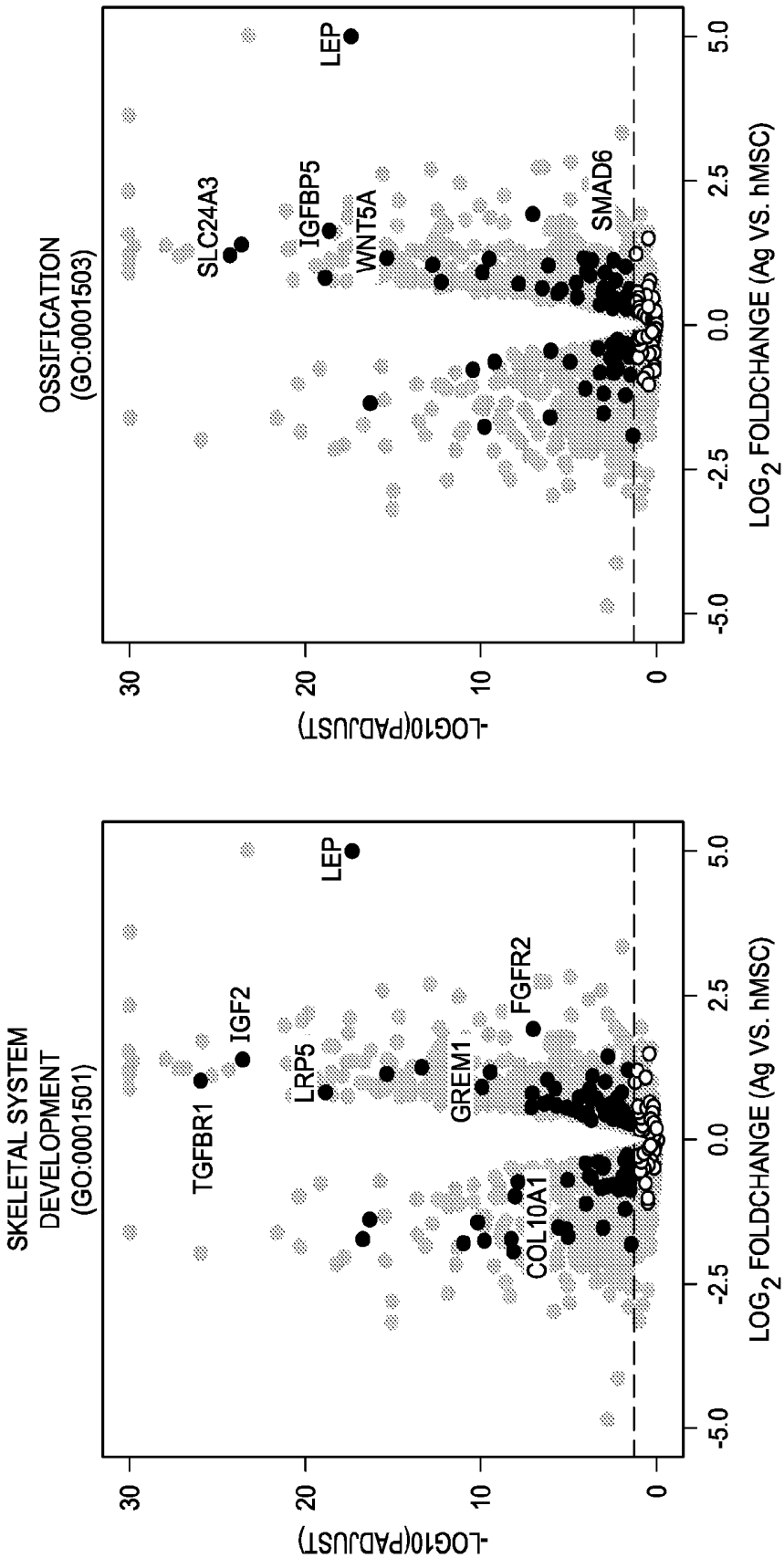
SKELETAL SYSTEM DEVELOPMENT (GO:0001501)
TGFBR1
IGF2
LRP5
LEP
GREM1
FGFR2
COL10A1
-LOG10(PADJUST)
LOG2 FOLDCHANGE (Ag VS. hMSC)
OSSIFICATION (GO:0001503)
SLC24A3
IGFBP5
WNT5A
LEP
SMAD6
-LOG10(PADJUST)
LOG2 FOLDCHANGE (Ag VS. hMSC)

FIG. 6B

FIG. 6C

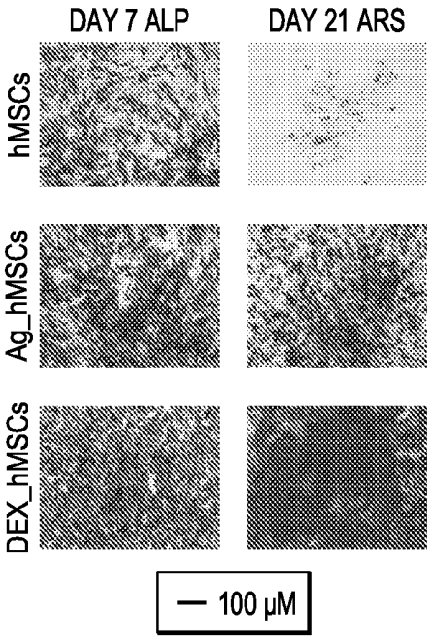

FIG. 6D

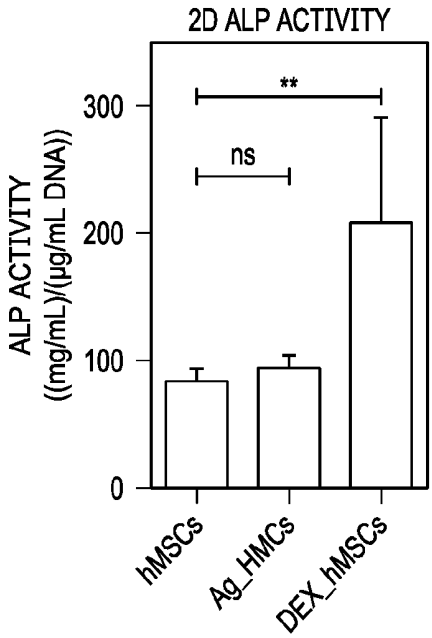

FIG. 6E

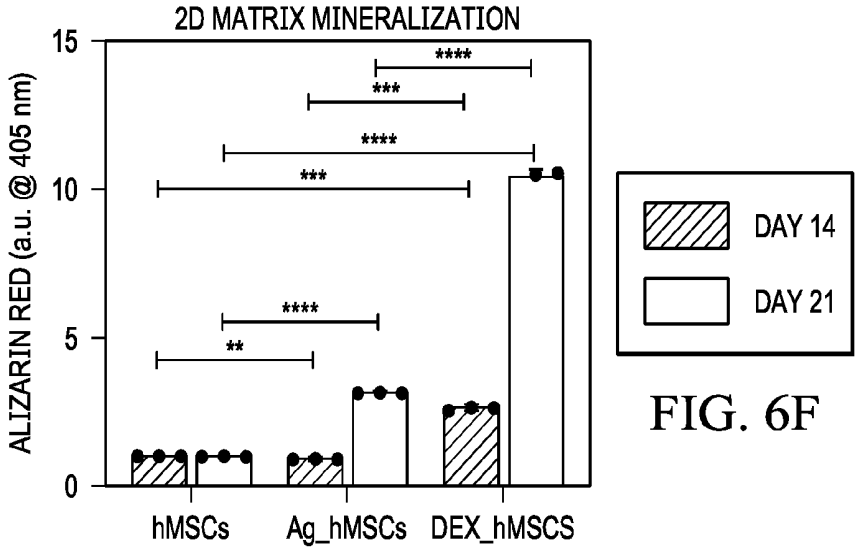

FIG. 6F

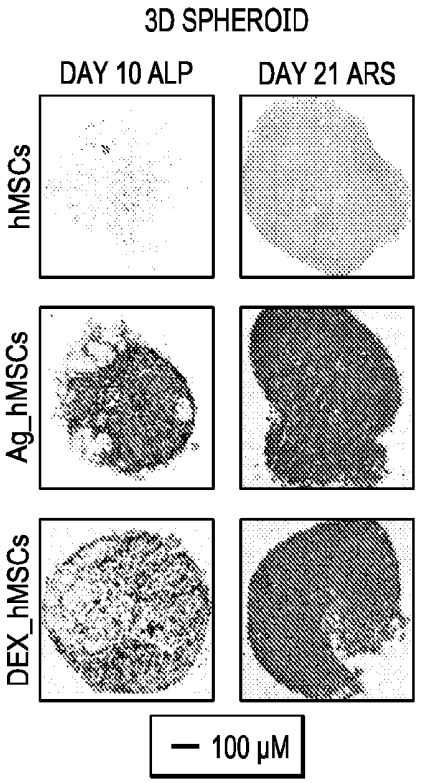
3D SPHEROID
DAY 10 ALP
DAY 21 ARS
hMSCs
Ag_hMSCs
DEX_hMSCs
100 μM

FIG. 6G

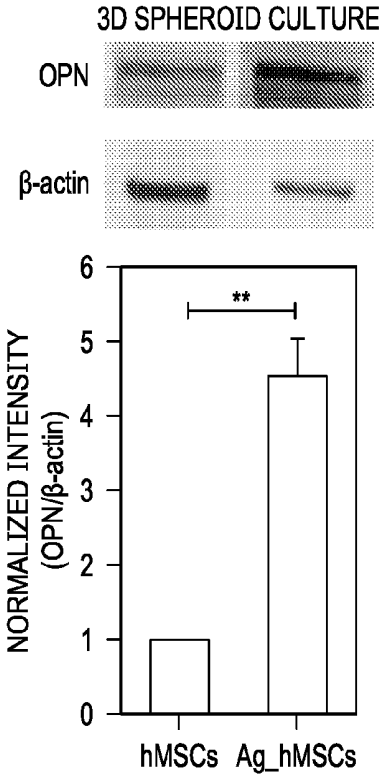
3D SPHEROID CULTURE
OPN
β-actin
NORMALIZED INTENSITY (OPN/β-actin)
**
0
1
2
3
4
5
6
hMSCs
Ag_hMSCs

FIG. 6H

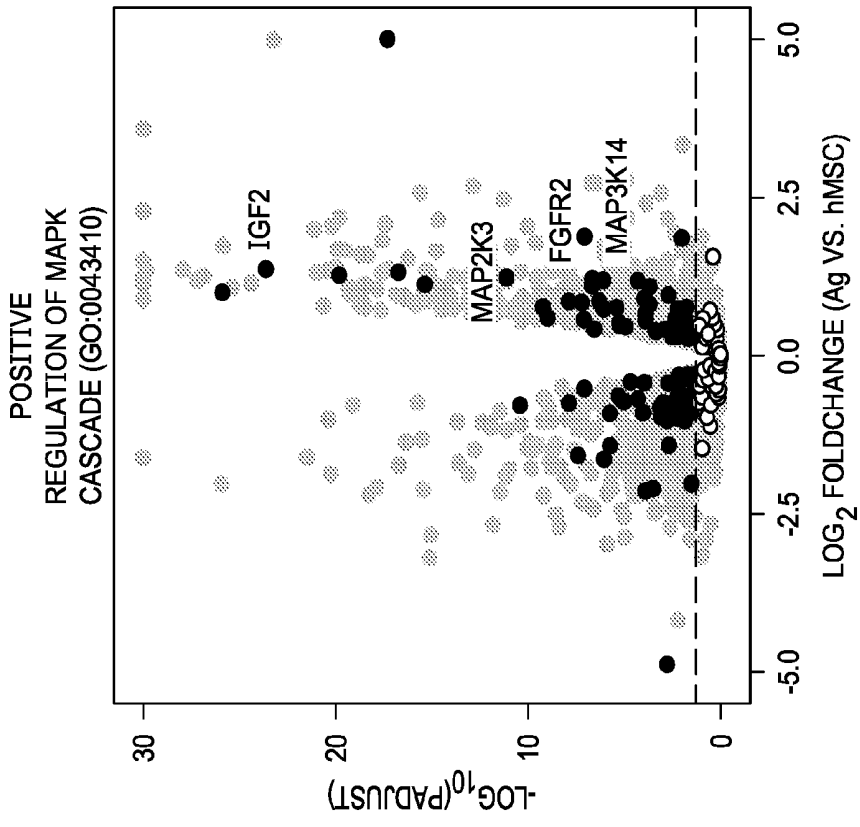
POSITIVE
REGULATION OF MAPK
CASCADE (GO:0043410)
IGF2
MAP2K3
FGFR2
MAP3K14
-LOG10(PADJUST)
LOG2 FOLDCHANGE (Ag VS. hMSC)
30
20
10
0
-5.0
-2.5
0.0
2.5
5.0

FIG. 7A

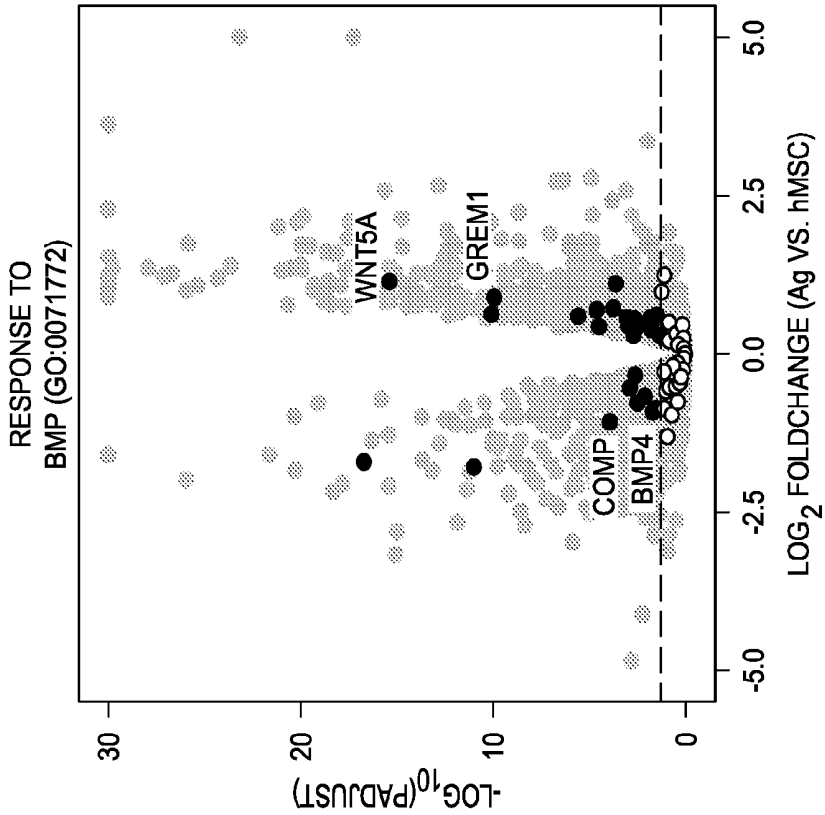
RESPONSE TO
BMP (GO:0071772)
WNT5A
GREM1
COMP
BMP4
-LOG10(PADJUST)
LOG2 FOLDCHANGE (Ag VS. hMSC)
30
20
10
0
-5.0
-2.5
0.0
2.5
5.0

FIG. 7B

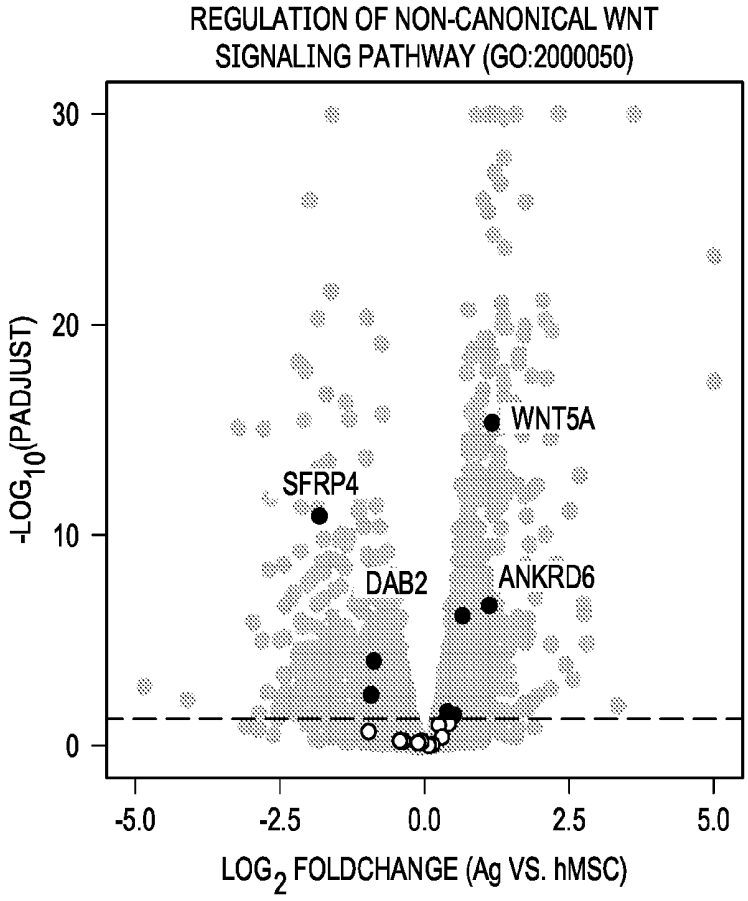
REGULATION OF NON-CANONICAL WNT SIGNALING PATHWAY (GO:2000050)
30
20
10
0
-LOG10(PADJUST)
WNT5A
SFRP4
DAB2
ANKRD6
-5.0
-2.5
0.0
2.5
5.0
LOG2 FOLDCHANGE (Ag VS. hMSC)

FIG. 7C

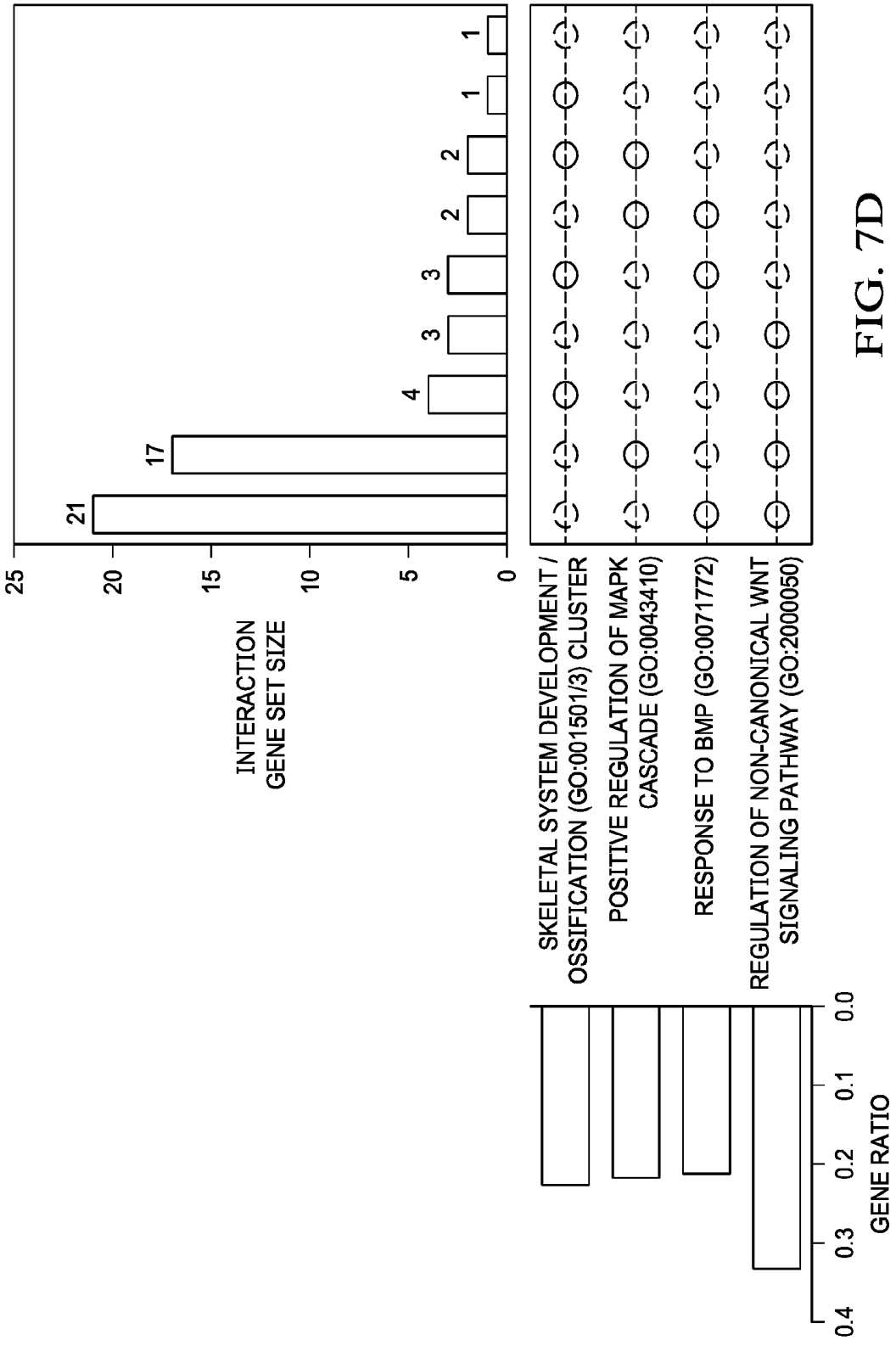
INTERACTION
GENE SET SIZE
25
20
15
10
5
0
21
17
4
3
3
2
2
1
1
SKELETAL SYSTEM DEVELOPMENT / OSSIFICATION (GO:001501/3) CLUSTER
POSITIVE REGULATION OF MAPK CASCADE (GO:0043410)
RESPONSE TO BMP (GO:0071772)
REGULATION OF NON-CANONICAL WNT SIGNALING PATHWAY (GO:2000050)
GENE RATIO
0.4
0.3
0.2
0.1
0.0

FIG. 7D

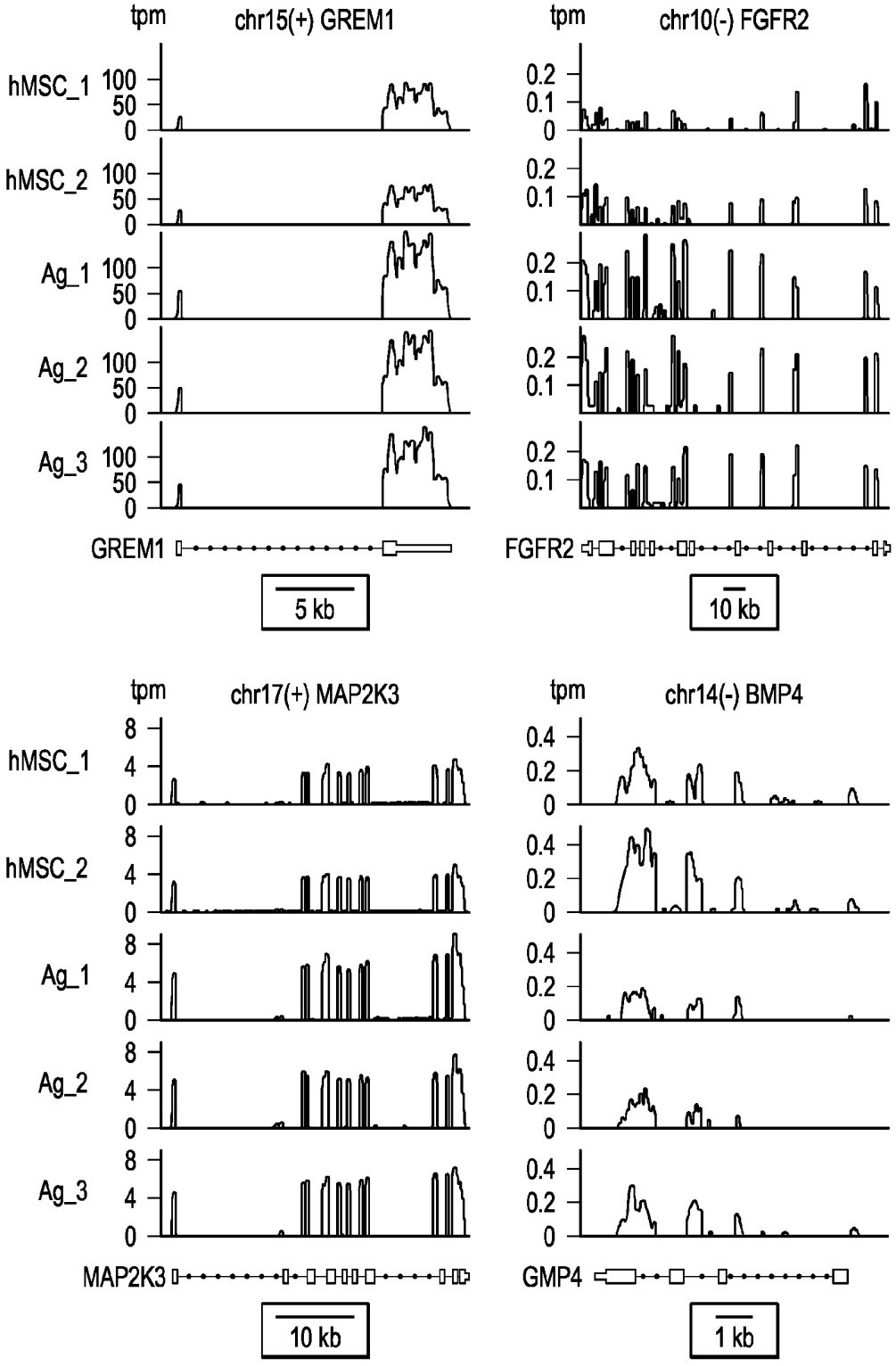
tpm
chr15(+) GREM1
hMSC_1
hMSC_2
Ag_1
Ag_2
Ag_3
100
50
0
GREM1
5 kb
tpm
chr10(-) FGFR2
0.2
0.1
0
FGFR2
10 kb
tpm
chr17(+) MAP2K3
8
4
0
MAP2K3
10 kb
tpm
chr14(-) BMP4
0.4
0.2
0
GMP4
1 kb

FIG. 7E

FIG. 7F

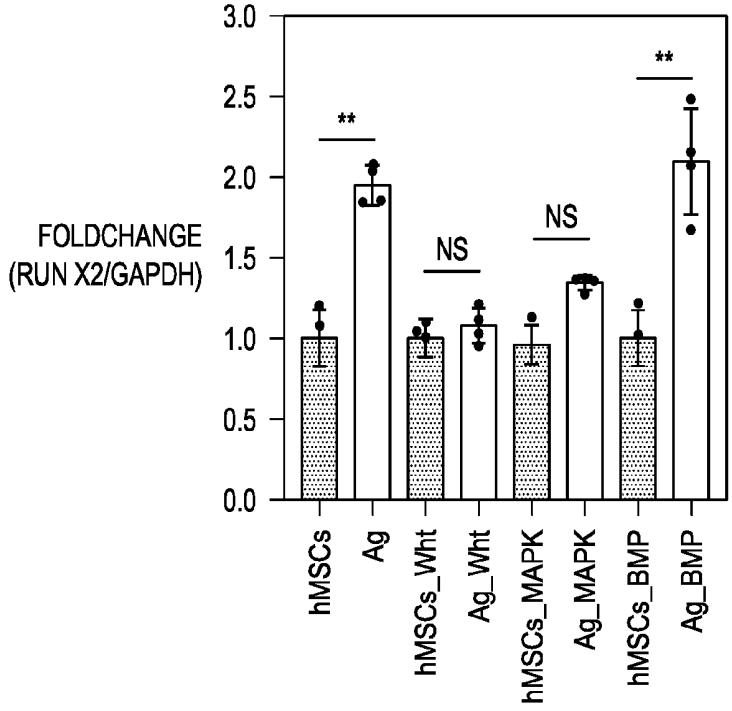
FOLDCHANGE
(RUN X2/GAPDH)
3.0
2.5
2.0
1.5
1.0
0.5
0.0
**
**
NS
NS
hMSCs
Ag
hMSCs_Wht
Ag_Wht
hMSCs_MAPK
Ag_MAPK
hMSCs_BMP
Ag_BMP

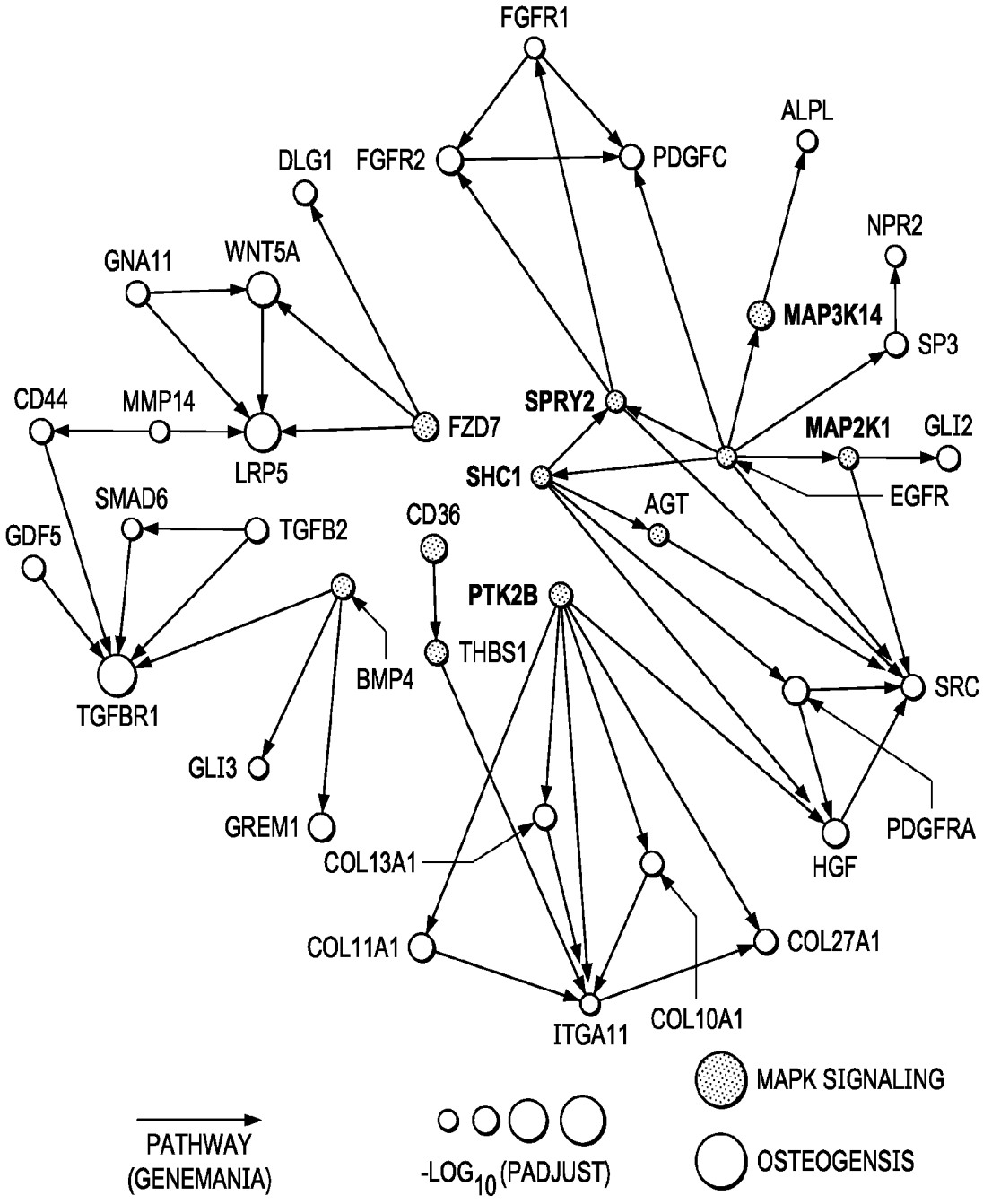
FGFR1
ALPL
DLG1
FGFR2
PDGFC
NPR2
GNA11
WNT5A
MAP3K14
SP3
CD44
MMP14
SPRY2
FZD7
MAP2K1
GLI2
LRP5
SHC1
EGFR
SMAD6
AGT
CD36
GDF5
TGFB2
PTK2B
THBS1
BMP4
SRC
TGFBR1
GLI3
GREM1
PDGFRA
COL13A1
HGF
COL11A1
COL27A1
ITGA11
COL10A1
MAPK SIGNALING
PATHWAY
(GENEMANIA)
-LOG10(PADJUST)
OSTEOGENSIS

FIG. 7G

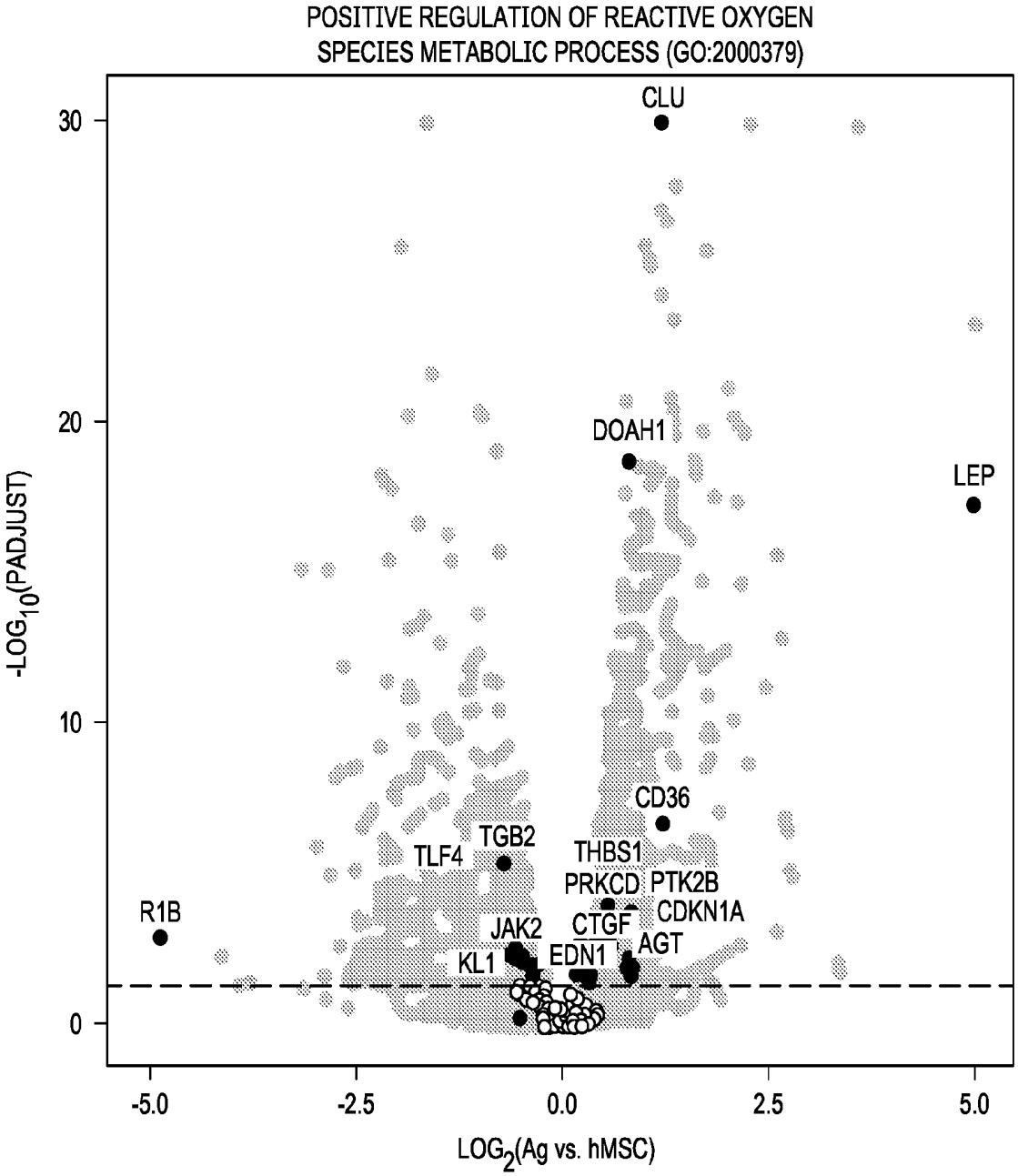
POSITIVE REGULATION OF REACTIVE OXYGEN SPECIES METABOLIC PROCESS (GO:2000379)
CLU
DOAH1
LEP
CD36
TGB2
TLF4
THBS1
PRKCD
PTK2B
CDKN1A
CTGF
AGT
EDN1
JAK2
KL1
R1B
30
20
10
0
-5.0
-2.5
0.0
2.5
5.0
-LOG10(PADJUST)
LOG2(Ag vs. hMSC)

FIG. 8A

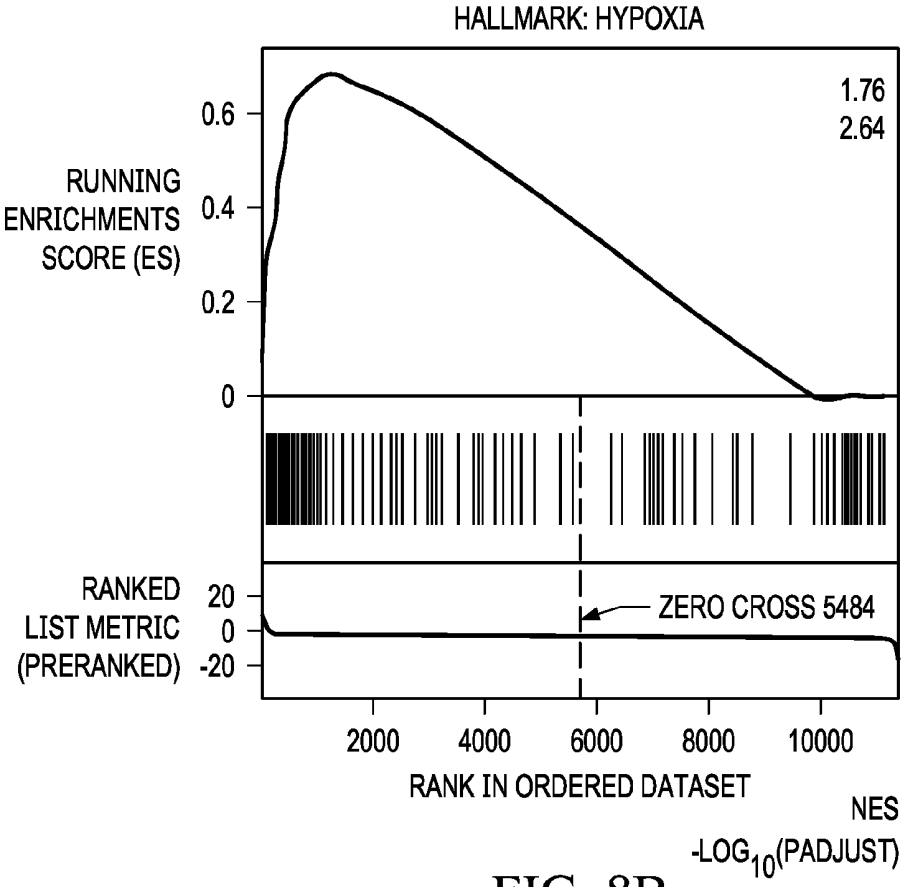
HALLMARK: HYPOXIA
1.76
2.64
RUNNING ENRICHMENTS SCORE (ES)
0.6
0.4
0.2
0
RANKED LIST METRIC (PRERANKED)
20
0
-20
ZERO CROSS 5484
2000
4000
6000
8000
10000
RANK IN ORDERED DATASET
NES
-LOG10(PADJUST)

FIG. 8B

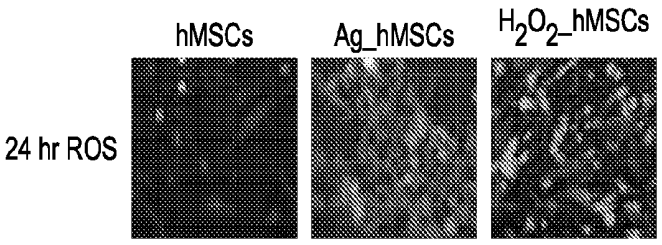
hMSCs
Ag_hMSCs
H2O2_hMSCs
24 hr ROS

FIG. 8C

FIG. 9

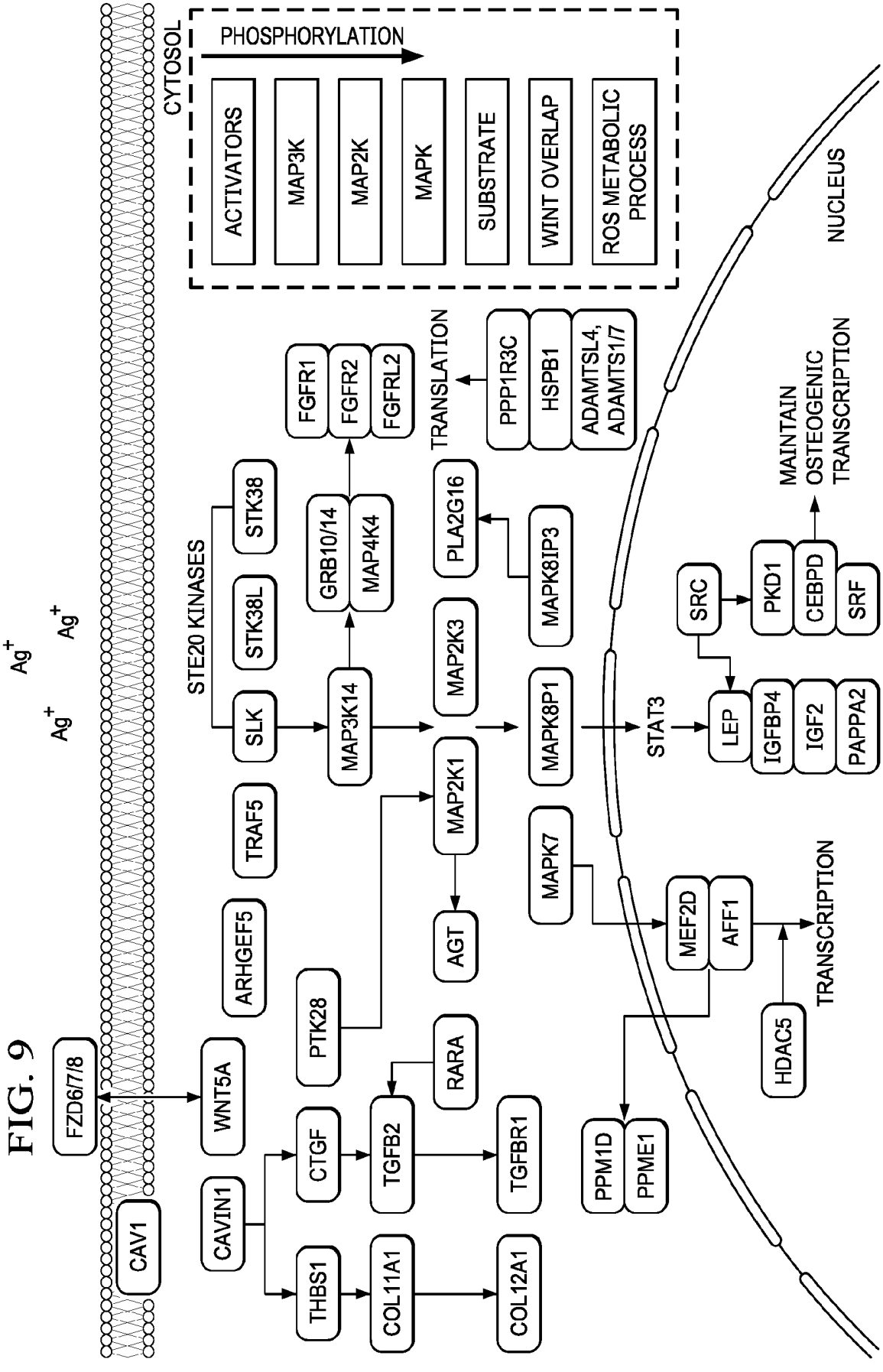
Ag+
Ag+
Ag+
CYTOSOL
PHOSPHORYLATION
ACTIVATORS
MAP3K
MAP2K
MAPK
SUBSTRATE
WINT OVERLAP
ROS METABOLIC PROCESS
NUCLEUS
FZD6/7/8
CAV1
WNT5A
CAVIN1
CTGF
THBS1
COL11A1
TGFB2
TGFBR1
ARHGEF5
TRAF5
PTK28
RARA
STE20 KINASES
SLK
STK38L
STK38
MAP3K14
GRB10/14
MAP4K4
FGFR1
FGFR2
FGFRL2
MAP2K1
AGT
MAP2K3
PLA2G16
MAPK8IP3
TRANSLATION
PPP1R3C
HSPB1
ADAMTSL4, ADAMTS1/7
MAPK8P1
MAPK7
STAT3
SRC
LEP
IGFBP4
IGF2
PAPPA2
PKD1
CEBPD
SRF
MAINTAIN OSTEOGENIC TRANSCRIPTION
MEF2D
AFF1
HDAC5
TRANSCRIPTION
PPM1D
PPME1

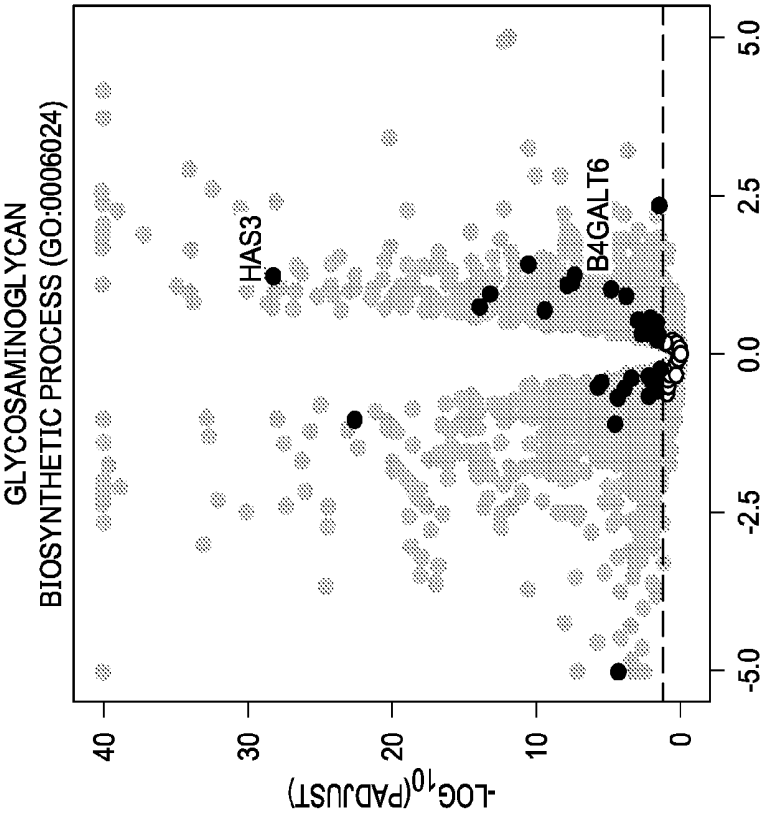

FIG. 10B

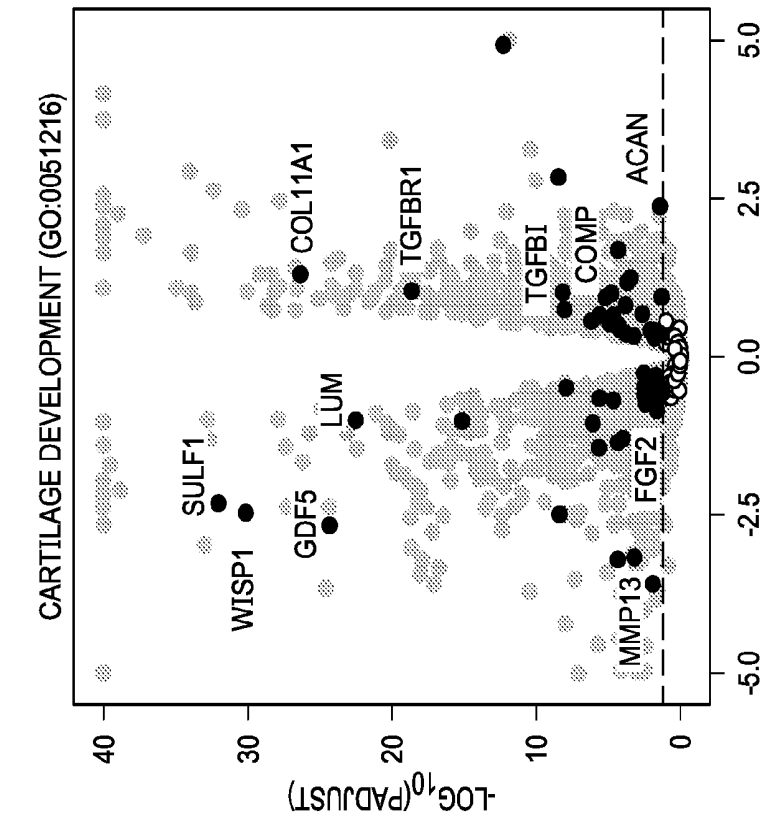

FIG. 10A

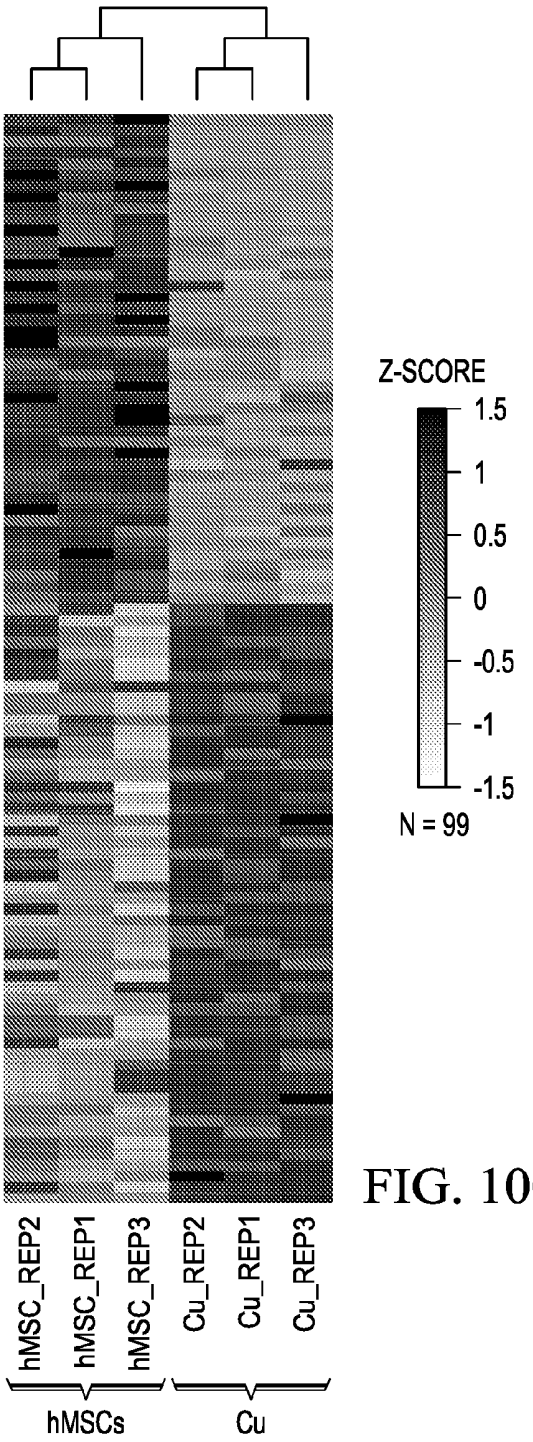
Z-SCORE
1.5
1
0.5
0
-0.5
-1
-1.5
N = 99
hMSC_REP2
hMSC_REP1
hMSC_REP3
Cu_REP2
Cu_REP1
Cu_REP3
hMSCs
Cu

FIG. 10C

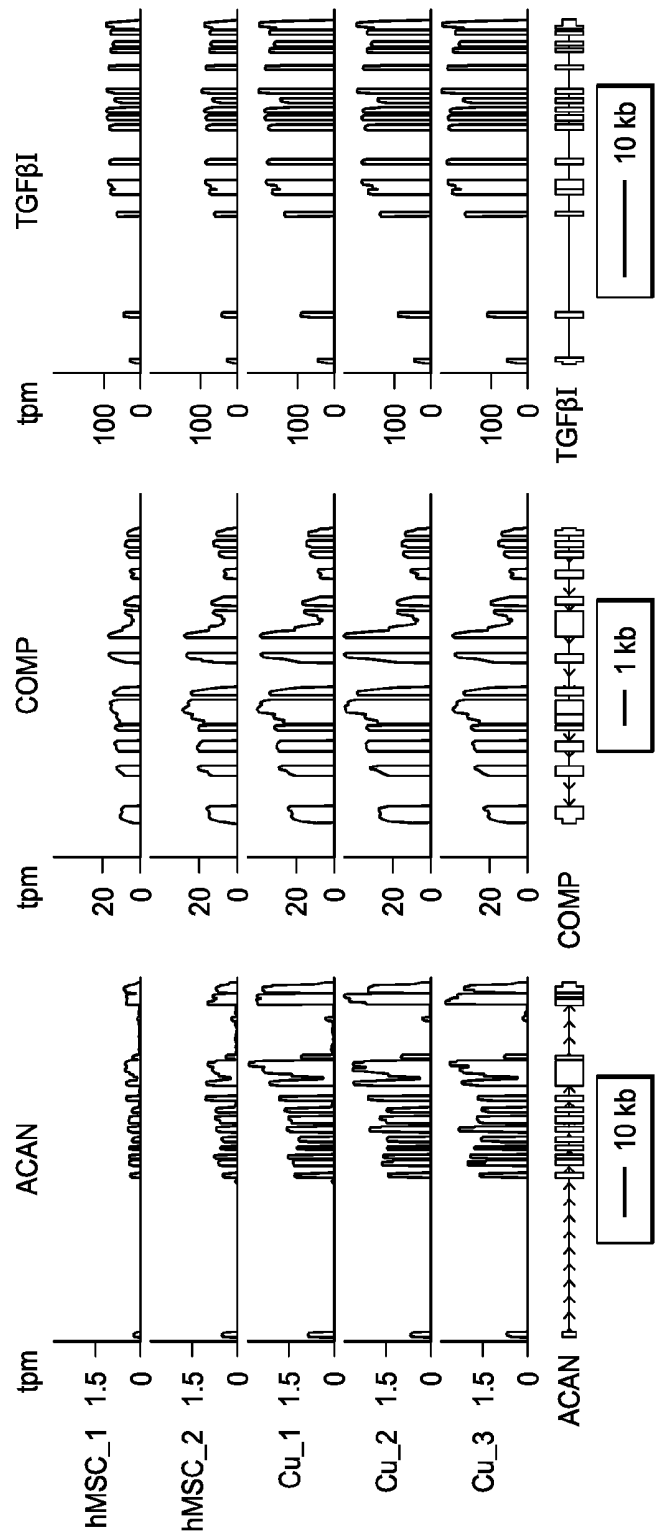
ACAN
COMP
TGFβI
tpm
hMSC_1
hMSC_2
Cu_1
Cu_2
Cu_3
1.5
0
20
100
10 kb
1 kb

FIG. 10D

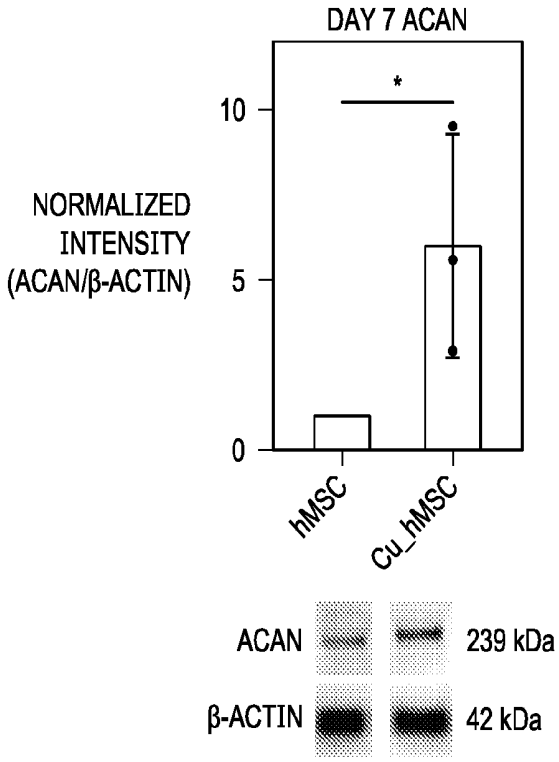

FIG. 10E

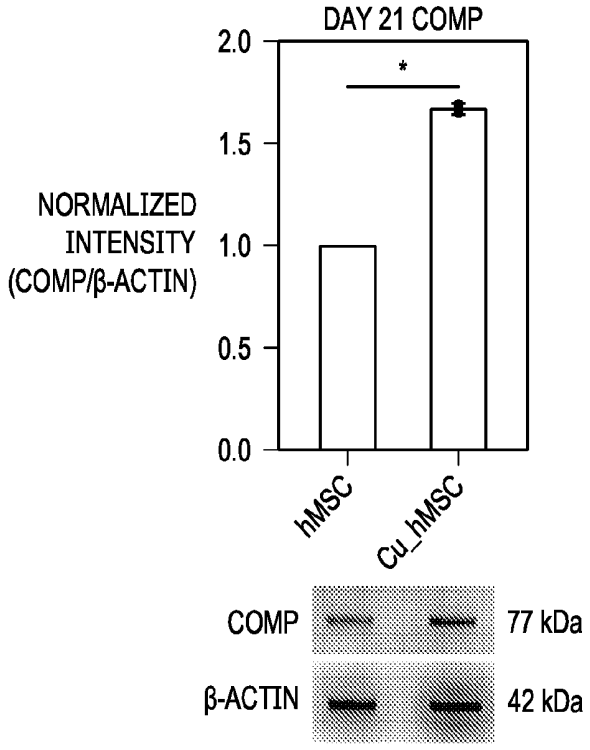

FIG. 10F

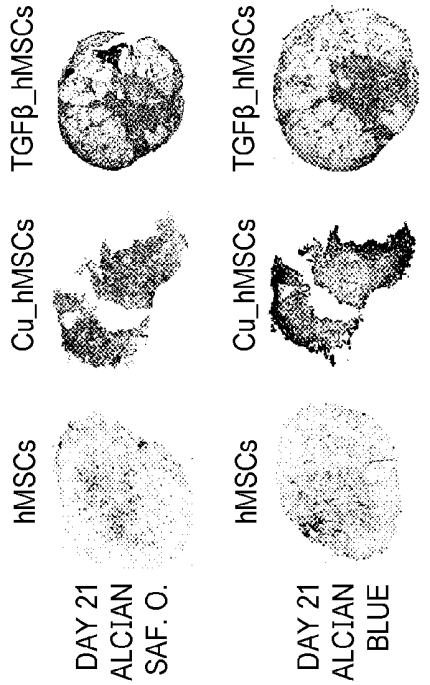

FIG. 10H

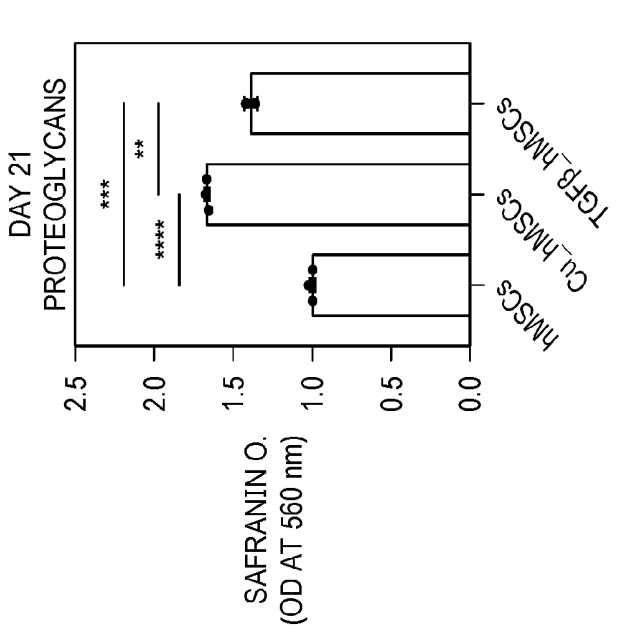

FIG. 10G

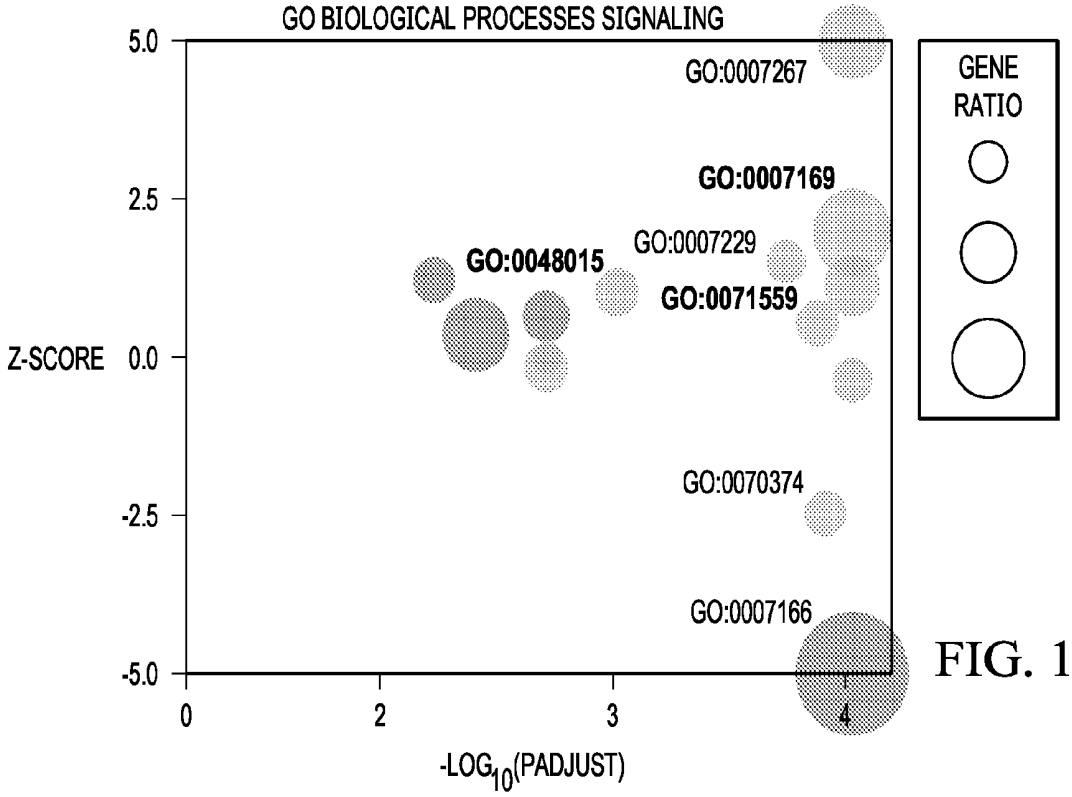

FIG. 10I

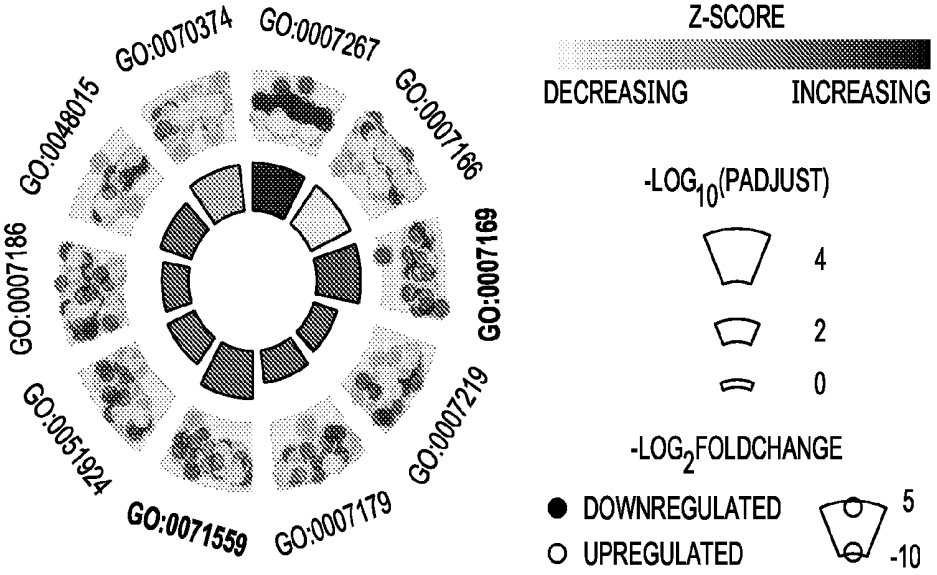

FIG. 10J

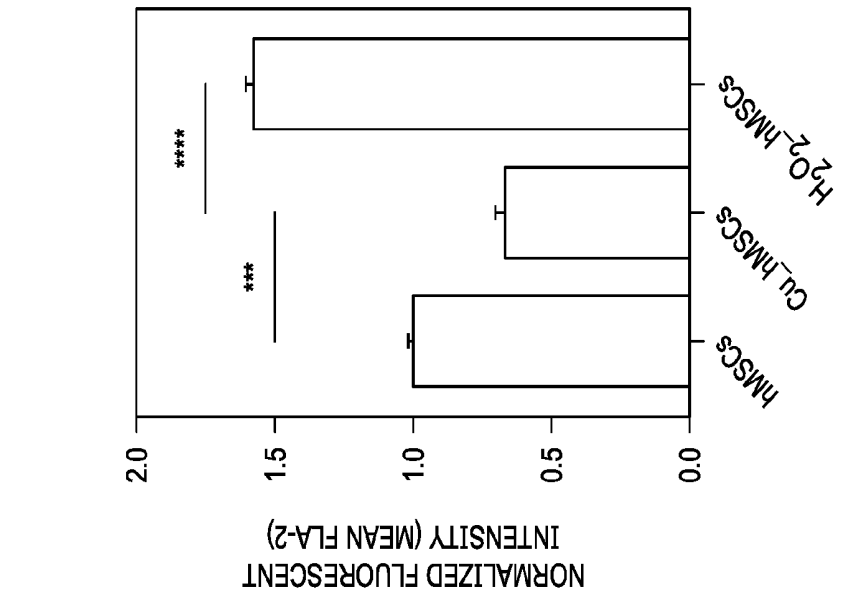

FIG. 11B

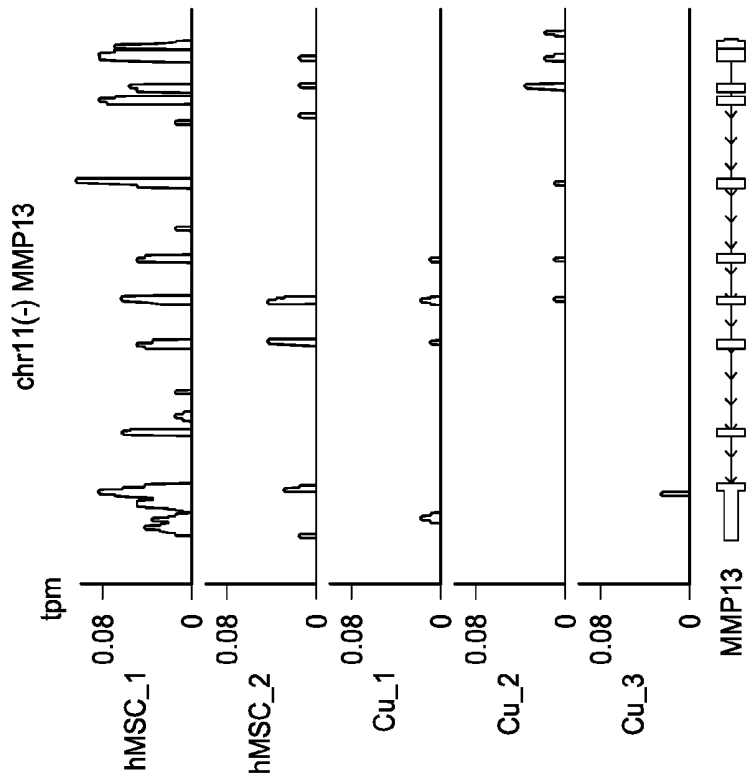

FIG. 11A

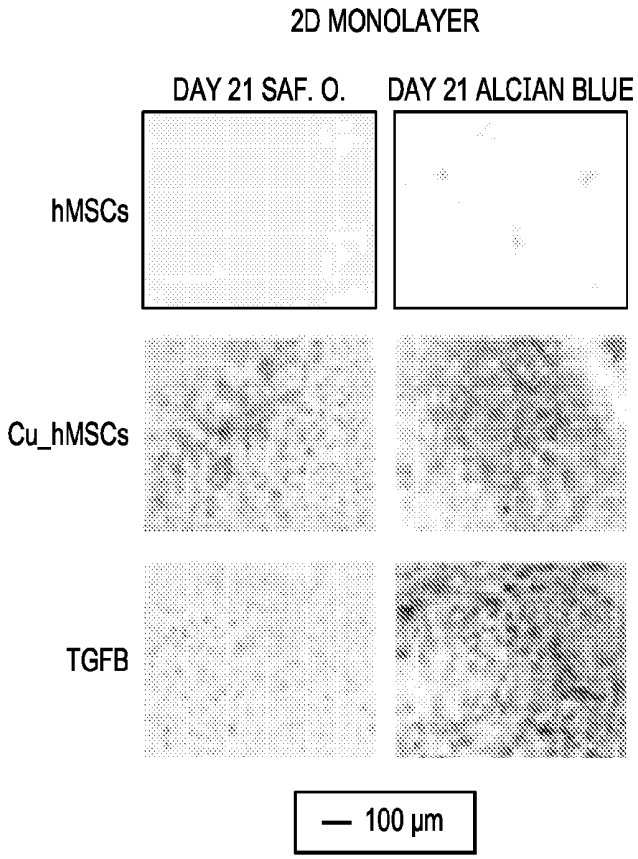

FIG. 12A

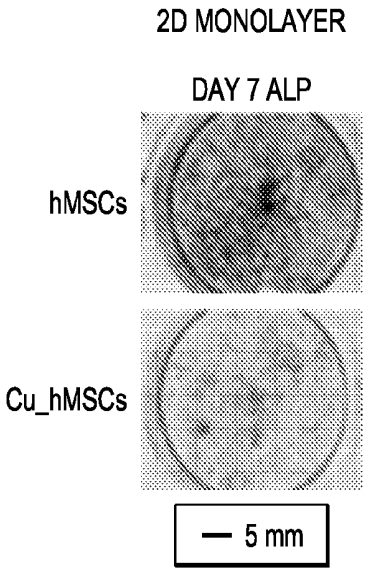

FIG. 12B

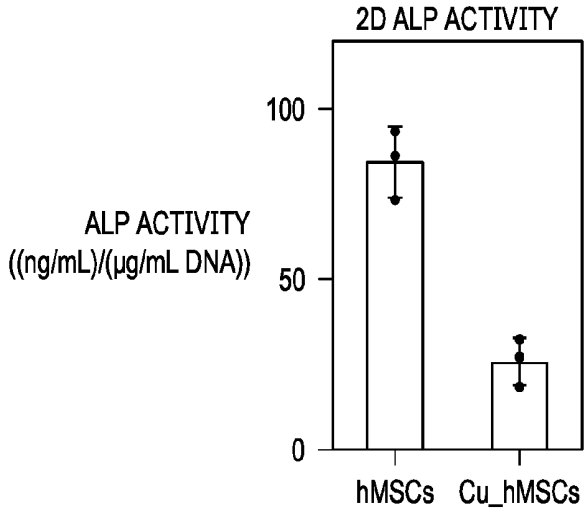

FIG. 12C

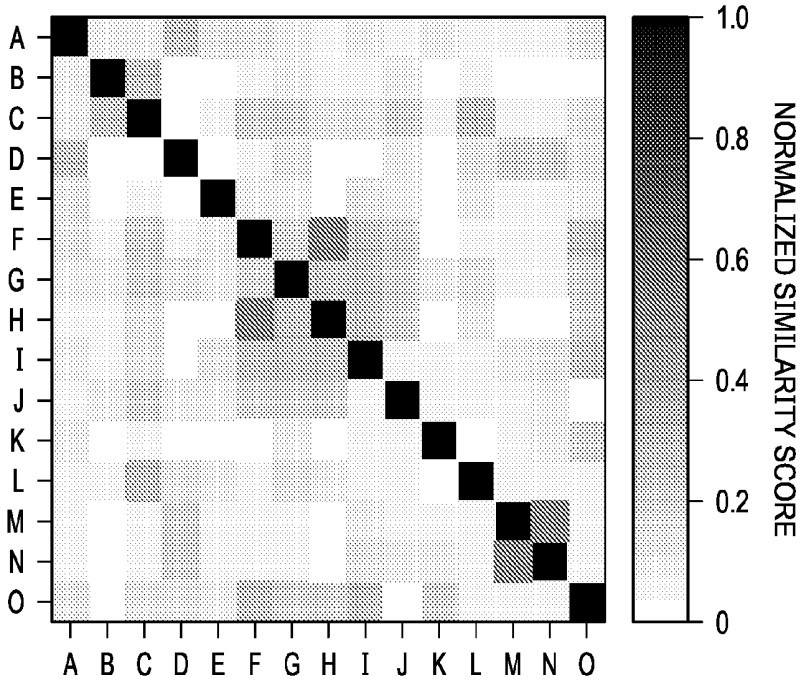

A: CELL-CELL ADHESION (GO:0007267)
B: CELL SURFACE RECEPTOR SIGNALING PATHWAY (GO:0007166)
C: G PROTEIN-COUPLED RECEPTOR SIGNALING PATHWAY (GO:0007186)
D: INTEGRIN MEDIATED SIGNALING PATHWAY (GO:0007229)
E: NOTCH SIGNALING PATHWAY (GO:0007219)
F: PHOSPHATIDYLINOSITOL-MEDIATED SIGNALING (GO:0048015)
G: POSITIVE REGULATION OF ERK1 AND ERK2 CASCADE (GO:0070374)
H: POSITIVE REGULATION OF PHOSPHATIDYLINOSITOL 3-KINASE SIGNALING (GO:0014068)
I: POSITIVE REGULATION OF PROTEIN KINASE B SIGNALING (GO:0043491)
J: REGULATION OF CALCIUM ION TRANSPORT (GO:0051924)
K: REGULATION OF FIBROBLAST GROWTH FACTOR RECEPTOR SIGNALING PATHWAY (GO:0040036)
L: REGULATION OF RHO PROTEIN SIGNAL TRANSDUCTION (GO:0035023)
M: RESPONSE TO TRANSFORMING GROWTH FACTOR BETA (GO:0071559)
N: TRANSFORMING GROWTH FACTOR BETA RECEPTOR SIGNALING PATHWAY (GO:0007179)
O: TRANSMEMBRANE RECEPTOR PROTEIN TYROSINE KINASE SIGNALING PATHWAY (GO:0007169)

FIG. 13

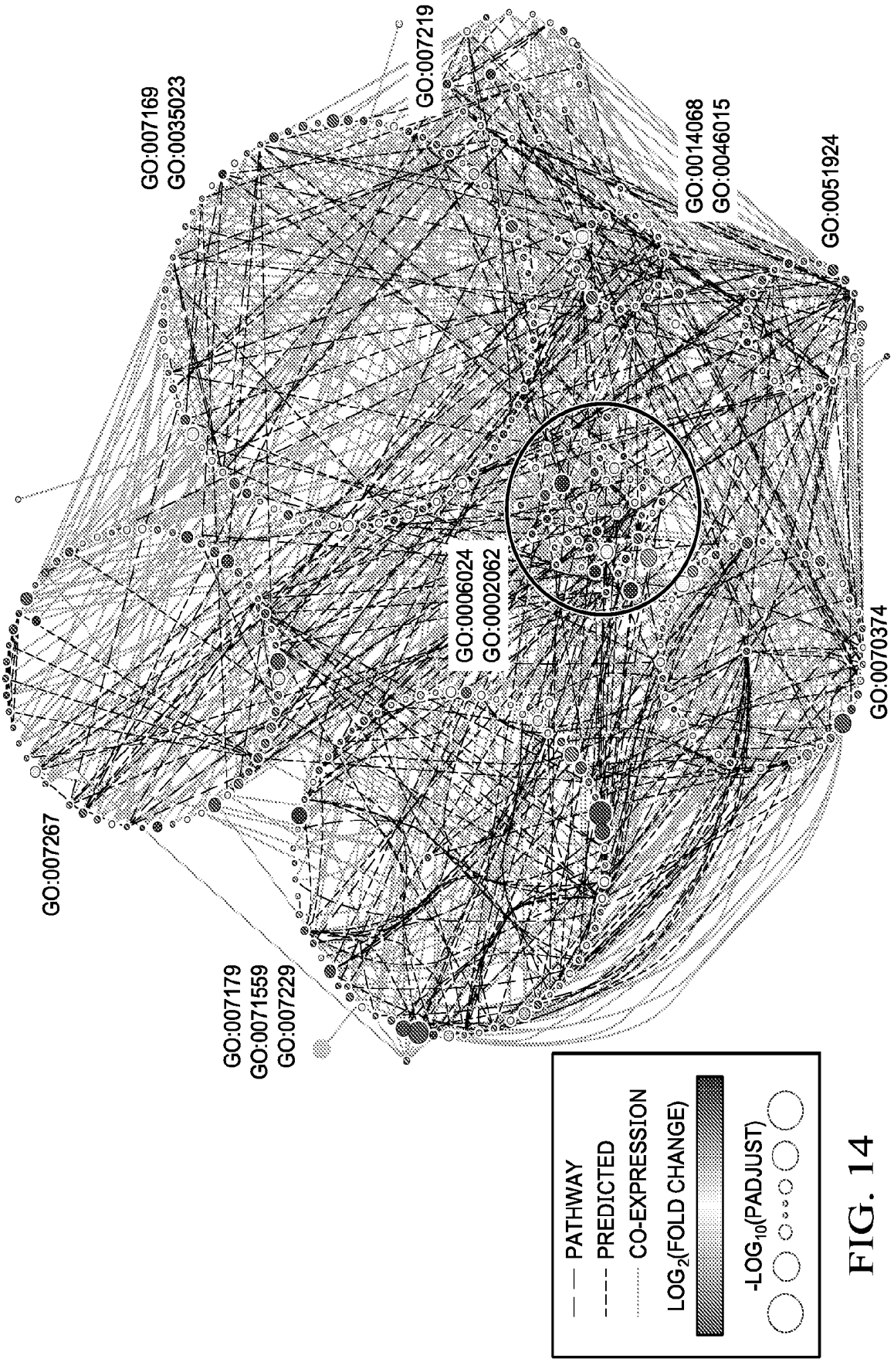
GO:007219
GO:007169
GO:0035023
GO:0014068
GO:0046015
GO:0051924
GO:0006024
GO:0002062
GO:0070374
GO:007267
GO:007179
GO:0071559
GO:007229
PATHWAY
PREDICTED
CO-EXPRESSION
LOG2(FOLD CHANGE)
-LOG10(PADJUST)

FIG. 14

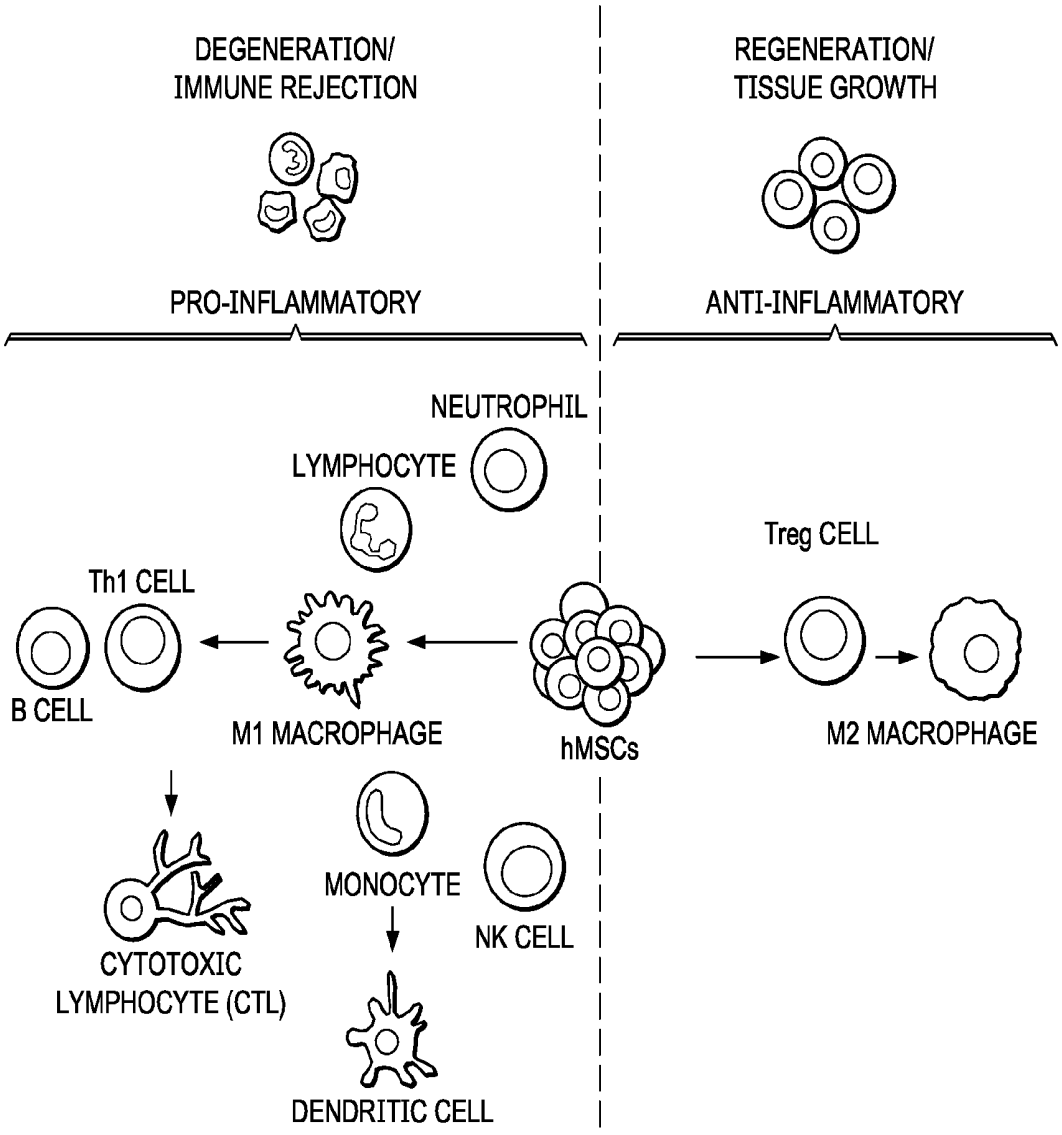
DEGENERATION/
IMMUNE REJECTION
REGENERATION/
TISSUE GROWTH
PRO-INFLAMMATORY
ANTI-INFLAMMATORY
NEUTROPHIL
LYMPHOCYTE
Th1 CELL
Treg CELL
B CELL
M1 MACROPHAGE
hMSCs
M2 MACROPHAGE
MONOCYTE
NK CELL
CYTOTOXIC
LYMPHOCYTE (CTL)
DENDRITIC CELL

FIG. 15A

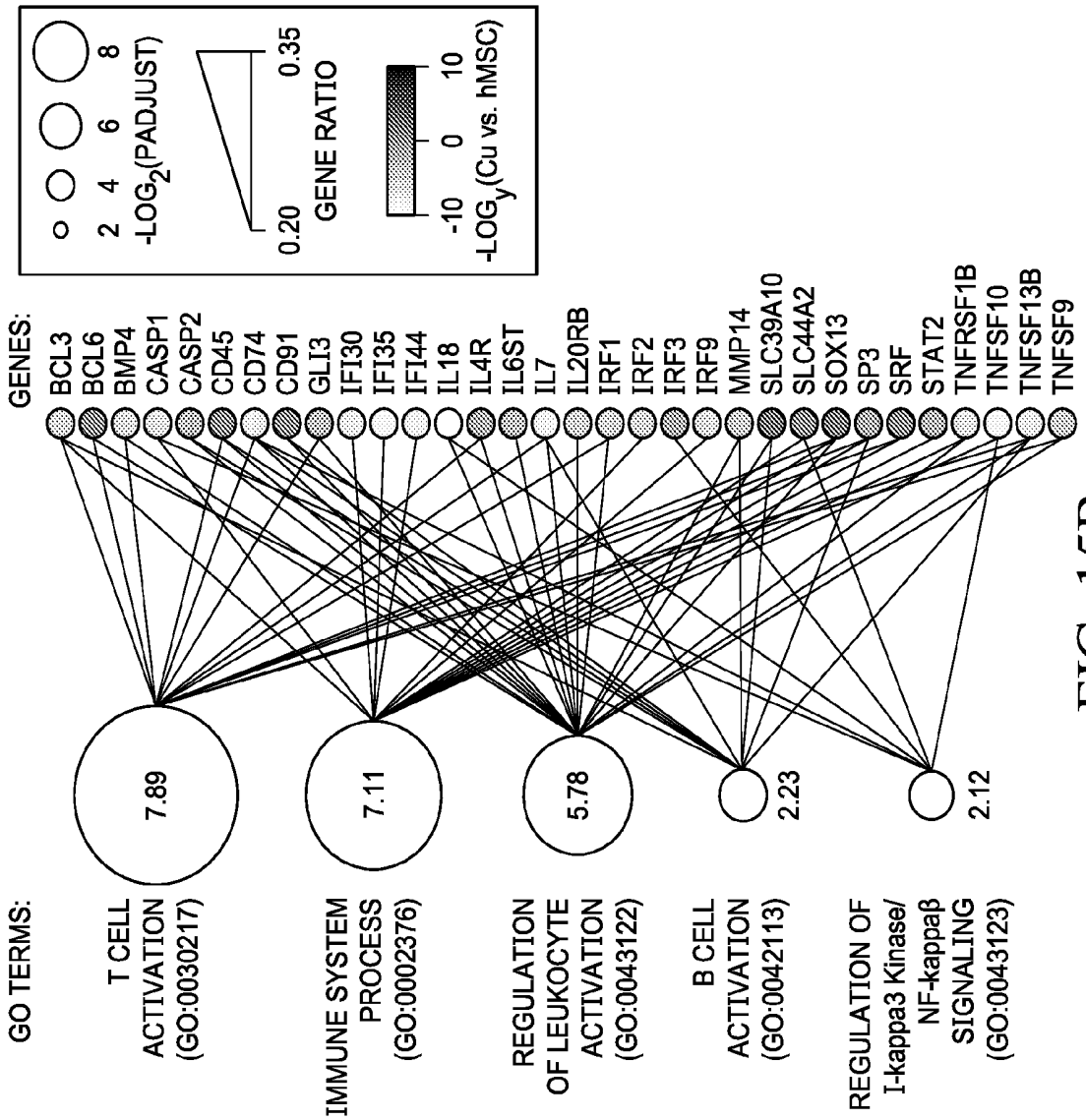

FIG. 15B

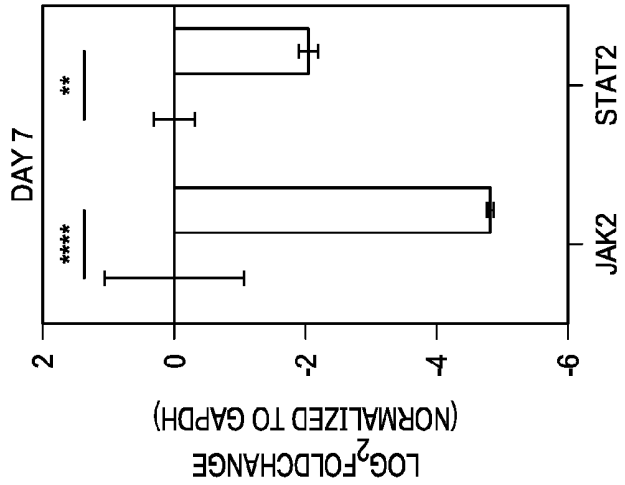

FIG. 15C

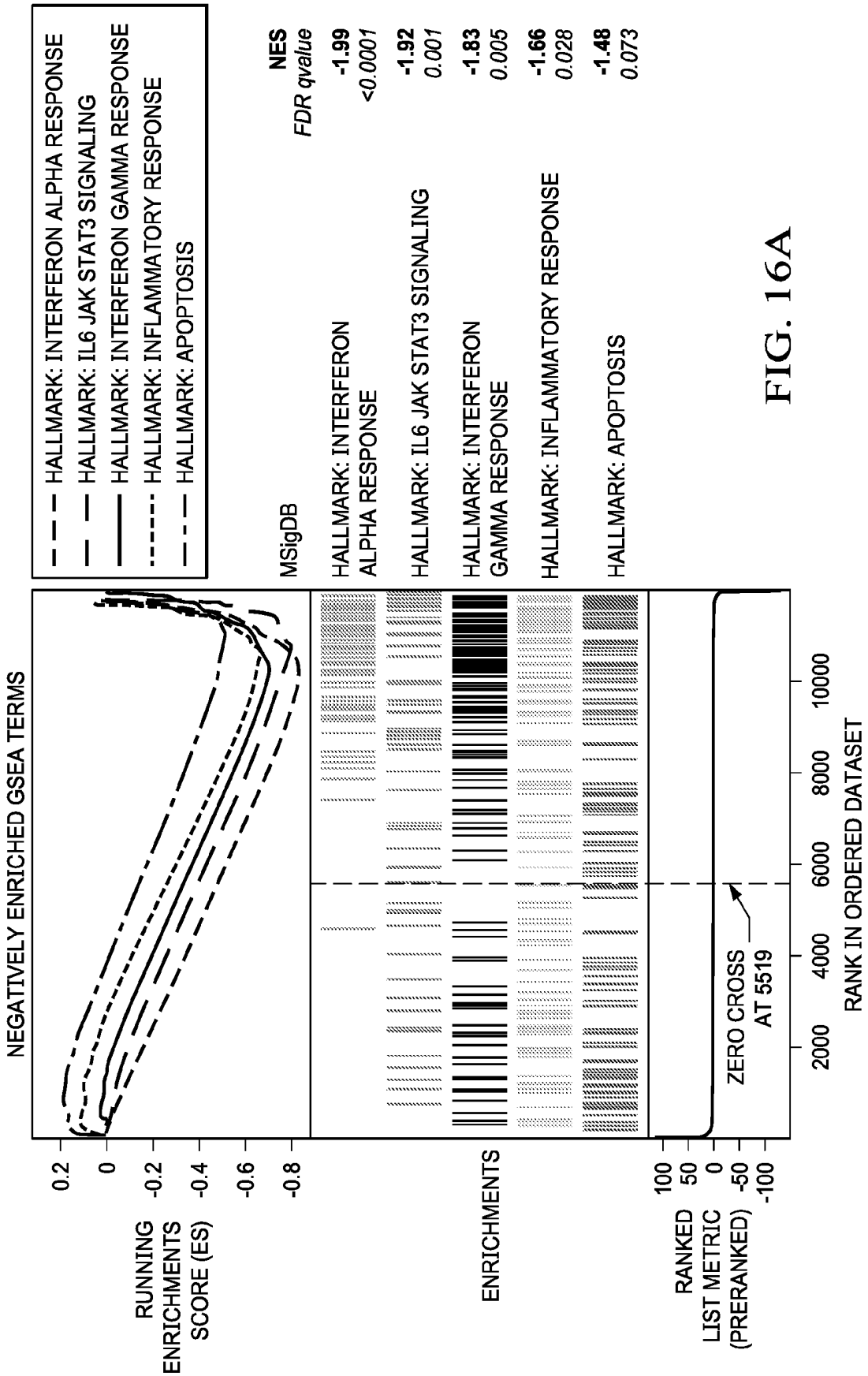
NEGATIVELY ENRICHED GSEA TERMS
HALLMARK: INTERFERON ALPHA RESPONSE
HALLMARK: IL6 JAK STAT3 SIGNALING
HALLMARK: INTERFERON GAMMA RESPONSE
HALLMARK: INFLAMMATORY RESPONSE
HALLMARK: APOPTOSIS
MSigDB
NES
FDR qvalue
HALLMARK: INTERFERON ALPHA RESPONSE
-1.99
<0.0001
HALLMARK: IL6 JAK STAT3 SIGNALING
-1.92
0.001
HALLMARK: INTERFERON GAMMA RESPONSE
-1.83
0.005
HALLMARK: INFLAMMATORY RESPONSE
-1.66
0.028
HALLMARK: APOPTOSIS
-1.48
0.073
RUNNING ENRICHMENTS SCORE (ES)
0.2
0
-0.2
-0.4
-0.6
-0.8
ENRICHMENTS
RANKED LIST METRIC (PRERANKED)
100
50
0
-50
-100
ZERO CROSS AT 5519
2000
4000
6000
8000
10000
RANK IN ORDERED DATASET

FIG. 16A

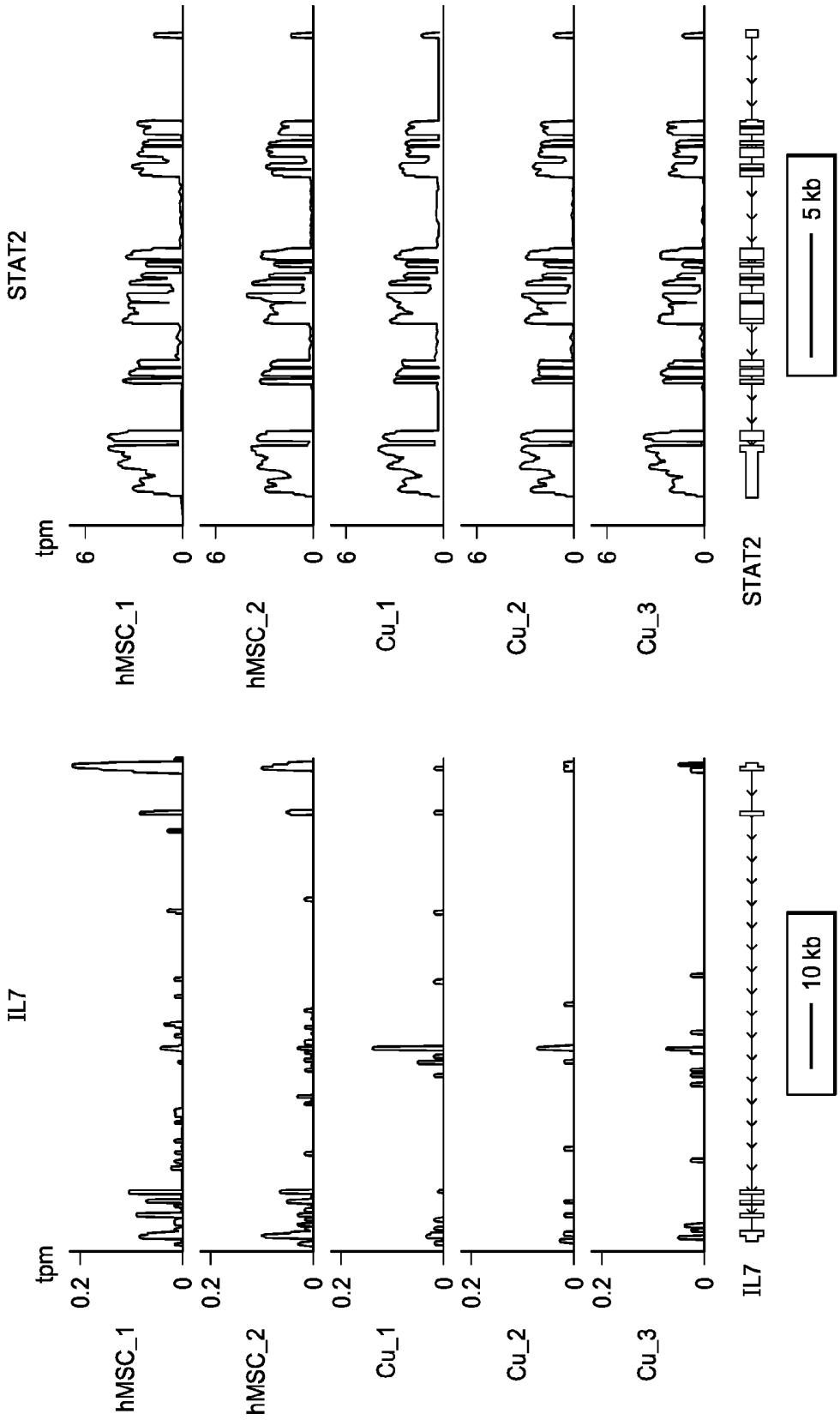
IL7
tpm
0.2
0
hMSC_1
hMSC_2
Cu_1
Cu_2
Cu_3
10 kb
STAT2
tpm
6
0
hMSC_1
hMSC_2
Cu_1
Cu_2
Cu_3
STAT2
5 kb

FIG. 16B

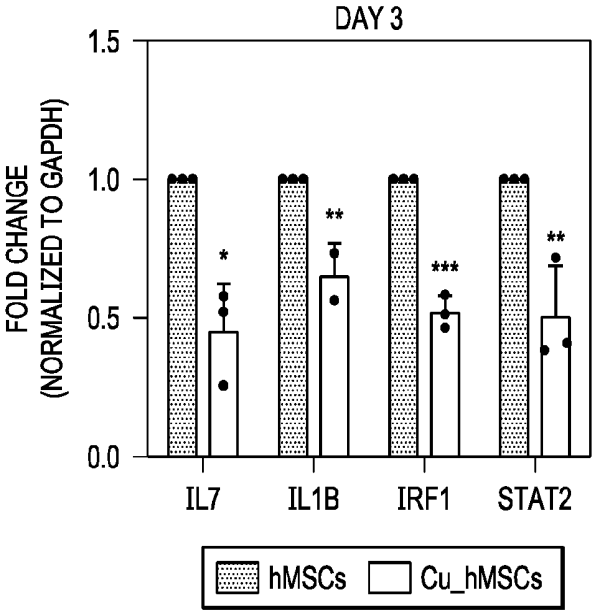

FIG. 16C

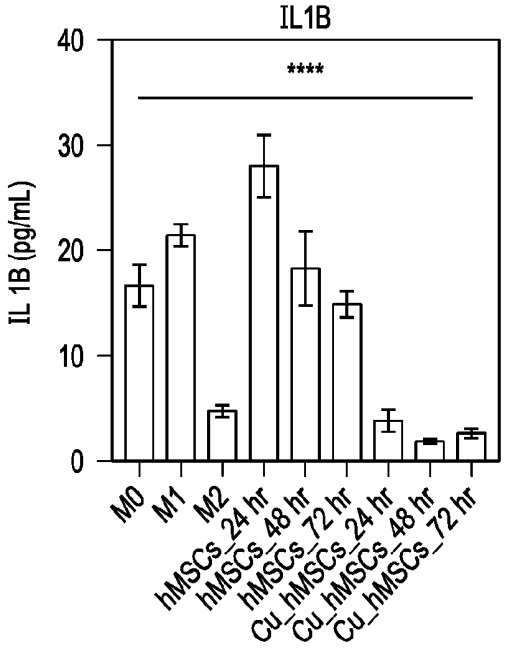

FIG. 16D

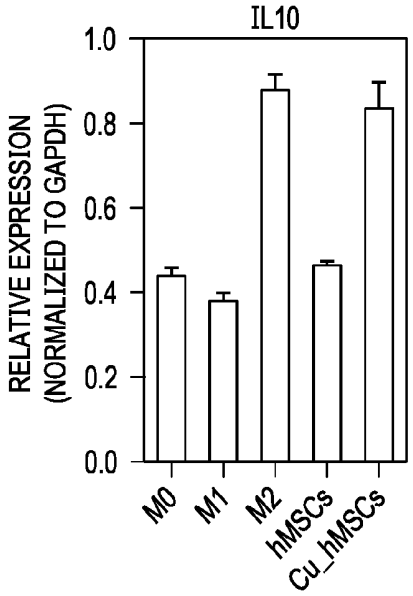

FIG. 16E

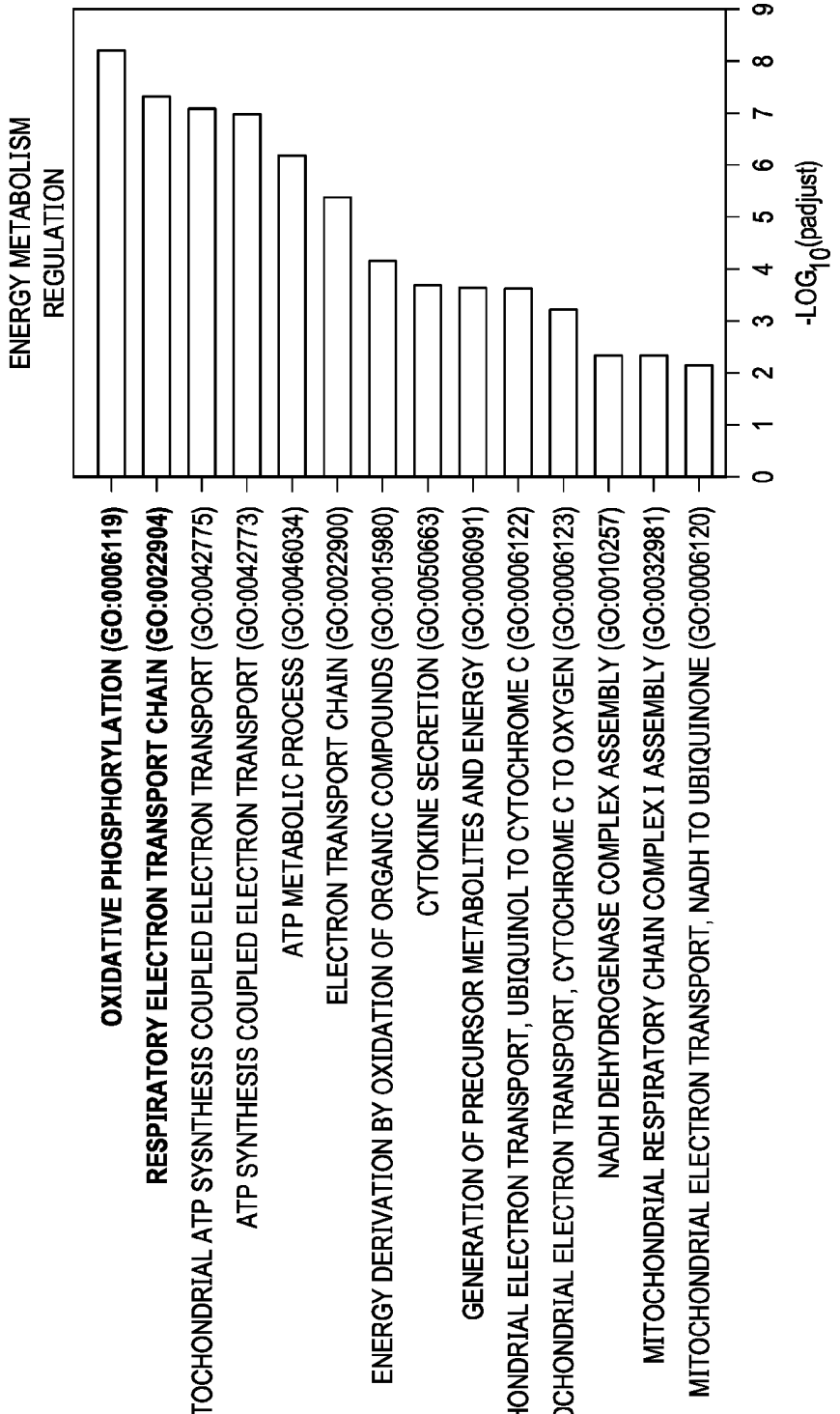
ENERGY METABOLISM
REGULATION
OXIDATIVE PHOSPHORYLATION (GO:0006119)
RESPIRATORY ELECTRON TRANSPORT CHAIN (GO:0022904)
MITOCHONDRIAL ATP SYSNTHESIS COUPLED ELECTRON TRANSPORT (GO:0042775)
ATP SYNTHESIS COUPLED ELECTRON TRANSPORT (GO:0042773)
ATP METABOLIC PROCESS (GO:0046034)
ELECTRON TRANSPORT CHAIN (GO:0022900)
ENERGY DERIVATION BY OXIDATION OF ORGANIC COMPOUNDS (GO:0015980)
CYTOKINE SECRETION (GO:0050663)
GENERATION OF PRECURSOR METABOLITES AND ENERGY (GO:0006091)
MITOCHONDRIAL ELECTRON TRANSPORT, UBIQUINOL TO CYTOCHROME C (GO:0006122)
MITOCHONDRIAL ELECTRON TRANSPORT, CYTOCHROME C TO OXYGEN (GO:0006123)
NADH DEHYDROGENASE COMPLEX ASSEMBLY (GO:0010257)
MITOCHONDRIAL RESPIRATORY CHAIN COMPLEX I ASSEMBLY (GO:0032981)
MITOCHONDRIAL ELECTRON TRANSPORT, NADH TO UBIQUINONE (GO:0006120)
0 1 2 3 4 5 6 7 8 9
-LOG10(padjust)

FIG. 17A

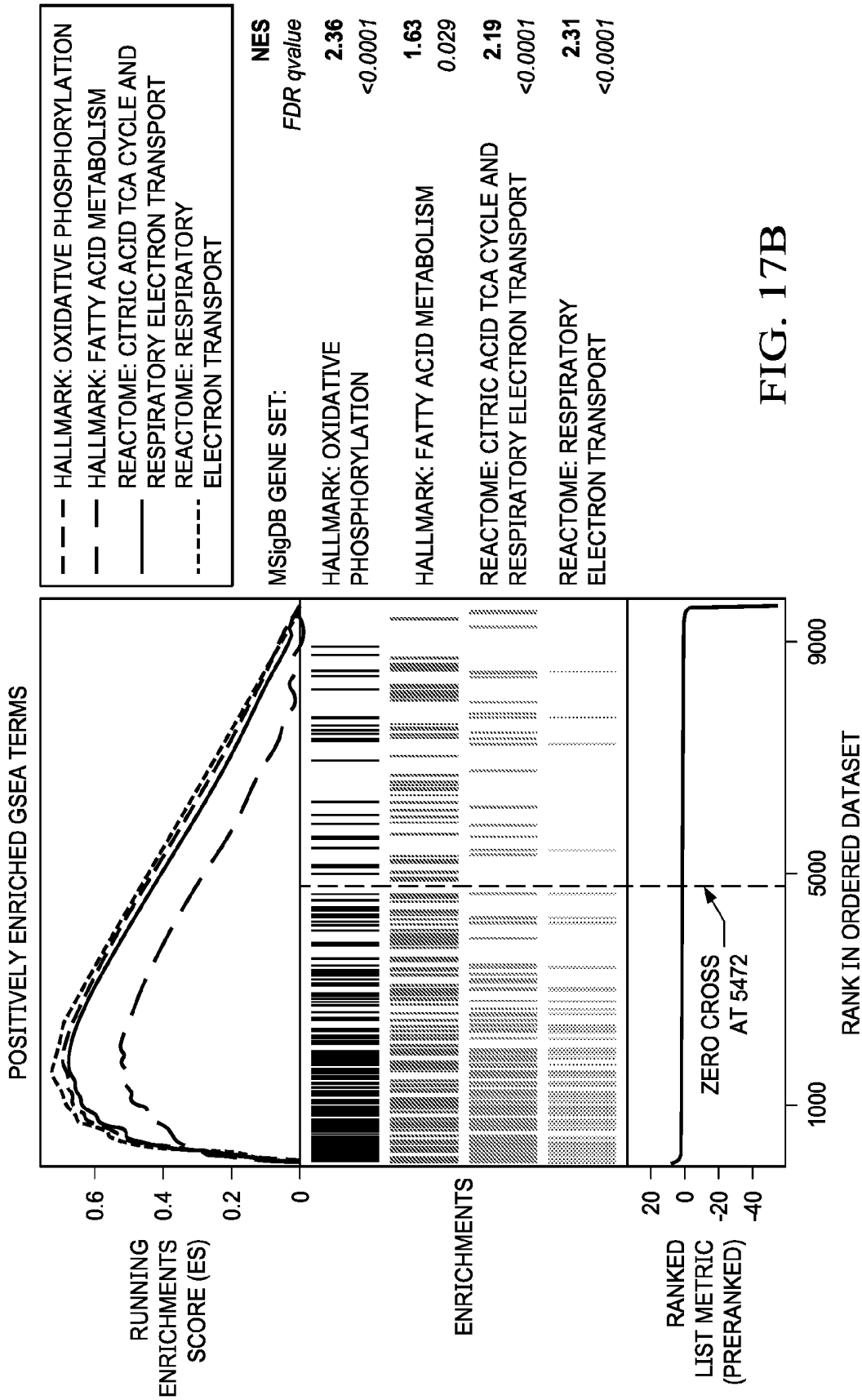
HALLMARK: OXIDATIVE PHOSPHORYLATION
HALLMARK: FATTY ACID METABOLISM
REACTOME: CITRIC ACID TCA CYCLE AND RESPIRATORY ELECTRON TRANSPORT
REACTOME: RESPIRATORY ELECTRON TRANSPORT
MSigDB GENE SET:
NES
FDR qvalue
HALLMARK: OXIDATIVE PHOSPHORYLATION
2.36
<0.0001
HALLMARK: FATTY ACID METABOLISM
1.63
0.029
REACTOME: CITRIC ACID TCA CYCLE AND RESPIRATORY ELECTRON TRANSPORT
2.19
<0.0001
REACTOME: RESPIRATORY ELECTRON TRANSPORT
2.31
<0.0001
POSITIVELY ENRICHED GSEA TERMS
RUNNING ENRICHMENTS SCORE (ES)
0.6
0.4
0.2
0
ENRICHMENTS
RANKED LIST METRIC (PRERANKED)
20
0
-20
-40
ZERO CROSS AT 5472
1000
5000
9000
RANK IN ORDERED DATASET

FIG. 17B

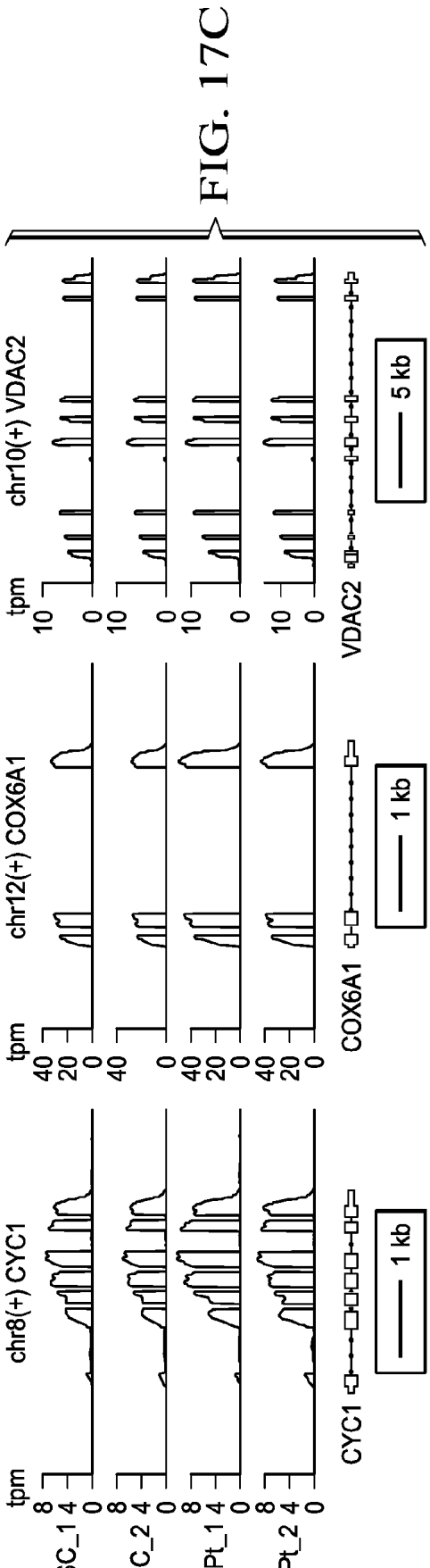

FIG. 17C

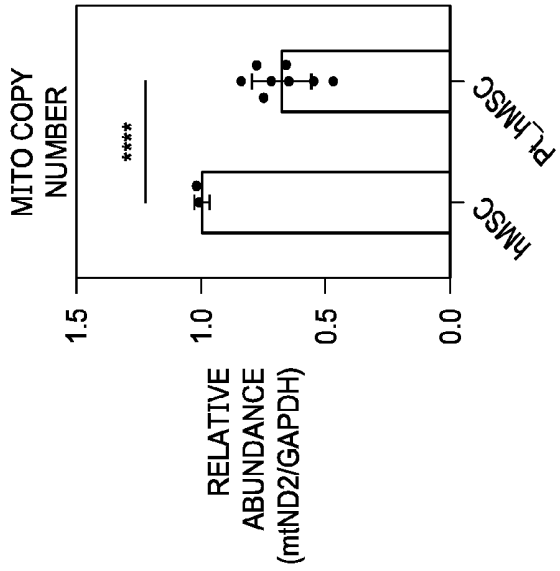

FIG. 17D

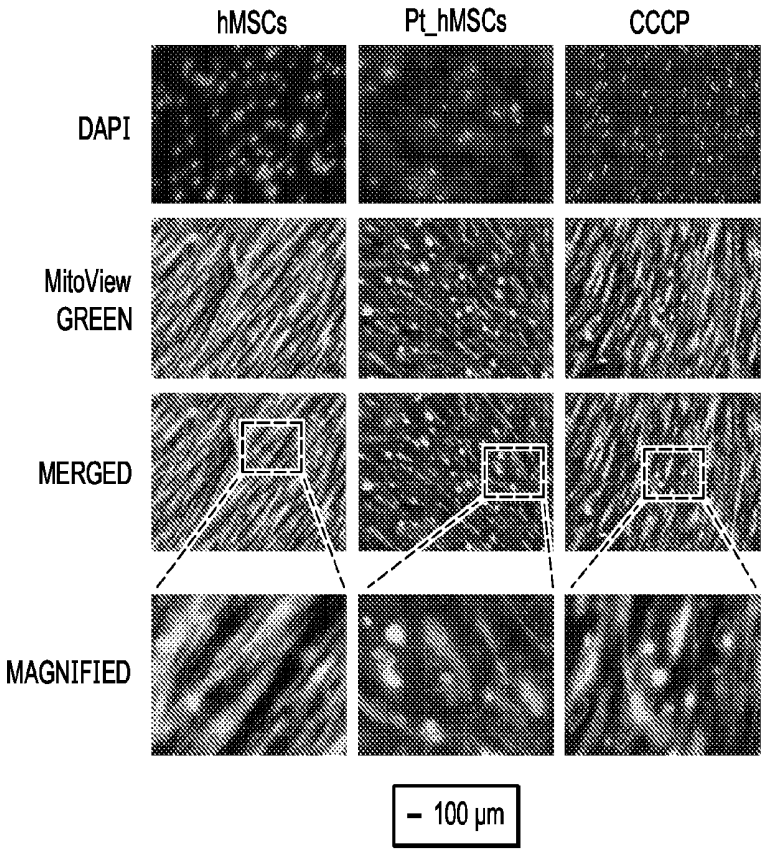

FIG. 17E

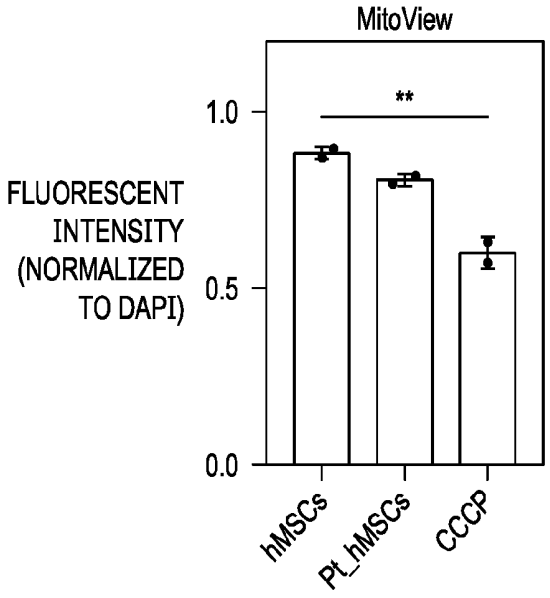

FIG. 17F

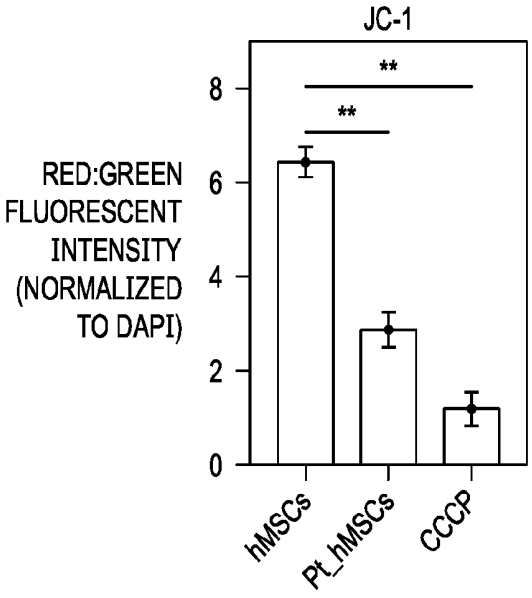

FIG. 17G

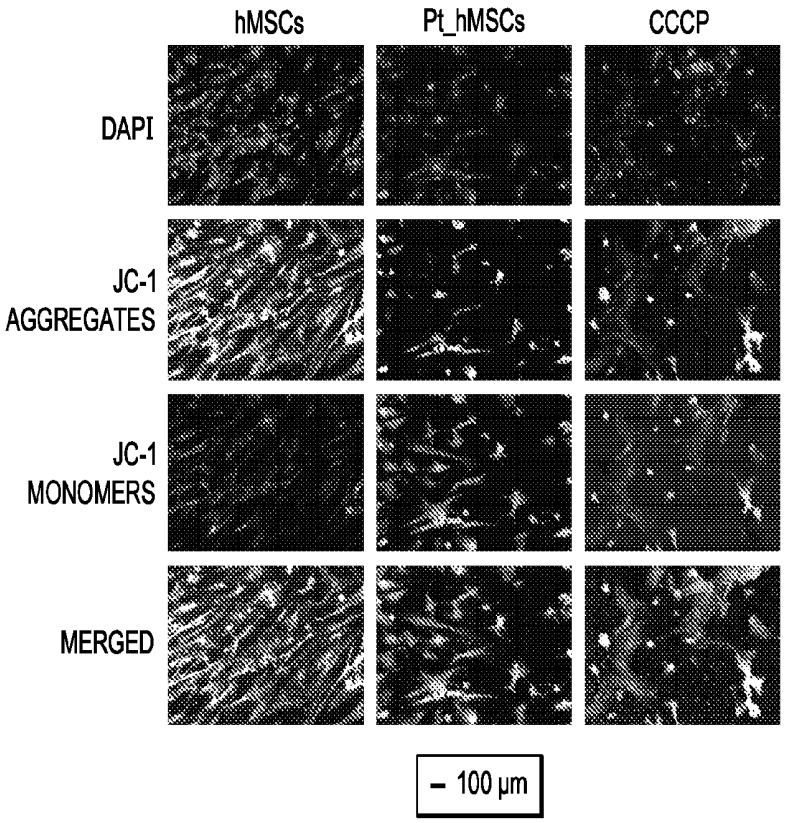

FIG. 17H

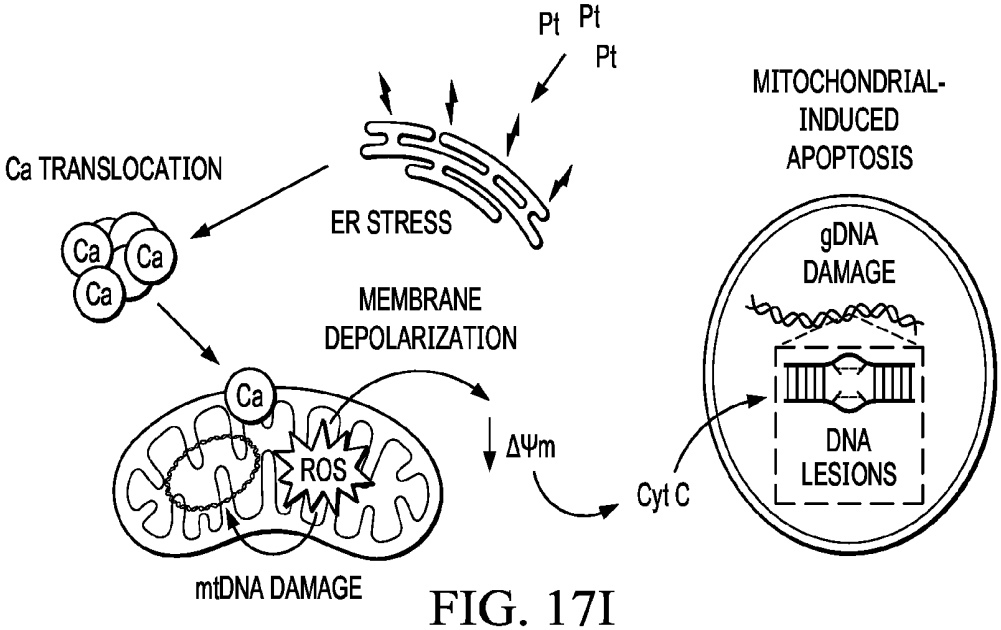

FIG. 17I

FIG. 18

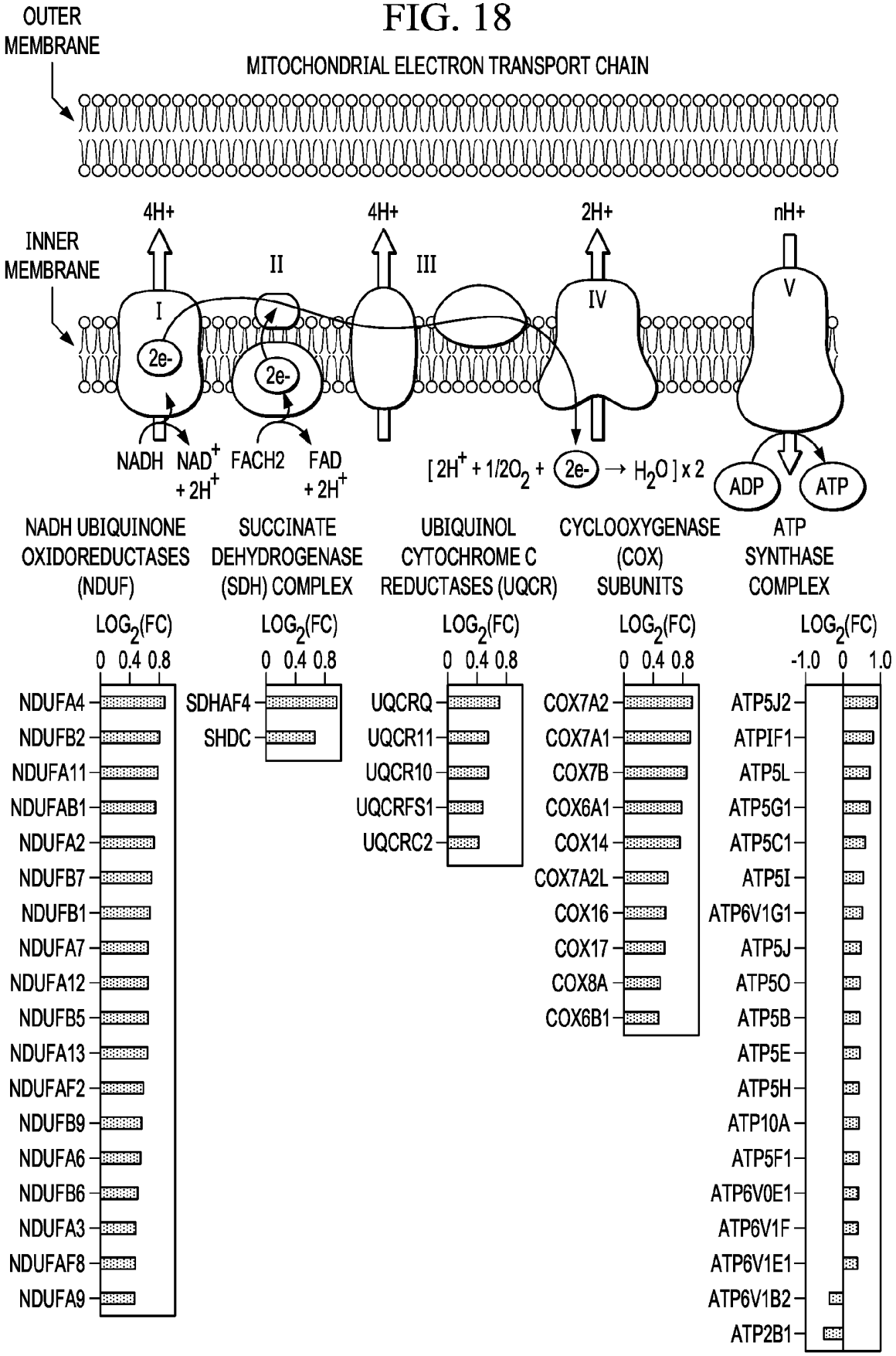
OUTER MEMBRANE
MITOCHONDRIAL ELECTRON TRANSPORT CHAIN
INNER MEMBRANE
4H+
4H+
2H+
nH+
I
II
III
IV
V
2e-
2e-
NADH
NAD+ + 2H+
FACH2
FAD + 2H+
[2H+ + 1/2O2 + 2e- → H2O] x 2
ADP
ATP
NADH UBIQUINONE OXIDOREDUCTASES (NDUF)
SUCCINATE DEHYDROGENASE (SDH) COMPLEX
UBIQUINOL CYTOCHROME C REDUCTASES (UQCR)
CYCLOOXYGENASE (COX) SUBUNITS
ATP SYNTHASE COMPLEX
LOG2(FC)
0 0.4 0.8
NDUFA4
NDUFB2
NDUFA11
NDUFAB1
NDUFA2
NDUFB7
NDUFB1
NDUFA7
NDUFA12
NDUFB5
NDUFA13
NDUFAF2
NDUFB9
NDUFA6
NDUFB6
NDUFA3
NDUFAF8
NDUFA9
SDHAF4
SHDC
UQCRQ
UQCR11
UQCR10
UQCRFS1
UQCRC2
COX7A2
COX7A1
COX7B
COX6A1
COX14
COX7A2L
COX16
COX17
COX8A
COX6B1
-1.0 0 1.0
ATP5J2
ATPIF1
ATP5L
ATP5G1
ATP5C1
ATP5I
ATP6V1G1
ATP5J
ATP5O
ATP5B
ATP5E
ATP5H
ATP10A
ATP5F1
ATP6V0E1
ATP6V1F
ATP6V1E1
ATP6V1B2
ATP2B1

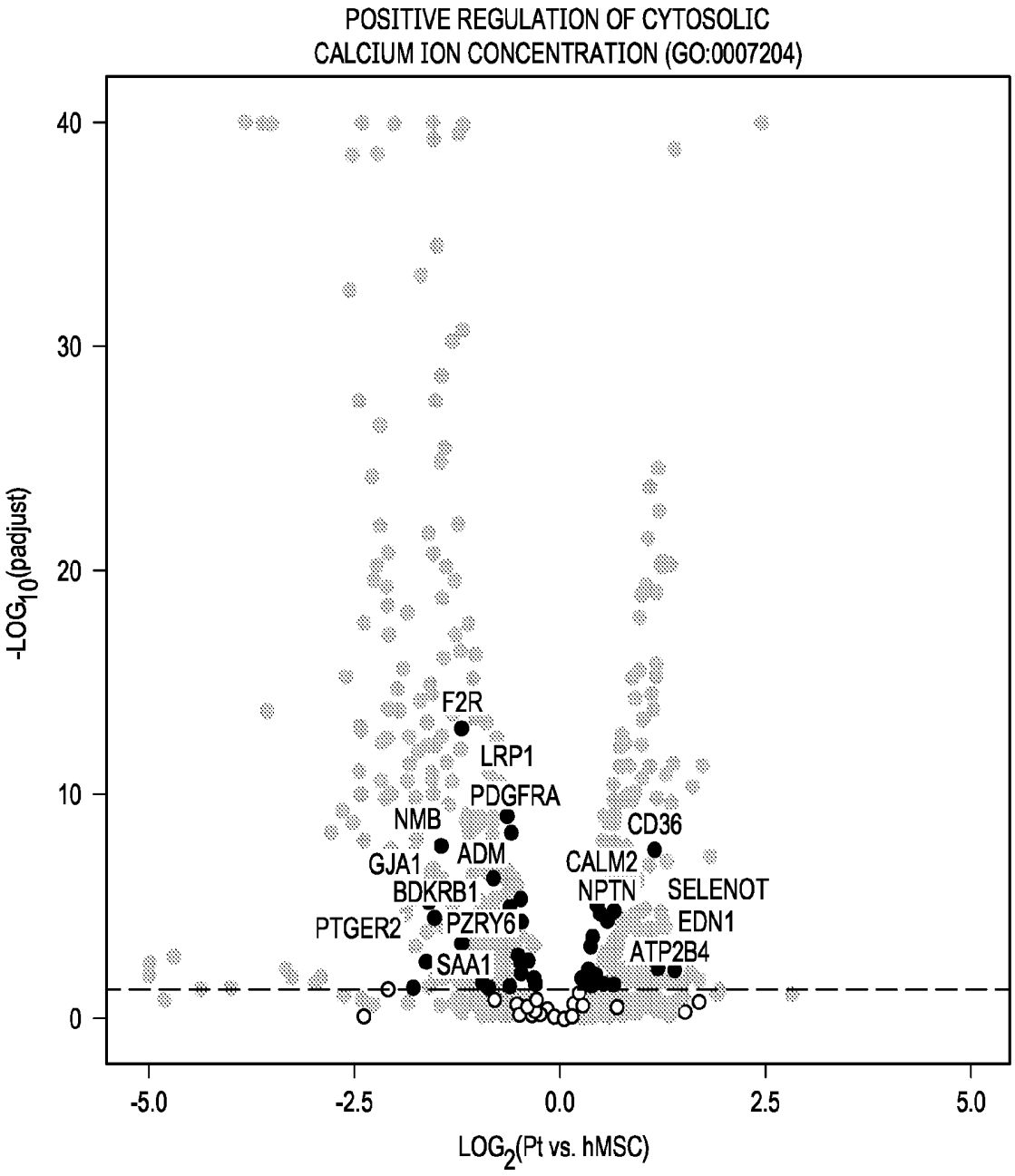
POSITIVE REGULATION OF CYTOSOLIC
CALCIUM ION CONCENTRATION (GO:0007204)
40
30
20
10
0
-LOG10(padjust)
F2R
LRP1
PDGFRA
NMB
CD36
ADM
GJA1
CALM2
BDKRB1
NPTN
SELENOT
PTGER2
PZRY6
EDN1
ATP2B4
SAA1
-5.0
-2.5
0.0
2.5
5.0
LOG2(Pt vs. hMSC)

FIG. 19A

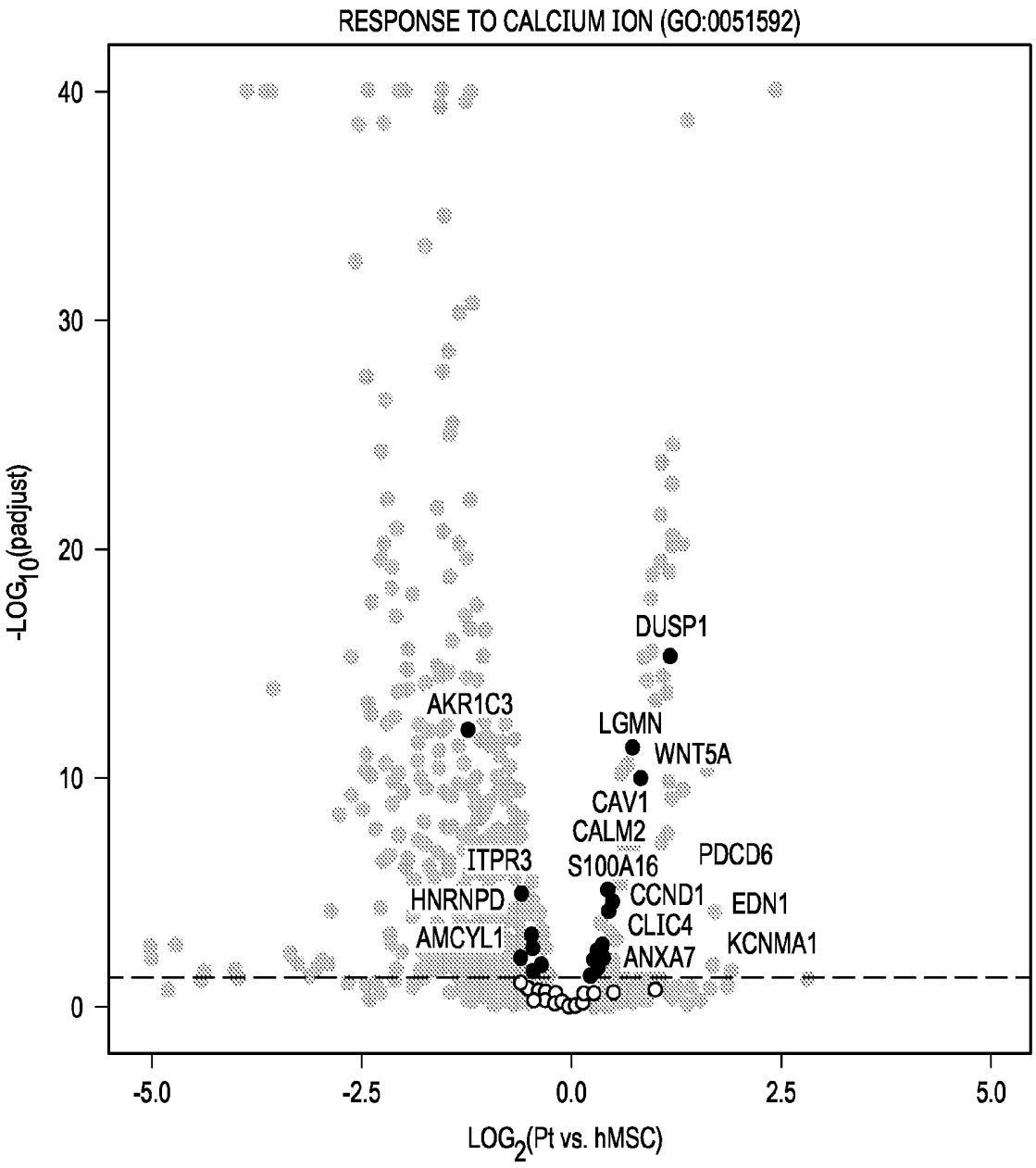
RESPONSE TO CALCIUM ION (GO:0051592)
40
30
20
10
0
-LOG10(padjust)
DUSP1
AKR1C3
LGMN
WNT5A
CAV1
CALM2
ITPR3
S100A16
PDCD6
HNRNPD
CCND1
EDN1
CLIC4
AMCYL1
KCNMA1
ANXA7
-5.0
-2.5
0.0
2.5
5.0
LOG2(Pt vs. hMSC)

FIG. 19B

INTERNATIONAL SEARCH REPORT

International application No.
PCT/US2024/059993

A. CLASSIFICATION OF SUBJECT MATTER

IPC: ***A61K 33/38*** (2025.01); ***A61K 47/62*** (2025.01); ***A61L 27/54*** (2025.01); ***A61P 19/10*** (2025.01); ***A61K 33/34*** (2025.01); *B82Y 5/00* (2025.01)

CPC: ***A61K 33/38; A61P 19/10; A61L 27/54; A61K 33/34; A61K 47/62;*** *A61K 2121/00; B82Y 5/00*

According to International Patent Classification (IPC) or to both national classification and IPC

B. FIELDS SEARCHED

Minimum documentation searched (classification system followed by classification symbols)

See Search History Document

Documentation searched other than minimum documentation to the extent that such documents are included in the fields searched

See Search History Document

Electronic data base consulted during the international search (name of data base and, where practicable, search terms used)

See Search History Document

C. DOCUMENTS CONSIDERED TO BE RELEVANT

Category*	Citation of document, with indication, where appropriate, of the relevant passages	Relevant to claim No.
	US 2020/0330510 A1 (BOARD OF TRUSTEES OF MICHIGAN STATE UNIVERSITY) 22 October 2020 (22.10.2020)	
X	entire document	1, 5-7, 9-13
Y	entire document	2-4, 8
	US 2010/0297200 A1 (SCHOENFISCH et al.) 25 November 2010 (25.11.2010)	
Y	entire document	8
	CN 111088225 B (LANCY PURCELL BIOTECHNOLOGY GUANGZHOU) 01 September 2020 (01.09.2020)	
A	see machine translation	1-13
	US 2024/0293448 A1 (KING FAISAL UNIVERSITY) 05 September 2024 (05.09.2024)	
P, X	entire document	1-13

☑ Further documents are listed in the continuation of Box C. ☐ See patent family annex.

* Special categories of cited documents:
"A" document defining the general state of the art which is not considered to be of particular relevance
"D" document cited by the applicant in the international application
"E" earlier application or patent but published on or after the international filing date
"L" document which may throw doubts on priority claim(s) or which is cited to establish the publication date of another citation or other special reason (as specified)
"O" document referring to an oral disclosure, use, exhibition or other means
"P" document published prior to the international filing date but later than the priority date claimed
"T" later document published after the international filing date or priority date and not in conflict with the application but cited to understand the principle or theory underlying the invention
"X" document of particular relevance; the claimed invention cannot be considered novel or cannot be considered to involve an inventive step when the document is taken alone
"Y" document of particular relevance; the claimed invention cannot be considered to involve an inventive step when the document is combined with one or more other such documents, such combination being obvious to a person skilled in the art
"&" document member of the same patent family

Date of the actual completion of the international search	Date of mailing of the international search report
27 January 2025 (27.01.2025)	**25 March 2025 (25.03.2025)**

Name and mailing address of the ISA/US	Authorized officer
COMMISSIONER FOR PATENTS **MAIL STOP PCT, ATTN: ISA/US** **P.O. Box 1450** **Alexandria, VA 22313-1450** **UNITED STATES OF AMERICA**	**TAINA MATOS**
Facsimile No. **571-273-8300**	Telephone No. **571-272-4300**

INTERNATIONAL SEARCH REPORT

International application No.
PCT/US2024/059993

Box No. I Nucleotide and/or amino acid sequence(s) (Continuation of item 1.c of the first sheet)

1. With regard to any nucleotide and/or amino acid sequence disclosed in the international application, the international search was carried out on the basis of a sequence listing:
   a. ☑ forming part of the international application as filed.
   b. ☐ furnished subsequent to the international filing date for the purposes of international search (Rule 13*ter*.1(a)),
      ☐ accompanied by a statement to the effect that the sequence listing does not go beyond the disclosure in the international application as filed.

2. ☐ With regard to any nucleotide and/or amino acid sequence disclosed in the international application, this report has been established to the extent that a meaningful search could be carried out without a WIPO Standard ST.26 compliant sequence listing.

3. Additional comments:

INTERNATIONAL SEARCH REPORT

International application No.
PCT/US2024/059993

Box No. III Observations where unity of invention is lacking (Continuation of item 3 of first sheet)

This International Searching Authority found multiple inventions in this international application, as follows:

This application contains the following inventions or groups of inventions which are not so linked as to form a single general inventive concept under PCT Rule 13.1. In order for all inventions to be examined, the appropriate additional examination fees need to be paid.

Group I: claims 1-13 are drawn to methods of inducing osteoblast differentiation of a stem cell in a subject in need thereof.

Group II: claims 14-26 are drawn to methods of inducing chondrocyte differentiation of a stem cell in a subject in need thereof.

Group III: claims 27-33 are drawn to pharmaceutical compositions.

The inventions listed in Groups I-III do not relate to a single general inventive concept under PCT Rule 13.1, because under PCT Rule 13.2 they lack the same or corresponding special technical features for the following reasons:

The special technical features of Group I, methods of inducing osteoblast differentiation of a stem cell in a subject in need thereof, are not present in Groups II and III; the special technical features of Group II, methods of inducing chondrocyte differentiation of a stem cell in a subject in need thereof, are not present in Groups I and III; and the special technical features of Group III, pharmaceutical compositions, are not present in Groups I and II.

Additionally, even if Groups I-III were considered to share the technical features of a method of inducing differentiation of a stem cell in a subject in need thereof, the method comprising administering to the subject an effective amount of an ion composition to induce differentiation, these shared technical features do not represent a contribution over the prior art as disclosed by US 2020/0330510 to Board of Trustees of Michigan State University (hereinafter, "MSU").

MSU teaches a method of inducing differentiation of a stem cell (bioactive glass-ceramic scaffold promotes proliferation and differentiation of cells that are in contact with the bioactive glass-ceramic scaffold, Para. [0057]) in a subject in need thereof (the Ag-doped glass-ceramic microparticles or the Ag-doped glass-ceramic nanoparticles… regenerate bone tissue in the subject, Para. [0056]) the method comprising administering to the subject an effective amount of an ion composition to induce differentiation (the source of silver ions is a plurality of silver-doped bioactive glass particles (Ag-BG), Para. [0019]; Ag-BG not only enhanced cell proliferation rate and osteoblastic differentiation in hBMSCs, but also promote bone formation in vivo, Para. [0308]).

The inventions listed in Groups I-III therefore lack unity under Rule 13 because they do not share a same or corresponding special technical feature.

INTERNATIONAL SEARCH REPORT

International application No.
PCT/US2024/059993

Box No. III Observations where unity of invention is lacking (Continuation of item 3 of first sheet)

1. ☐ As all required additional search fees were timely paid by the applicant, this international search report covers all searchable claims.

2. ☐ As all searchable claims could be searched without effort justifying additional fees, this Authority did not invite payment of additional fees.

3. ☐ As only some of the required additional search fees were timely paid by the applicant, this international search report covers only those claims for which fees were paid, specifically claims Nos.:

4. ☑ No required additional search fees were timely paid by the applicant. Consequently, this international search report is restricted to the invention first mentioned in the claims; it is covered by claims Nos.: **1-13**

Remark on Protest

☐ The additional search fees were accompanied by the applicant's protest and, where applicable, the payment of a protest fee.

☐ The additional search fees were accompanied by the applicant's protest but the applicable protest fee was not paid within the time limit specified in the invitation.

☐ No protest accompanied the payment of additional search fees.

C. DOCUMENTS CONSIDERED TO BE RELEVANT

Category*	Citation of document, with indication, where appropriate, of the relevant passages	Relevant to claim No.
Y	SENGSTOCK et al. Effect of silver nanoparticles on human mesenchymal stem cell differentiation, J Nanotechnol, Vol. 5, Pgs. 20158-2069, 10 November 2014 [retrieved on 28.01.2025]. Retrieved from the internet: <URL: https://www.beilstein-journals.org/bjnano/content/pdf/2190-4286-5-214.pdf> entire document	2-4